2010

On The Use Of Polyurethane Matrix Carbon Fiber Composites For Strengthening Concrete Structures

Zachary Haber
University of Central Florida

ON THE USE OF POLYURETHANE MATRIX CARBON FIBER COMPOSITES FOR STRENGTHENING CONCRETE STRUCTURES

by

ZACHARY BENJAMIN HABER
B.S.C.E. University of Central Florida, 2007
B.S. University of Central Florida, 2008

A thesis submitted in partial fulfillment of the requirements
for the degree of Master of Science
in the Department of Civil, Environmental and Construction Engineering
in the College of Engineering and Computer Science
at the University of Florida
Orlando, Florida

Spring Term
2010

Major Professor: Kevin R. Mackie

ABSTRACT

Fiber-reinforced polymer (FRP) composite materials have effectively been used in numerous reinforced concrete civil infrastructure strengthening projects. Although a significant body of knowledge has been established for epoxy matrix carbon FRPs and epoxy adhesives, there is still a need to investigate other matrices and adhesive types. One such matrix/adhesive type yet to be heavily researched for infrastructure application is polyurethane. This thesis investigates use of polyurethane matrix carbon fiber composites for strengthening reinforced concrete civil infrastructure. Investigations on mirco- and macro-mechanical composite performance, strengthened member flexural performance, and bond durability under environmental conditioning will be presented. Results indicate that polyurethane carbon composites could potentially be a viable option for strengthening concrete structures.

To my Mother.

ACKNOWLEDGMENTS

This research was supported by the Florida Department of Transportation (FDOT). The work would not have been possible without the assistance of the following individuals at the FDOT Structures Research Center in Tallahassee, Florida: Marcus Ansley, Steve Eudy, Frank Cobb and William Potter. Following individuals, groups, or companies are also thanked for support:

- Franz Worth and the Air Logistics Co.
- Michael Olka of Metz and Associates in Orlando, Fl
- Charles Williams
- Jun Xia
- Jansa Tomasevic
- Paul Anderson
- Richard Bertrand
- Andrew Warren
- Kirk Scammon (AMPAC – UCF)
- Dr. Lei Zhao (AMICO – Seasafe)
- Dr. Kevin Coffey (MMAE Dept. UCF)
- Nicholas S. Gurney
- Rafiq Chowdhury
- Cara Brown
- Erik Stewart
- Robert Slade

TABLE OF CONTENTS

LIST OF FIGURES

LIST OF TABLES

1. INTRODUCTION

1.1 Background

Increasing service loads, extreme loading events, and constant exposure to an ever-changing ambient environment are just a few reasons why civil structures, over extended service periods, degrade and ultimately become structural deficient. In many cases, it is economically more feasible to repair/strengthen the damaged structure than full demolition and re-construction. Traditional methods of strengthening include steel jacketing/plating, addition of concrete, and near surface mounting additional steel. Although these methods have been proven effective, they can be cumbersome, time inefficient, and susceptible to corrosion. The 1980s saw the advent of more cost effective means to manufacture advanced fiber-reinforced polymer (FRP) composite materials; making the use of such materials more suitable for construction purposes. By the late 1980's, numerous researchers began investigating the possibilities of using FRPs to strengthen reinforced concrete structures. With excellent corrosion resistance, high strength-to-weight ratio, and stiffness-to-weight ratio, externally bonded FRP composites provided a time and strength efficient means to strengthen reinforced concrete (RC) structures.

Since its beginnings in the 1980s, the use of FRP for civil strengthening applications has been heavily researched over the past 20 year. Yet, virtually all work related to FRP strengthening of concrete has been focused on composites utilizing epoxy matrices and adhesives. Although these composites have been proven very effective, they do have some drawbacks:

-During the curing process, epoxies tend to release volatiles and fumes that can be irritating to the eyes and skin.

-In wet lay-up applications, epoxy matrices and adhesives have to be prepared in the field. Furthermore, fibers have to be field impregnated prior to application. Such processes can lead to quality control issues of the composite material and the bond to the substrate.

-Epoxy's bond to concrete has been shown to be sensitive to the application environment; the presence of moisture is a specific concern

Given this drawbacks, it is important that newer matrix systems and adhesives be investigated. Recently there have been developments with matrix materials such that issues observed with typical epoxy resins were mitigated (Bazinet et al. 2003). One such system utilizes polyurethane (PU) as both the matrix material and laminate adhesive. Some benefits of this system are as follows:

-The composite laminate is a pre-impregnated system that comes in a hermetically sealed pouch. Hence this system can be delivered to the job site ready to use or can be stored for a period up to 1 year. Furthermore, pre-preg manufacturing results in high quality saturation of fibers and laminate quality.

-The curing catalyst for the PU matrix and adhesive is water. This means that underwater environments are not a significant obstacle.

-The only byproduct of matrix curing is CO_2 which is not hazardous to the environment or humans.

1.2 Scope and Objectives

This thesis describes the experimental tests completed to preliminarily characterize polyurethane (PU) matrix composites for strengthening and/or retrofitting reinforced concrete structures. . Emphasis is put on areas that have been deemed critical for externally bonded FRP systems for strengthening concrete infrastructure by the literature. In order to evaluate the system in question, a wide spectrum of experimental tests were conducted. Tests can be groups into two main sets; small-scale tests and large-scales. Small-scales tests focused on evaluation of bond and material durability under various environmental conditions. Methods of evaluating bond and material durability included the use of scanning electron microscopy (SEM), material tensile tests, and flexural tests on unreinforced FRP-strengthened concrete beams. All small-scale tests were conducted at University of Central Florida facilities. Large-scale tests focused on comparing the flexural performance of 16' reinforced concrete beam specimens strengthened with PU matrix CFRP to those strengthened with epoxy matrix CFRP systems; flexural performance under cyclic mechanical and thermal loading were considered. SEM was used to characterize the effect of cyclic mechanical and thermal loading on the CFRP laminate systems. Large-scale beam test were conducted at the Florida Department of Transportation Structures Research Center in Tallahassee, FL.

The objective of this study was to determine answers to the following questions in regard to polyurethane matrix carbon fiber composites:

- How do various environments affect the tensile properties of PU composites along with the matrix/fiber interaction at the micron level?

- Does the polyurethane bond to concrete tend to degrade under environmental conditioning?

- How do polyurethane matrix composites behave compared to epoxy matrix composites when externally bonded to reinforced concrete beams?

- What is the failure mechanism for PU-FRP strengthened RC beams?

In completing these objectives, this thesis will provided insight to researchers and engineers on the PU matrix carbon fiber composites and how those composites would perform in infrastructure applications.

1.3 Thesis Outline

The following section provides an outline of the work presented and briefly describes the contents of each section.

Literature Review: The literature review for this document is presented in Chapter 2 and is meant provide a brief introduction on FRP materials in terms of the two main constituents; the reinforcing fiber and the polymer matrix that binds the fibers. The Application of polymer composites in civil infrastructure is then discussed with emphasis on the externally bonded systems and their performance. Finally, polyurethane composite materials are briefly reviewed

Specimen Details: Chapter 3 discusses the design, details, and preparation of all specimen types used in this research. First, the details and materials properties of the 4 different CFRP systems are discussed. This is followed by design and preparation details of small-scale and large-scale beam specimens respectively.

Test Methods And Evaluation Procedures: Chapter 4 discusses the procedures by which specimens were conditioned (either mechanically or environmentally), loaded, and by other means evaluated. Test schedules for all specimen types will be discussed in respective subsections along with loading procedures and conditioning environments described in detail. SEM evaluation procedures are also presented.

Results: Chapter 5 presents that results from the tests conducted. The results section has been limited to tables, plots, and figure integral to characterization of the PU CFRP system. The results chapter is broken into two distinct sections; the first discusses the small-scale (durability tests) tests and the other describes the large-scale tests.

Conclusions and Recommendations: Chapter 6 provides the final conclusions, recommendations, and directions for future research.

2. LITERATURE REVIEW

2.1 Fiber Reinforced Polymers Composites

Fiber Reinforced Polymer (FRP) composites consist of two main constituents: a reinforcing fiber, which is the main load-carrying component, and a polymeric matrix which is used as a stress transferring mechanism, binder, and to protect the reinforcing fibers from the ambient environment. The matrix material also ensures that reinforcing fibers maintain their designed orientation in the structural component.

2.1.1 Reinforcing Fibers

There are a number of different types of reinforcing fibers. This portion of the report will focus on carbon, glass, and aramid reinforcing fibers. Research has shown that these are the best suited for infrastructure applications. Table 1 contains a good representation of commercially available fibers and their mechanical and physical properties.

Table 1. Typical Reinforcing Fiber Material Properties†

Fiber Type	Fiber Identification	Density (g/cm^3)	Tensile Modulus (Msi)	Tensile Strength (ksi)	Failure Strain (%)	Coefficient of Thermal Expansion (10^{-6} /ºF)	Poisson's Ratio
Glass	*E-glass*	2.54	10.5	500	4.8	8.99	0.2
	S-glass	2.49	12.6	625	5	5.22	0.22
Carbon	*T-300*	1.76	33.5	530	1.4	-1.08	0.2
	P-100	2.15	110	350	0.32	-2.61	0.2
	AS-4	1.8	36	590	1.65	-1.08	0.2
	IM-7	1.78	43.5	770	1.81	-1.35	0.2
Aramid	*Kevlar 49*	1.45	19	525	2.8	-3.60	0.35
	Techora	1.39	10.1	435	4.6	-10.79	0.35

†All Values taken from (Mallick, 2008)

2.1.1.1 Glass Fibers

Glass fibers are one of the most common and popular types of reinforcing fibers. Glass fibers are low cost compared to carbon or aramid fiber and have a high commercial availability. Some of the notable advantages of glass fibers are high ultimate strength, relatively high elongation until failure compared to other fiber types, non-conductive, good resistance to chemicals. The disadvantages of glass fibers are low tensile modulus, high specific gravity compared to carbon and aramid fibers, and surface abrasion sensitivity. Glass fibers also have some critical durability issues with mechanical fatigue (both static and cyclic), prolonged exposure to hydro-thermal loads, and alkali or acidic environments.

2.1.1.2 Carbon Fibers

As seen in Table 1, carbon fibers can be found with various mechanical properties. Yet, generally speaking, carbon fibers have high strength-to-weight ratios, stiffness-to-weight ratios, chemical resistivity, and excellent resistance to mechanical fatigue. Also, carbon fibers have negative coefficients of thermal expansion (CTE) which means that combine with the correct resin matrix system can yield a composite with a zero CTE. Some of the disadvantages of carbon fibers are poor impact resistance, high cost compared to other fibers, limited availability, low strain-to-failure, and high electric and thermal conductivity.

Tavakkolizadeh et al. (2001) discusses the issue of carbon-to-steel galvanic corrosion. It was found that the corrosion rate was primarily dependent on the matrix thickness, direct carbon-to-steel contact area, and presence of salt solutions.

2.1.1.3 Aramid Fibers

Aramid fiber technology saw its first commercial appearance in the 1960s under the DuPont Company. Aramid fibers have the highest tensile strength-to-weight ratio amount the popular reinforcing fibers. Some advantages of aramid fibers are high resistance to extreme heat, high tensile strength, a negative CTE, excellent resistance to impact damage, and good chemical resistance. The disadvantages of aramids are difficult to machine, low compressive strength, and have durability issues with UV light and prolonged exposure to moisture (Mallick, 2008).

2.1.2 Polymeric Matrix Materials and Adhesives

There exists a wide variety of matrix material materials used in the manufacturing of FRP composites. Matrices can be organic or inorganic and can come from different material families i.e. ceramic, metallic, or polymeric. The matrices that will be of focus in this section are epoxy and polyurethane.

2.1.2.1 Epoxy Resins

Epoxy resin is one of the most popular matrix types used with carbon, glass, and aramid fibers in infrastructure applications. This is due to the number of advantageous chemical and mechanical properties that epoxy resins possess. Table 2 displays some general material properties of epoxy resin. Of these properties, the two worth mentioning are the Poisson ratio and the cure shrinkage. With a Poisson value in the range of 0.2-0.33, cured epoxy resins have a similar Poisson values to steel and concrete which are normally the bonding substrates in civil applications. The low cure shrinkage for epoxies, which is in the low range for polymeric matrices, means that cure-induced residual strains at the substrate level are low.

Table 2. Generic Cast Epoxy Resin Properties

Density (g/cm^3)	Tensile Strength, (ksi)	Tensile Modulus, (ksi)	Poisson Ratio	CTE, 10^{-6} (10^{-6} in/in/F)	Cure Shrinkage (%)
1.2 - 1.3	8-19	400-5,950	0.2-0.33	(28-44)	1-5

†All Values taken from (Mallick, 2008)

Epoxy resins also have a number of attractive chemical properties such as absence of volatile matter during cure, excellent resistance to chemicals, and excellent adhesion properties. The disadvantages of epoxy matrices are high cost and prolonged cure time (Mallick, 2008)

2.1.2.2 Polyurethanes

Polyurethane is generic name used more for convenience than accuracy. Polyurethanes are not produced by polymerizing urethane monomers and do not consist solely of urethane groups; they can contain a number of different chemical groups. The development of polyurethane based adhesives began in the late 1930's with the first structural use introduced in 1968 by Goodyear (Szycher, 1999). Urethane adhesives have vast range of attractive properties making them a good candidate for a variety of substrate applications:

- Effectively wet the surface of most substrates.
- Have small molecular size that allows the adhesive to permeate porous substrates.
- Rapid cure time that is adjustable with catalyst.
- Cost effective.
- Excellent at low temperature.

Some of the disadvantages of polyurethane adhesives are as follows:

- Limited thermal stability due to molecular constituents.
- Issues with hydrolytic stability.
- Sensitive to moisture in bulk.
- Conditions under which application/curing occurs are critical.
- Some substrates require the use of primers.

There does not exist a significant amount of research available on the use of polyurethanes as matrix materials for FRPs. The majority of early work published on the subject is related to fiber reinforced elastomeric polyurethanes (Andreopoulos et al.1989) and thermoplastic polyurethane composites (Kutty et al. 1991 and Kutty et al. 1991) which do not exhibit mechanical performance suitable for infrastructure load-bearing applications.

2.2 Applications of FRP Composites in Civil Infrastructure

Today there is a growing popularity of using FRPs in civil construction. Typically, FRP composites are selected as a structural or load bearing component when significant strength and stiffness are needed and component self-weight is a critical design factor. Other instances where FRP composites have been a design option are scenarios where harsh and/or corrosive environments are encountered.

One such application is the use FRPs for strengthening and retrofit of damaged, deficient, and degraded reinforced concrete (RC) flexural members. Typically, flexural strengthening is achieved by bonding pre-formed FRP plates or field impregnated fiber sheets to the tension soffit of the member. Plates and sheets can be bonded to the concrete substrate using a number of different adhesive systems, i.e., epoxy, polyester, vinylester, and polyurethane. Furthermore, different types of reinforcing fiber can be selected depending on the application environment, i.e., glass, aramid, carbon, and basalt. The composite strengthening system is defined as the combination of reinforcing fibers and impregnating resin. Strengthening systems may or may not include a substrate adhesive primer layer to promote bonding.

Investigations on externally bonded flexural strengthening began in the late 1980s (Ritchie et al., 1991). It was found that applying externally bonded FRP to the tension soffit of an RC beam could significantly increase the load bearing capacity of the member. Although increase in strength observed the increase came at the cost of decreased member deformation and abrupt non-ductile failure modes.

The failure mode most commonly associated with flexural strengthening of concrete with externally bonded FRPs is laminate debonding. This failure mechanism occurs when the bonded laminate, either locally or globally, separates from the concrete member. A study by Bonacci and Maalaj (2001) involved compiling a database of laboratory beam specimens that were tested in flexure with bonded FRP laminates. The results of the study indicated that as many as 69% of laboratory specimens failed via laminate debonding. Debonding is a complex mode of failure that is depended on a number of variables such as concrete strength, FRP type, adhesive properties, and the environmental conditions during composite curing (Buyukozturk & Yu, 2006). Various debonding failure modes are depicted in Figure 1.

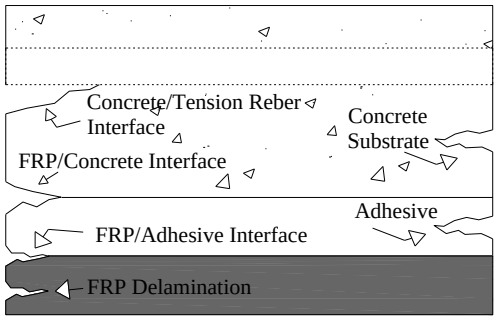

Figure 1. Typical Debonding Failure Mechanisms

Research has shown that there are a number of different factors that affect the performance of RC beams externally strengthened with bonded FRP laminates. One area of particular interest to design engineers and researchers is the long-term durability of strengthened members. The subsequent sections describe how mechanical fatigue/cyclic loading and harsh environments affect the performance of strengthened members.

2.2.1 Fatigue and Cyclic Loading

A critical factor effecting the long-term performance and durability of RC members strengthened with externally bonded FRP systems is repeated or fatigue loading. There only exist a limited number of available studies that have investigated the fatigue response of FRP strengthened members.

One of the earliest studies conducted was by Meier, et al. (1992) at EMPA (The Swiss Laboratories for Material Testing and Research at Dubendorf). In this study an RC beam with length 2000mm, depth 250mm, and wide 300mm, was strengthened in flexure with a glass/carbon hybrid sheet that was bonded to the tension face of the beam. The member was loaded in 4-point bending at a frequency of 4 Hz with a loading range of 1 to 19 kN (stress in the tension reinforcement was in the order of 400 MPa). Ultimate failure of the member occurred at 805,000 cycles.

Two more fatigue tests were conducted by Meier at EMPA. In these tests other test parameters were investigated such as slight increase in temperature and humidity during fatigue loading and pre-stress of the composite plate. Complete failure occurred at 14 and 30 million cycles. It must be noted that stress range for the second and third tests was not as intense as the initial test.

Barne, et al. (1999) conducted a similar fatigue study on CFRP strengthened RC beams. In their study, 5 RC beam specimens were constructed with the following dimensions and reinforcement: a span length 2.3m, depth 230mm, width 130mm, and 3 T12 rebars as tension reinforcement. Of the 5 beams, 3 beams were strengthened with pultruded CFRP composite plates. The plates were bonded to the tension face of the beams using SikaDur 31 two part structural epoxy. Moreover, all of the strengthened specimens incorporated plate-end anchorage consisting of two steel anchor bolts and a steel plate. The remaining two beams were used as control specimens.

Fatigue loading was conducted at 1 Hz in a 4-point bending configuration. The maximum load range considered for fatigue testing was between 25.9% and 39% of the predicted ultimate capacity of the beams (stress in the tension steel between 198 and 303 MPa). All strengthened specimens failed via fatigue rupture of the tension steel reinforcement.

The results of this study concluded that the fatigue stress range and the amount of tension steel were the most critical parameters when considering fatigue life of a CFRP strengthened member.

Ferrier, et al. (2005) conducted a study that employed the use of small-scale single and double lap shear test specimens. The purpose of the study was to determine the allowable shear bond strength and FRP strength as a function of number of load cycles. The test parameters considered in this study were epoxy type and stress range.

The results from this study concluded that as the number of fatigue cycles increase there is a proportional decrease in failure strength and composite elastic modulus. Moreover, it could also be observed that the stress range applied during fatigue loading had a significant impact on fatigue life. Recall, this result was noted by Barnes and Mays (1999) as well.

Ferrier et al. also describes the syntax of progressive failure during the fatigue life of the specimen as follows:

- *10% - 15% of fatigue life:* Debonding begins to occur near the loaded end of the specimen.

- *50% - 75% of fatigue life:* Epoxy adhesive begins to undergo softening and fatigue induced degradation.

- 75% - *100% of fatigue life:* Crack propagation at the concrete/FRP interface leading to failure.

The fatigue and monotonic strength of RC beams strengthened with externally bonded CFRP was investigated by Gheorghiu, et al. (2006). Fifteen RC beam specimens were constructed with dimensions: length 1215mm, width 100mm, and depth 150mm. All beams were strengthened with one layer of Sika CarboDur (50mm width). A 260mm portion of the composite laminate was left unbounded at the mid-span of all beams to ensure that specimen failure would occur via debonding.

Thirteen beams were subjected to cyclic loading and then to monotonic loading until failure. The two beams not subjected to cyclic loading were used as reference specimens and only subjected to monotonic loading.

Cyclically loaded beams were subjected to 400,000 to 2,000,000 load cycles at one of two load intensities. A low-range load intensity that varied from 15-35% of specimen yield strength and a high-range load intensity that varied from 35-75% of specimen yield strength. Beams were tested at 2 Hz (10 beams) or 3 Hz (3 beams).

The study concluded that the number of fatigue cycles at the low-range load intensity did not have a significant effect on the strengthened beams. Yet, the converse was true for the beams fatigued at the higher load intensity range. After about 200 cycles there was a significant increase in laminate strain and crack presence. Although the higher load range had an effect on observed strain and cracking, it was concluded that fatigue loading did not have a significant effect on member ultimate load (monotonic to failure).

Toutanji, et al. (2006) investigated the cyclic behavior of RC beams strengthened with CFRP sheets impregnated and bonded with an inorganic matrix. The main objective of the study was to investigate the relationship between fatigue strength, crack width, and number of fatigue cycles. Seventeen beam specimens were cast for the experiment. Thirteen beams were strengthened with three layers of externally bonded CFRP fabric. Strengthened specimens also incorporated externally bonded 45 degree shear strengthening CFRP strips.

The fatigue load applied ranged between 50% and 80% (strengthened specimens) of the ultimate static load capacity. The study concluded that member deflections and laminate strains do not vary significantly after the fatigue rupture of tension steel. It was also concluded that due to CFRP's higher ultimate strength compared to that of steel that the application of CFRP can increase the fatigue load capacity of a strengthened RC member. Finally it was concluded that crack initiation and propagation occurs during that first few hundred fatigue cycles.

Grace, et al. (2005) conducted an experimental study investigating the effect of repeated loading on the flexural response of CFRP strengthened RC beams. Twelve beam specimens with the following dimensions were used: length 2740mm, length 254mm, and width 152mm. Beams were strengthened with either externally bonded CFRP plates or sheets. Specimens were loaded in a 4-point bending configuration at 3.25 Hz for 2 million cycles. The loading ranges were 15%, 25%, or 40% of the ultimate flexural capacity. The study concluded that fatigue had no adverse effect on the ultimate load carrying capacity of the strengthened beam. It was noted that for the 40% of ultimate load range that specimens for both CFRP plate and fabric experienced softening without increase in applied load.

A study by Aidoo, et al. (2004) investigated the fatigue performance of large-scale RC bridge girders retrofitted with CFRP materials. Particular attention was paided to the bond between CFRP and concrete and fatigue life of strengthened specimens. Test parameters taken into consideration were CFRP system (plates and sheets) and fatigue stress range (60% and 80% of tension steel yeild stress). Eight 6.1m (20') reinforced concrete T-beams were prepared for the study. The construction details of the specimens prepared represented a 62% scaling of beams removed from an interstate bridge constructed in 1961. Fatigue loading was applied with a servo-controlled MTS hydraulic actuator under load control at 1Hz.

It was observed that strengthened specimens for both stress ranges failed in the following manner:

- Initial failure was caused by fatigue rupture of the extreme tension layer of reinforcing steel. In some specimens, multiple tension bars experienced fatigue rupture.

- Shear cracking/deformation near mid-span initiated CFRP debonding.

- Complete CFRP delamination from concrete. In some cases delamination was induced by steel rupture.

It was concluded that the addition of externally bonded CFRP can increase the fatigue life of RC beams. The increase in fatigue life is limited by the CFRP-to-concrete bond quality and ability to resist fatigue induced bond degradation. It was also found that the preformed CFRP strip preformed better than the fabric retrofit.

The following general conclusions can be drawn from past research on the fatigue durability of CFRP strengthened RC beams:

- Fatigue stress range seems to play an important role in the fatigue performance of CFRP strengthened members.

- The majority of studies reported softening in strengthened members due to fatigue induced degradation of the FRP-to-concrete interface.

- Studies report mixed results in regard to post-fatigue monotonic ultimate flexural capacity.

2.2.2 NaCl Solution

There are numerous situations in externally strengthening applications where the FRP composite system could be subjected to salt exposure i.e. road de-icing salts and sea water. Although FRP composites have a high tolerance against corrosion, the FRP-to-concrete interface could be compromised due to such exposure. There have been a few studies conducted on the effects of salt exposure on RC members externally strengthened with FRP materials.

One of the earliest studies to investigate exposure to chlorides was done by Karbhari, et al. (1996). The study focused on the FRP-to-concrete bond behavior under short term exposure to various environments. Two different commercially available epoxy resin systems were investigated with glass and carbon reinforcing fibers. Small-scale mortar (1:3 – cement:sand) beam specimens were used with dimensions of 13”(length) x 2”(width) x 1”(height). Three layers of epoxy impregnated reinforcing fiber were applied to each strengthened specimen. After a one week cure period specimens were subjected to 60 days (1440 hours) of immersion in a 5% NaCl solution. Upon completion of environmental conditioning specimens were subjected to 4-pt monotonic loading until failure.

All four composite systems tested experienced decreased flexural performance in terms of ultimate load bearing capacity, deflection capacity, and flexural stiffness (*EI*). The decreases in performance were reported as follows: 13-47%, 15-53%, and 7-31% for ultimate load, deflection, and flexural stiffness respectively. It must be noted that the epoxy systems with the lower glass transition temperature experienced the most severe degradation for both glass and carbon fibers. Furthermore, it was determined that the epoxy system was more critical to the post-conditioned behavior than the reinforcing fiber.

The effect of immersion in NaCl solution was investigated as a portion of the study conducted by Grace, et al. (2005). 12 beam specimens, with dimensions 9'(length) x 6"(width) x 10"(height) and ρ=1.15%,were exposed to immersion in a NaCl solution for 1000, 3000, or 10,000 hours at 73°F ± 3°F. Beams were strengthened with either CFRP plates or fabric sheets. The CFRP systems were adhered to the concrete surface using one of two types of structural epoxy. Both epoxy systems had similar material properties. Ultimate load testing was conducted under 4-point bending in three stages.

Results from load tests show no significant decrease in ultimate load bearing capacity for either CFRP strengthening system. The system employing CFRP plates actually showed an increase in ductility for all exposure periods. The system employing CFRP sheets showed a 16.6% decrease in ultimate deflection capacity. Ultimate strains values for both systems at all exposure periods experienced slight or no reductions from baseline values. In conclusion there did exist any type of definitive relationship between time of exposure and mechanical response.

An experimental study on the durability characterization of wet lay-up carbon/epoxy composites was conducted by Abanilla, et al. (2006). A portion of the study was focused on the effect of a salt solution on CFRP at the material level. The carbon fabric used had the following properties: ρ = 1.80 g/cm^3, E = 230 GPa, and f_{frp} = 4900 MPa. Specimens exposed to saline solution immersion consisted of either 2 or 6 layers of carbon fabric. After curing, a standard ASTM D3171 acid digestion test was conducted and it was determined that specimen volume fractions ranged from 34 to 43%.

Specimens where subjected to 100 weeks of immersion in a 5% NaCl solution at 23 °C. The effect of saline immersion was quantified via uniaxial tension (ASTM D3039), 3-point flexure (ASTM D790), glass transition temperature T_g (ASTM E1640), and moisture uptake testing. Specimens were tested throughout the 100 week period of exposure (5 specimens per time interval).

It was concluded that the presence of NaCl in solution had a negligible effect on the rate of moisture uptake and T_g. Tensile test (2-layer specimens) results showed an 18 and 12% decrease in tensile strength and modulus respectively after 100 weeks of exposure. 3-point bending test (6-layer specimens) results showed a 25 and 9.4% decrease in flexural strength and modulus respectively after 100 weeks of exposure. It must be noted that the respective strength and modulus decreases seen over the 100 week period for both tests were progressive and had a tendency to stabilize over time.

Soudki, et al. (2007) conducted an experimental study which examined the ability of externally bonded CFRP plates (Sika CarboDur) and sheets (Forca-Tow) to prevent chloride intrusion of concrete. A total of 11 RC beams (2400mm-length x 150mm-width x 250mm-height and ρ=0.6%) were cast. Of which 8 beams were cracked and strengthened with CFRP and 3 beams remained uncracked. There were two strengthening schemes employed: beams strengthened with CarboDur plates incorporated U-wrap plate-end anchorage and beams strengthened with Forca-Tow sheets employed lateral CFRP anchorage strip throughout the length of the beam shear span. It must be noted that both the sides and tension face of the beams strengthened with Forca-Tow were covered with saturating epoxy.

Beams were subjected to 0, 100, 200, or 300 wet/dry cycles in the presence of 3% NaCl solution. Each wet/dry cycle took 2 days to complete (1 day for the wet cycle and 1 day for the dry cycle). Upon completion of the wet/dry conditioning beams were loaded monotonically to failure in a 4-point bending configuration.

Results of the study showed that beams strengthened with CarboDur plates yielded 19, 25, and 28% reduction in load bearing capacity for 100, 200, 300 wet/dry cycles respectively. Beams strengthened with the Forca-Tow system showed 2, 6, and 11% reductions in ultimate capacity for 100, 200, and 300 wet/dry cycles respectively. The performance of the Forca-Tow system verses the CarboDur system was attributed to the epoxy coverage of the beam. It is also concluded by the authors that the Forca-Tow system was not greatly affected by the applied conditioning. It must be noted that the authors of this document believe that the performance of the Forca-Tow system can be attributed to the amount of additional transverse anchorage that was used.

2.2.3 Moisture & Humidity

Karbhari, et al. 2003 identified exposure to moisture and humidity to be a critical area in need of investigation for externally strengthening. This is due to the susceptibility of the resin matrix to be infiltrated by moisture. Moisture intrusion of the matrix can lead to a number of negative effects. On the matrix level, this can cause hydrolysis, plasticization, and saponification. At the fiber/matrix interface level, moisture intrusion can cause both chemical and mechanical fiber/matrix bond degradation. If moisture is allowed to reach the reinforcing fibers, in the cases of aramid and glass fiber, can cause deterioration of the fiber and a higher possibility of premature fiber rupture.

Although significant work has been completed on the investigation of humidity and moisture effects of FRP composites (Marom and Broutman 1981, Apicella et al. 1983, Zheng and Morgan 1993, and Schutte 1994) the same is untrue for externally reinforced RC members. The following section discusses some of the available studies conducted on moisture/humidity effects on FRP strengthened RC members

The study conducted by Karbhari, et al. (1996), as discussed earlier, was one of the earliest experimental investigations on environmental effects on FRP strengthened concrete. A portion of this study focused on the immersion of specimens in water at 68°F (20°C) for 60 days (1440 hours).

Results showed that of the four composite systems tested there were 15-35% and 15-52% reductions ultimate load and deflection at failure respectively. It was also found that immersion in water did not have an effect on the glass transition temperature for all systems. It was concluded that the resin matrix system used in creating the externally bonded composite had the greatest effect on the post-immersion load deflection behavior of the specimens.

The study conducted by Grace, et al. (2005), previously discussed, included a portion of the experimental program that exposed specimens to 100% humidity for periods of 1000, 3000, and 10,000 hours at 100±3°F (38±2°C) per ASTM D 2247. Recall that both CFRP plates and sheets were used to strengthen beam specimens.

Results of the study showed that beams strengthened with CFRP sheets exhibited more stable post-humidity performance than those strengthened with CFRP plates. Of the various exposure environments used in the study (dry heat, humidity, NaCl solution, freeze-thaw, alkali solution, and fatigue) it was found that the beams strengthened with CFRP plates showed a greater tendency to experience decreased flexural performance in terms of ultimate load bearing capacity and maximum flexural strain due to humidity exposure (at 10,000 hours); decrease of 31.9% and 54% from baseline ultimate capacity and maximum strain respectively. The post-exposure behavior of the specimens strengthened with CFRP sheets was not nearly as critical for 10,000 hours of exposure; 9.67% , 11.4%, and 19.9% decreases from baseline results in terms of ultimate load, deflection, and mid-span strain respectively. All specimens failed via CFRP debonding and/or concrete cover delamination.

2.2.4 Temperature Effects

In infrastructure service environments, variations in ambient temperature are to expected. Therefore, the effect of temperature variation on the FRP-to-concrete interface is of importance when considering the long-term durability of strengthened members. There have been three types of temperature oriented tests conducted in relation to infrastructure applications:

1) Exposure to a constant temperature (either elevated or decreased).

2) Cyclic temperature exposure (such as freeze/thaw or heat/cool).

3) Steady-state or transient temperature exposure during the loading (both experimental and analytical conducted).

The study conducted by Grace, et al. (2005), previously discussed, included portions of the experimental program that exposed specimens to constant elevated temperatures and freeze/thaw cycles. Twelve RC (4 per exposure period) beam specimens were exposed to 1000, 3000, or 10,000 hours of 60°C (140°F) dry heat in a specially design chamber. Eight (4 per exposure period) beam specimens were exposed to 350 or 700 freeze/thaw cycles where temperature cycled between -17.8°C and 4°C (0°F and 40°F). Air was used to freeze beams while water was used for thawing. After the conditioning period, specimens were loaded monotonically until failure.

Results revealed that freeze/thaw conditioning resulted in reduced loading bearing capacity of RC member strengthened with FRP plates and sheets by 3.3-9.5% and 6-13% respectively. There was no significant decrease in flexural performance observed in specimens subjected to dry heat conditioning. All specimens failed via CFRP debonding.

Gamage, et al. (2006) investigated, via analytical means, the bond properties of CFRP to concrete under elevated temperatures. More specifically, the study focused on bond performance under transiant thermal loads like those associated with structural fires. 13 single-lap shear specimens (2 of which were coated with an insulating material) were prepared to calibrate a non-linear heat transfer finite element model (FEM). Test specimens were loaded using displacement control. During testing, non-insulated specimens were subjected to a constant rate applied temperature of 10°C/min (50°F/min). Parameters investigated via FEM were bond length, bond slip, failure load, temperature rate, fire resistance level, and insulation thickness.

Based on both experimental and analytical results, the study by Gamage, et al. concluded the following:

- The epoxy adhesives currently being used for construction applications are extremely sensitive to temperature variations.

- A maximum service temperature of 70°C (158°F) is recommended to maintain force transfer between concrete and CFRP.

- Bond strength, under elevated temperatures, is not dependent on bond length.

- Un-insulated concrete-CFRP composites will reach the point of bond failure in the standard fire within 5-6min.

Karbhari, et al. (2003) suggested that for civil infrastructure applications freeze/thaw conditons are to be considered the most critical temperature related service environment.

2.3 Polyurethane Matrix Composites

Sen et al. (2006) completed a demonstration field project that focused on the repair of severely damaged underwater bridge piles using the same polyurethane composite system considered in this study and other more conventional systems. After two years of service, direct tension bond pull-off tests revealed that the polyurethane system tended to exhibit inter-layer failure. Such a failure indicates good bond to concrete but poor layer-to-layer adhesion. Furthermore, the ease in which the system could be used was noted. Mechanical testing to determine the ultimate load-bearing capacity of strengthened piles was not completed.

Setiadi et al. (2005) conducted a study on random fiber reinforced polymer composites and the damage sequence induced onto the composite by cyclic loading. Two different types of polymeric matrices were considered for the study; a modifed polyester employing a methyl ethyl ketone peroxide (MEKP) initiator and a thermosetting polyurethane. Test specimens (of dogbone geometery per ASTM D 628-01) were reinforced with 5 layers of random oriented E-glass mat and manufacured via resin tranfer molding (RTM). The approximate fiber fractions for each matrix type where 25 to 28% for the polyester-based FRP and 23 to 25% for the urethane-based FRP. Fatigue testing was conducted at 0.3 Hz within a stress range of 0 to 50% of the ultimate stress of the respective specimen types.

Results from static loading show that the urethane matrix composite had significantly higher strain at failure, ultimate strength, and energy absorption at failure than the polyester composite at the cost of lower tensile stiffness. Furthermore, the fracture plane and the observed post-failure cracking was more localized for that of the urethane composite.

Results from fatigue loading indicate that both matrix types show increased strains with cycle number. Yet, the strain increases in the urethane composite were smaller than those observed in the polyester composite. Furthermore, a decrease in elastic modulus was observed for both specimen types but was less significant in the urethane composite. The urethane matrix composite also exhibited a lower amount of matrix cracking at 1000 cycles. Moreover, cracks in the urethane matrix were observed to originate from micro-voids caused by CO_2 during cure. It was concluded that urethane matrix composite performed better, under the inposed conditions, than of the polyester matrix composite.

3. SPECIMEN DETAILS

Two groups of specimens were constructed for the work presented in this thesis. The first group was comprised of small-scale beams and composite plates that would be used to evaluate the short-term durability of PU carbon composite system being considered. The second group of specimens was a set of large-scale reinforced concrete beams use to evaluate the performance of the PU system versus an epoxy based system. The following section describes the composite systems used, how specimens were constructed, how CFRP was applied, and how specimens were instrumented for testing. Test matrices will also be presented.

3.1 CFRP Systems

For this study there were four CFRP systems used in experimental testing; 2 polyurethane matrix systems and 2 epoxy matrix systems. The principle material properties, i.e. elastic modulus, rupture strength and strain, for all systems were experimental determined at the University of Central Florida's Structural Analysis Laboratory. Tensile coupons were prepared according to ASTM D3039 for all composite types and testing on a Satec 200kip universal testing machine. The following section describes system constituents and the composite material properties.

3.1.1 Polyurethane Matrix Carbon Fiber Composite Systems

Two polyurethane matrix carbon fiber composite systems used in this study; the first (denoted the "PU1" system) utilized a uniaxial carbon fabric and the second (denoted the "PU2" system) utilized a biaxial carbon fabric. Both systems are commercially known as Aquawrap-Black and are produced by the Air-Logistics Company in Azusa, CA. The PU composite systems were pre-impregnated with a polyurethane resin and came ready to use in a hermetically sealed foil package. The matrix hardening process for the PU matrix was catalyzed by misting the pre-impregnated composite with water. The PU composite systems also employed the use of an adhesive base primer (know as BP-1) to promote laminate adhesion to rough surfaces; a two-part polyurethane adhesive that came in pre-measured quantities ready for mixing. The BP-1 system also contained glass fibers for additional strength. General properties of the BP-1 base primer system can be found in Table 3.

Table 3. BP-1 Base Primer Properties

BP-1 Adhesive Primer	
Working Time	45 min @ 77 ^{0}F
Application Temperature	33 - 100^{0}F
Service Temperature	0 - 250^{0}F
Cure Time	60-90 min @ 77^{0}F
Bond Strength (Concrete)	225 psi

A total of 5 tensile test coupons were constructed to determine that material properties of the PU1 CFRP system. The stress-strain material behavior and results summary for acceptable samples can be found in Figure 3 and Table 4 respectively.

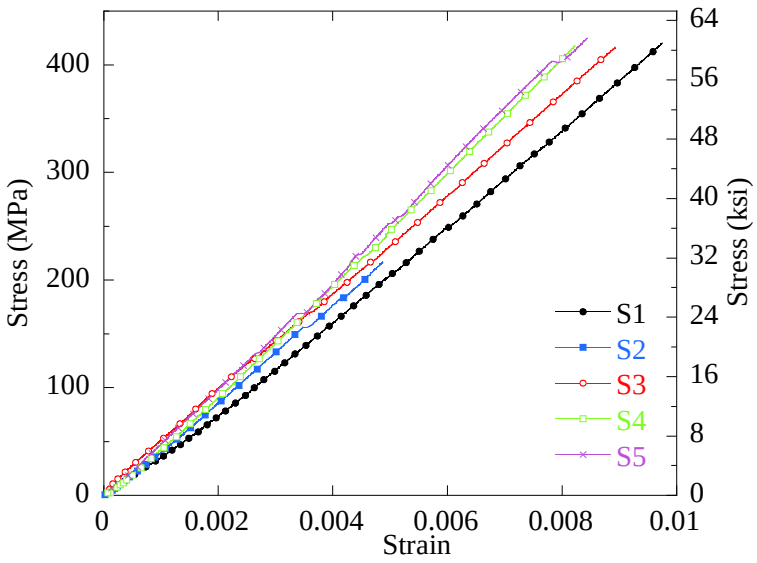

Figure 2. PU1 System Stress-strain Material Behavior

Table 4. PU1 System Tensile Test Results Summary

Sample ID	Elastic Modulus (ksi)
S1	6459
S2	6861
S3	6621
S4	7611
S5	7578
Average	7026

A total of 9 tensile test coupons were constructed to determine that material properties of the PU2 CFRP system. Of the 9 test samples, 7 were considered to produce acceptable results. Samples 1 and 7 were not included due to substantially low numerical results and data acquisition malfunction respectively. The stress-strain material behavior and results summary for acceptable sample can be found in Figure 3 and Table 5 respectively.

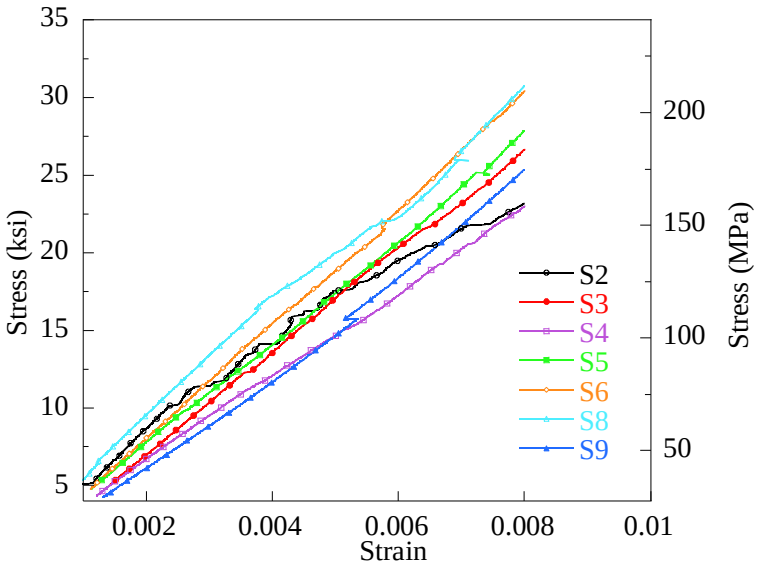

Figure 3. PU2 System Stress-strain Material Behavior

Table 5. PU2 System Tensile Test Results Summary

Sample ID	Elastic Modulus (ksi)	Rupture Strain (%)	Ultimate Stess (ksi)
S2	2356	1.52	35.8
S3	3221	1.24	39.8
S4	2679	1.39	37.1
S5	3353	1.03	34.5
S6	3716	1.01	37.4
S8	3235	1.24	40.0
S9	3348	1.03	34.6
Average	3130	1.21	37.0

3.1.2 Epoxy Matrix Carbon Fiber Composite Systems

There were two epoxy matrix systems used in this study. Both systems utilized the same 12” width uni-directional carbon fiber. The carbon fabric was produced by the Hexcel Corporation (product identification GA130). Fiber details can be found in Table 6.

Table 6. Carbon Fabric Properties

GA130 Carbon Fabric	
Weight (oz/yd2)	13.2
Thickness (in.)	0.02
Fibers/Tow	12000
Weave	Unidirectional

The first epoxy matrix carbon fiber composite system was designated the "EP1" system. The resin system used was a two-part medium viscosity epoxy produced by the PTM&W Company commercially known as Aeropoxy (PR2032 resin and PH3660 catalyst). The Aeropoxy system was previously used by the FDOT in previous research studies. The mix ratio used, as specified by the manufacturer, was 3:1 resin to catalyst by weight or volume. Test specimens were constructed using two layers of CFRP fabric. Test results for elastic modulus and rupture strength are found in Table 8.

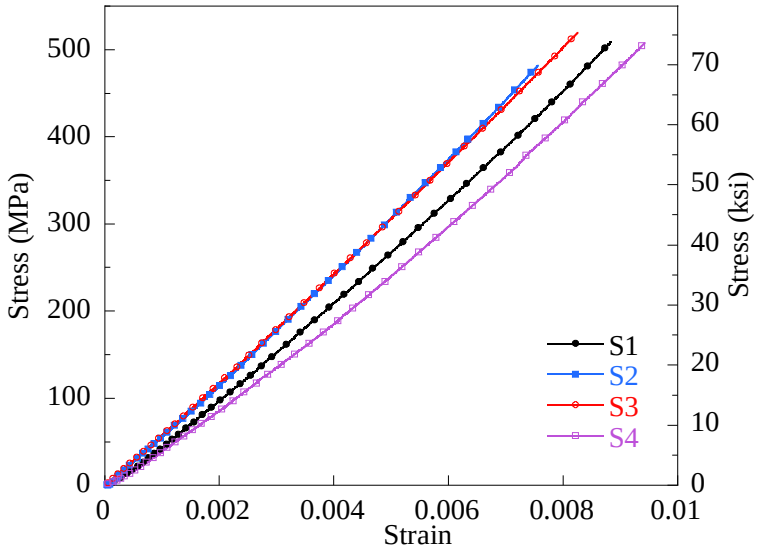

Figure 4. EP1 System Stress-Strain Behavior

Table 7. EP1 System Tensile Test Results Summary

Sample ID	Elastic Modulus (ksi)	Rupture Strain (%)	Rupture Stress (ksi)
S1	9084	1.12	103
S2	9801	1.09	101
S3	9055	1.09	101
S4	8918	0.96	88.6
S5	-	1.04	96.2
Average	9214	1.065	98.1

The second epoxy matrix system, designated at the "EP2" system, employed an epoxy matrix that incorporated resin and catalyst from different manufacturers. The epoxy resin used was D.E.R.™ 383 produced by the DOW Company. The resin catalyst was Jeffamine® D-230 produced by Huntsman. The mix ratio used was 3.29:1 resin to catalyst by weight; this mix ratio yields an epoxy of medium viscosity. Tensile test coupons were prepared with two layers of CFRP fabric. Results can be found in Figure 5 and Table 8.

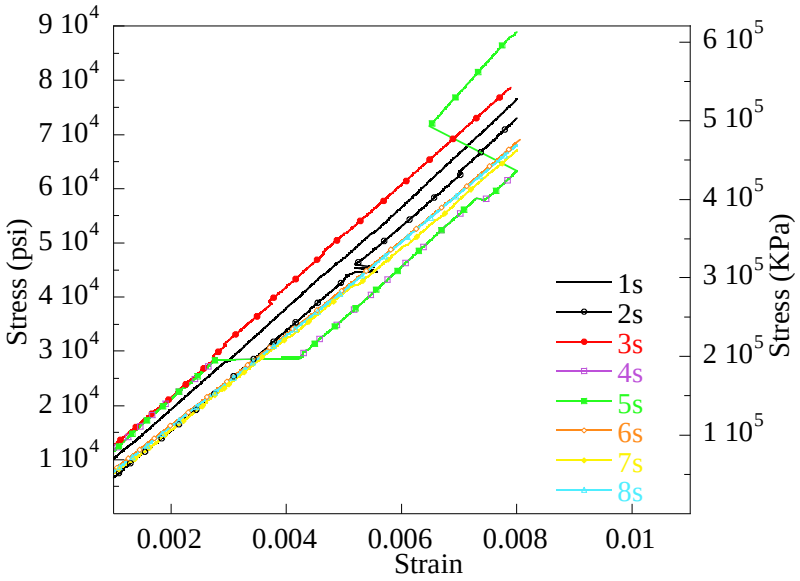

Figure 5. EP2 System Stress-Strain Behavior

Table 8. EP2 System Tensile Test Results Summary

Sample ID	Elastic Modulus (ksi)	Rupture Strain (%)	Ultimate Stress (ksi)
S1	9549	0.98	93.8
S2	9681	0.92	88.6
S3	9531	0.83	78.7
S4	9242	0.93	85.9
S5	8764	1.22	106
S6	8764	-	-
S7	8552	1.26	107
S8	8745	1.26	110
Average	9103	1.06	95.9

3.2 Small-scale Beam Specimens

Small-scale specimens were poured on August 31st 2009 in the UCF structures laboratory (refer to Figure 6). A total of 77 beams were poured measuring 6" x 6" x 24" of which 34 beams would be used for the work presented in this thesis. During casting, 72 (4" x 8") concrete cylinders were poured according to ASTM C39. Details regarding the concrete mix used for small-scale beam specimens can be found in Table 9. Beams were allowed to cure undisturbed in forms for a minimum of 7 day prior to removal. During curing, forms were covered with plastic to ensure minimal escape of moisture.

Figure 6. Concrete Pour in Structures Lab

Table 9. Concrete Mix Details

Cement Type	Portland Type I/II
Maximum Aggregate Size	1"
Specified 28 Day Strength	5000 psi
Measured Slump	3.5"
14 Day Strength	5527 psi
28 Day Strength	6360 psi

Once removed from forms, beams were prepared for application of CFRP. The substrate surface of each beam was treated with a handheld grinder to remove the thin layer of cement paste covering the aggregate. Each beam specimen was to have a single layer of PU2-CFRP. Small-scale specimen details can be found in

Figure 7.

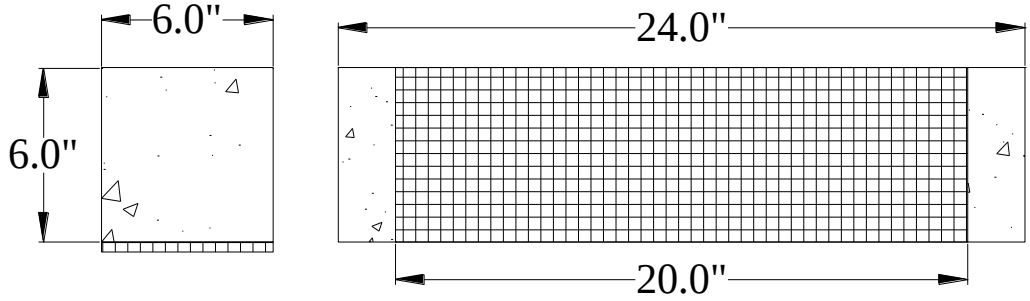

Figure 7. Small-scale Beam Specimen Details

The CFRP laminate was applied to small-scale specimens in 3 groups. This was done to ensure adequate working time of the PU base primer and pre-preg laminate. In order to reduce the time required for lay-up, specimen were clamped together in groups of two and laminated with a single 12" wide layer of CFRP. The seam between specimens was filled with a small continuous bead of silicone caulk to prevent leakage of base primer between beams. The caulk was allowed to set for 45min prior to beginning lay-up procedures. The following procedure was followed to apply the Aquawrap CFRP to the surface of small-scale beams:

1) The concrete surface was brushed with a steel-wire brush to remove any loose particle matter.
2) The brushed surface was then cleaned with acetone to remove any residual chemicals or fine particles
3) The tension soffit of each beam was then marked to identify the location of the applied laminate.
4) Two beams were then placed side-by-side and secured tightly with a clamp.
5) The seam between beams was then filled with caulk to prevent the urethane primer from leaking between beams. The caulk was allowed to dry for 45 min before proceeding.
6) A can of BP-1 Aquawrap primer Part B was then mixed into a can of BP-1 Part A and mixed by hand for approximately 3min.
7) A thin layer of primer was applied to the tension face of each set of beams with a paint roller and was allowed to become tacky for proceeding.

8) The Aquawrap CFRP was then removed from its sealed package and cut into 20” long sheets.
9) Sheets were then misted with water and depressed into the tension face of each beam-set with an FRP roller.
10) Applied sheets were rolled for 20min to ensure minimal formation of voids between CFRP and concrete.

Specimens were left undisturbed for 24 hours to allow for proper curing of the CFRP laminate. After 24 hours, clamps were removed and the laminate was cut along the specimen seam. To ensure a full cure of the CFRP laminate, specimens would not be exposed to conditioning environments for at least 7 days. It should be noted that the laminate length was altered prior to flexural tested to ensure that debonding failure would occur. That length was shortened from 20” to 12” by cutting that laminate with a small rotary tool.

3.3 Large-scale Beam Specimens

3.3.1 Beam Design

Large-scale concrete beam were cast at the FDOT Structural Research Center (SRC) in Tallahassee, FL. Beams were poured in eight separate batches with two beams per batch. Standard 6" x 12" compression cylinders were cast and tested according to ASTM Standard C39 for each batch. Details regarding the concrete mix used for large-scale beam specimens can be found in Table 10. Consecutive batches were poured a minimum of seven days apart allowing all beams to cure undisturbed in the forms. Refer to Table 11 for the pour dates, batch numbers, and the compressive strength results from seven and twenty-eight day test cylinders. After seven days of curing, beams were removed from the forms and stored outdoors at the SRC for further curing. As noted in Table 11, beams 13 and 14 were damaged during handling. These beams were not incorporated in the study.

Table 10. Large-scale Beam Concrete Mix Details

Cement Type:	Class II
Target Slump:	3in
Minimum f '$_c$:	4,500 psi
Max Water to Cement Ratio:	0.44
Minimum Cementitious Material:	611lb/yd^3
Air Content Range:	1% - 6%

Table 11. Large-scale Beam Concrete Details

Batch No.	Pour Date	Beam ID	Compressive Strength (psi)	
			7 Day	28 Day
1	5/11/2005	1 & 2	3205	5149
2	5/18/2005	3 & 4	4830	7397
3	6/1/2005	5 & 6	5105	7121
4	6/8/2005	7 & 8	4656	6773
5	6/15/2005	9 & 10	4249	6396
6	6/22/2005	11 & 12	5018	7440
7	6/29/2005	13[1,2,3] & 14[1,2,3]	2335	3872
8	8/31/2005	15[2] & 16	4598	7498

[1]Under Strength [2]Damaged [3]Excluded

Beam reinforcement cages were comprised of three longitudinal No. 7 deformed steel bars for tensile reinforcement (reinforcement ratio of 1.0%) and No. 3 bars for compression and shear reinforcement. It was experimentally determined that the yielding strength and ultimate strength for reinforcing steel was 74.8ksi and 110ksi respectively. A design schematic for the beams cast can be found in Figure 8.

Figure 8.

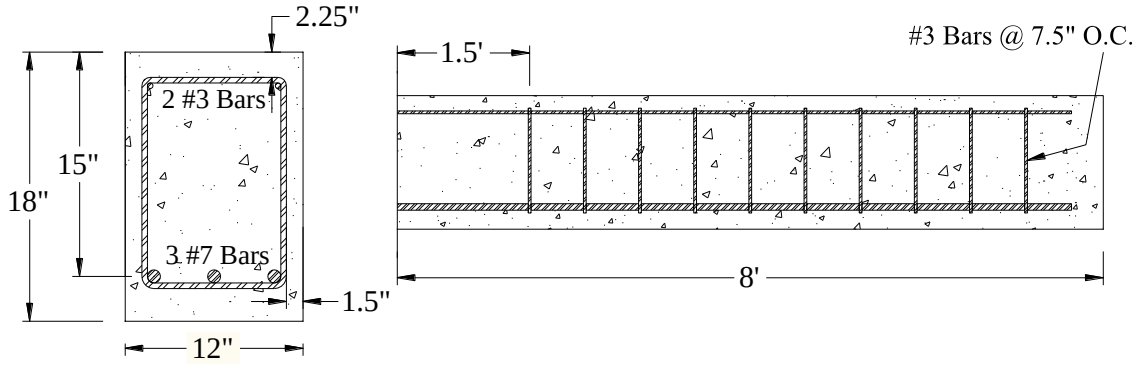

Figure 8. Beam Dimensions and Reinforcing Details

3.3.2 Specimen Preparation

Of the 14 beams used for experimental testing, 12 beams were strengthened with two layers of CFRP fabric. For this portion of the study, there were 3 CFRP systems used to strengthen beams; the PU1, EP1, and the EP2 systems. For each composite system there was a set of 4 beams strengthened. Prior to applying the CFRP laminate, the tension soffit of each beam was cleaned to ensure the surface was free of grit and other particles. For all resin systems, the composite laminate was applied to the tension face of the beams using a hand lay-up process; beams were positioned tension face up during the application process. In all cases, the CFRP laminate was applied to the full width of the tension soffit. The first layer and second layers of CFRP measured lengths of 14’4” and 13’10” respectively. This lay-up configuration results in a staggered bond-end to reduce an abrupt change in stiffness (Figure 9).

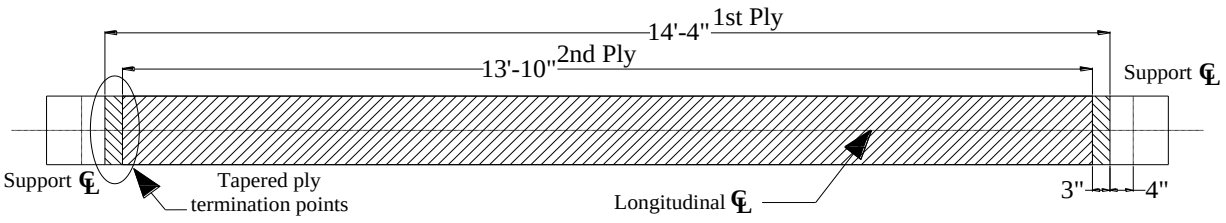

Figure 9. Laminate Lay-up Diagram

The CFRP laminates utilizing epoxy (EP1 and EP2) matrices were both installed using the same wet lay-up process. First, a thick coat of resin was applied to the prepared tension soffit in order to prime the concrete surface for adhesion; the resin primer coat was the same epoxy resin used to impregnate the fibers. The first dry fiber sheet was then laid down and depressed into the resin with an FRP roller. A saturating layer of resin was then applied to the fiber and impregnation was achieved using a FRP roller. This process was repeated for the second layer of fabric applied to complete the laminate installation. It should be mentioned that during the installation of the CFRP laminate that utilized the EP2 resin system, there were some issues encountered regarding premature gelling of the epoxy resin. This problem was mitigated by mixing new resin and reapplying new fabric. Although this solution was effective, it most likely led to some interlaminar and CFRP-to-concrete interface discontinuities in bond.

Unlike the epoxy systems that used the same resin to both bond and impregnate the fiber, the PU1 system utilized a separate two-part base primer to promote adhesion to the concrete surface. Hence, prior to installation of the PU1 system strengthened beams, the concrete tension surface was coated with a thin layer of the Air-Logistics BP-1 polyurethane base primer. Once the base primer became tacky, the pre-impregnated Aquawrap fabric was removed from its sealed package and applied to the beam. During the lay-up process, the laminate was misted with water using spray bottles to initialize matrix hardening. After the installation process, the fabric was rolled every 10 minutes with FRP rollers to push out air bubbles. During the installation process of the PU system, a representative from the Air-Logistics Company was present to provide assistance and ensure proper installation procedures were followed. Photos taken during installation can be found in Figure 10.

After the installation of CFRP on the beams, all specimens were left undisturbed for at least 24 hours to allow proper curing of the bonded CFRP sheets. After the laminate was allowed sufficient cure time, a class V finish (FDOT classification for a coating that withstands cracking under the thermal and elastic expansion ranges of the substrate) was applied to the exposed face of the CFRP sheet.

One beam specimen was dedicated for the use of performing direct bond pull-off testing according to ASTM D4541. A small 2-layer patch of CFRP laminate, one patch per CFRP system, was applied to the beam in the same manner as described previous.

(a) Preparing Adhesive Primer

(b) Primed Concrete Surface

(c) Rolling CFRP Laminate

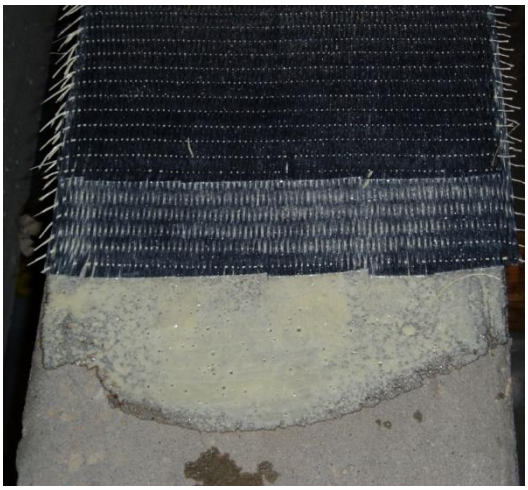

(d) CFRP Termination Point

Figure 10. PU1 CFRP Installation

4. TEST METHODS & EVALUATION PROCEDURES

4.1 Small-scale Specimens

4.1.1 Conditioning Environments

The following section discusses the procedures and environments used to environmentally condition small-scale beam specimens, composite plates and concrete cylinders. Five conditioning environments, considered to be critical for civil infrastructure, were selected: H_2O, high pH, seawater, dry heat, and ambient environment/UV. During the conditioning periods, all environments were monitored to ensure the quality of the conditioning was uniform for specimens. Conditioning periods for all specimens were not initiated on the same day. Table 12 provides a log of start dates and duration dates for all environments and conditioning periods.

Table 12. Conditioning Dates

Exposure Time (days)	Dry Heat	Roof	H20		Seawater		Concrete Leachate	
			Group 1	*Group 2*	*Group 1*	*Group 2*	*Group 1*	*Group 2*
Start	10/15/09	10/15/09	10/19/09	10/20/09	10/20/09	10/21/09	10/30/09	11/4/09
30	11/13/09	11/13/09	11/17/09	11/18/09	11/18/09	11/19/09	11/28/09	12/3/09
60	12/13/09	12/13/09	12/17/09	12/18/09	12/18/09	12/19/09	12/28/09	1/2/10

4.1.1.1 H2O Conditioning Environment

The H_2O conditioning environment consisted of pure tap water (pH ≈ 8). During the conditioning period the H_2O tank was periodically emptied and re-filled to minimize leaching of concrete pore water.

4.1.1.2 Concrete Leachate Conditioning Environment

Research as shown that water absorbed into the micro-pores of concrete can chemically react with the cement paste and create a high pH (>12) solution. Therefore, it was determined that the polyurethane strengthening system under investigation be able to withstand such an environment. A high-pH concrete leactate solution was created by letting concrete specimens and cylinders soak in H_2O while monitoring solution pH. pH was measured using a hand held Extech PH60 pH/temperature pen. Prior to taking measurements, the pen was calibrated using a two-point pH7 buffer and pH-10 buffer calibration. A plot of pH vs. time can be seen in Figure 11. The pH of the leachate solution reached a steady-state valve of approximately pH ≈ 12. A photo of the concrete leachate conditioning environment can be seen in Figure 12.

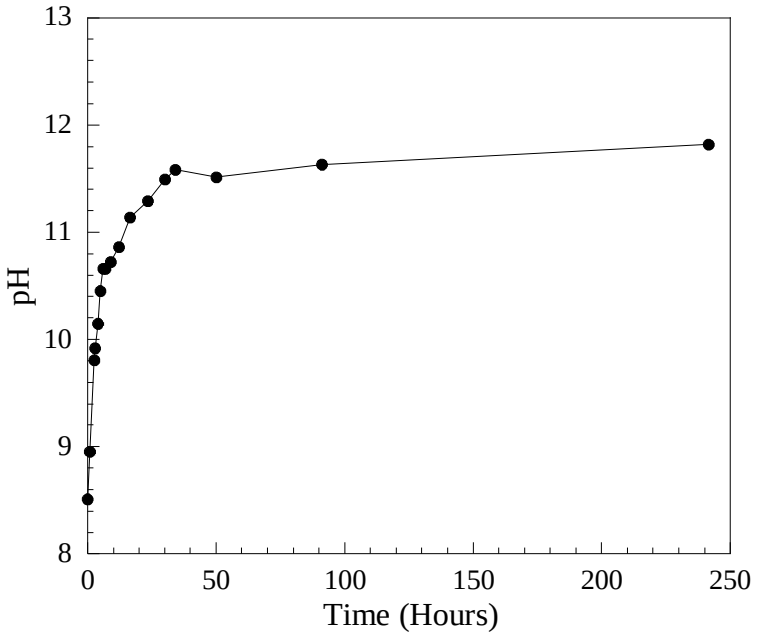

Figure 11. Concrete Lecheate Solution pH Measurements

Figure 12. Concrete Leachate Conditioning Environment

4.1.1.3 Seawater Conditioning Environment

A synthetic seawater solution was created used *Instant Ocean ® Sea salt*. The dry salt material was mixed according to manufactures recommendations: approximately 1.5lb of salt with 5 gallons of water. The water used to create the salt solution was normal tap water. The pH of the tap water was measured prior to mixing in salt material; a pH of approximately 8 was measured. During the conditioning period, pH of the seawater solution was measured once a week. It was determined that the pH of the solution reached a steady-state value of approximately pH ≈ 10. Furthermore, during conditioning the seawater solution was changed every 2 – 4 weeks.

4.1.1.4 Dry Heat Conditioning Environment

In order to provide constant and continuous dry heat, specimens were placed in a Blue M 146 Series industrial oven (refer to Figure 13 and Figure 14). A schematic of specimen location within the oven can be found in Figure 15. The oven temperate was set at 120 °F. During the first week of conditioning, oven internal, specimen concrete, and CFRP temperatures were monitored with a Westword 2ZB46 laser temperature measurement device to determine whether steady-state operation was being achieved. It was determined that the oven was not producing a steady-state environment due to overheating. In order to achieve steady-state operation, the oven's exhaust was adjusted until the internal temperature of the oven stabilized. Temperature measurement prior to and once steady-state operation was achieved can be found in Table 13/Table 14 and Table 15/Table 16 respectively. The average concrete and CFRP surface temperatures (steady-state) were determined to be 126.2 °F and 126.1°F respectively.

Figure 13. Dry Heat Oven

Figure 14. Specimens During Conditioning

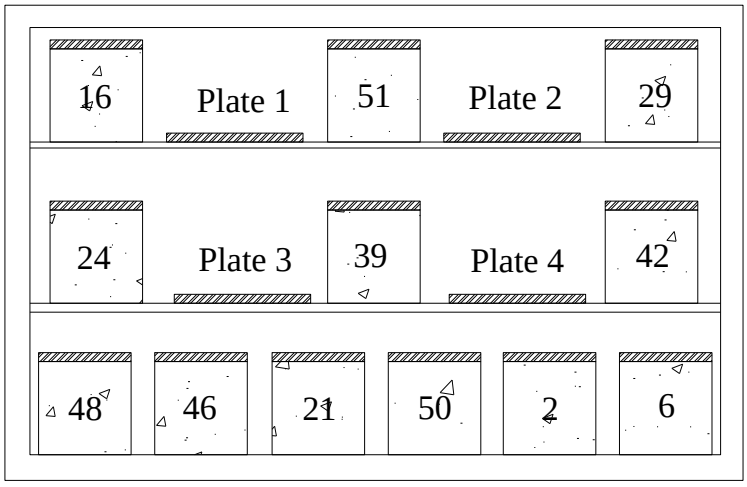

Figure 15. Specimen Locations within Dry Heat Oven

Table 13. Beam Specimen Dry Heat Oven Temperature Measurements: Prior to Steady State Operation

Measurements Taken: 10/18/2009 Before Steady-State Temperature operation		
Beam No.	CFRP Surface Temperature (F)	Concrete Temperature (F)
2	116.6	118.3
6	117.3	117.1
50	115.5	118.1
21	118	114
46	115	114
48	118.1	117
42	120.6	120.6
39	123.6	123.1
24	120.8	120.8
16	122.1	121.5
51	121.9	121.5
29	125.9	120
Average	119.6	118.8
Standard Dev.	3.39	2.93
C.O.V.	0.028	0.025

Table 14. Plate Dry Heat Oven Temperature Measurements: Prior to Steady State Operation

Measurements Taken: 10/18/2009	
Plate No.	Temperature (F)
1	124.1
2	128.5
3	123.6
4	125
Average	125.3
Standard Dev.	2.21
C.O.V.	0.018

Table 15. Beam Specimen Dry Heat Oven Temperature Measurements: Steady State Operation

Measurements Taken: 11/5/2009 After Steady-State Temperature operation		
Beam No.	CFRP Surface Temperature (F)	Concrete Temperature (F)
2	124.5	124.8
6	124.6	123.9
50	128.4	127.6
21	125.6	125.6
46	126.8	126.4
48	125.6	126.3
42	127.8	128.2
39	125.7	125.9
24	124.6	125.9
16	125.6	125.7
51	126	126.3
29	127.8	127.8
Average	126.1	126.2
Standard Dev.	1.33	1.23
C.O.V.	0.011	0.010

Table 16. Plate Dry Heat Oven Temperature Measurements: Steady State Operation

Measurements Taken: 11/5/2009	
Plate No.	Temperature (F)
1	127.5
2	127.3
3	127.5
4	127.1
Average	127.4
Standard Dev.	0.19
C.O.V.	0.002

4.1.1.5 Ambient Outdoor Conditioning Environment

The ambient outdoor conditioning environment was completely uncontrolled. Specimens were placed laminate-face up on the rooftop of the University of Central Florida's Engineering Building II (Figure 16). During the period in which specimens were conditioning, whether data was collected from the National Oceanic and Atmospheric Administration's (NOAA) online database. Figure 17 depicts the daily maximum, minimum, and average temperature measures collected for the Orlando area. Figure 18 shows a graphical representation of the precipitation recorded for the conditioning period.

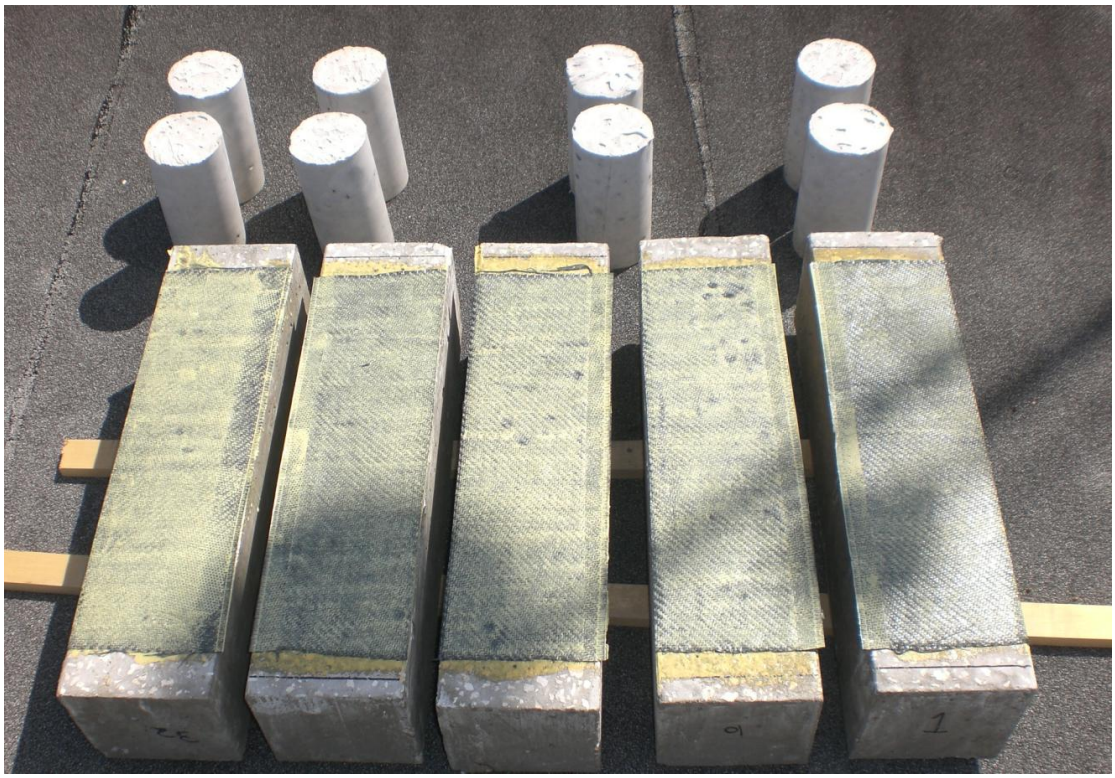

Figure 16. Ambient Environment Specimens on the Roof

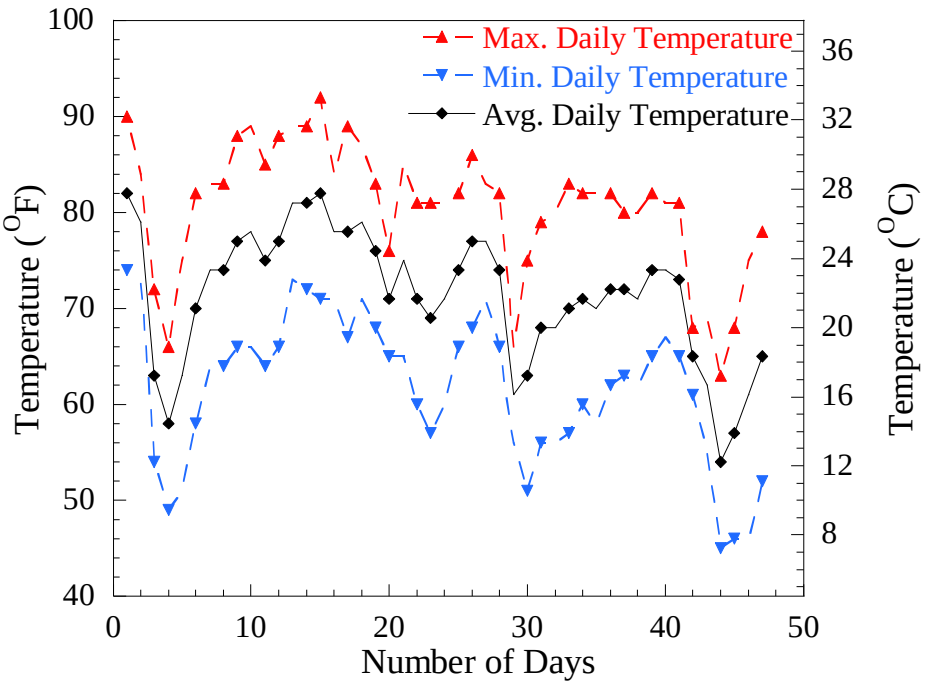

Figure 17. Orlando Temperature Measurements

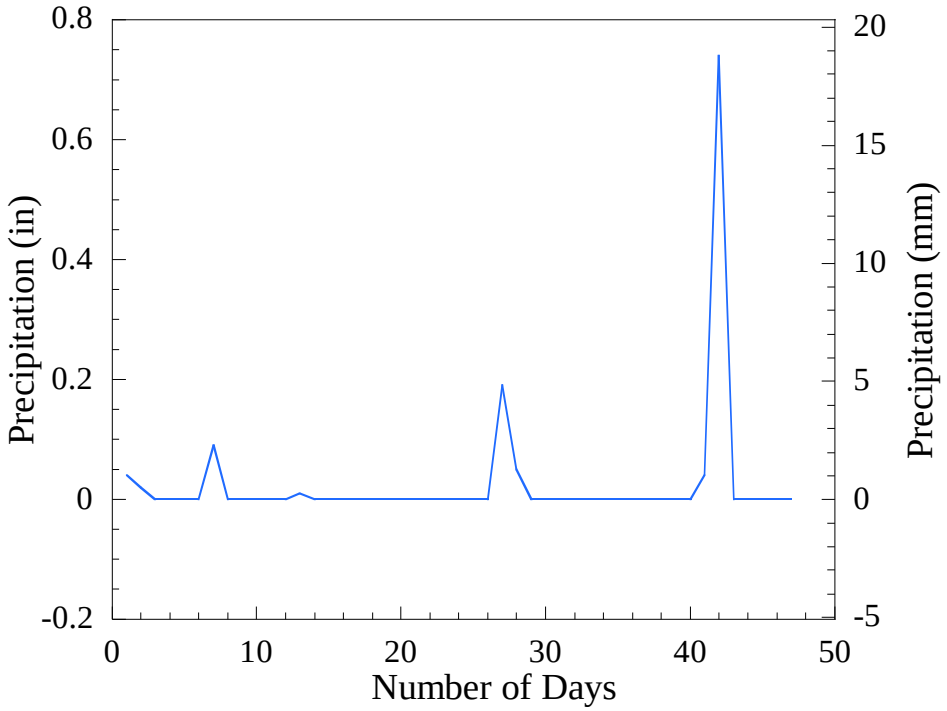

Figure 18. Orlando Precipitation Measurements

4.1.2 Test Set-up and Instrumentation

Once the conditioning period was completed for beam specimens, they were prepped for flexural testing. The sides of all beam specimens were painted white such that cracks would be easily identified during and after testing. A single 120 Ohm resistive foil-backed strain gage was installed at the mid-span of the CFRP laminate. Gages were applied using X60 two-part strain gauge adhesive.

Flexural testing of specimens was completed on a Satec 200kip universal testing machine (UTM). All specimens were loaded at a rate $0.1^{in}/_{min}$ in a 4-point bending configuration with a shear span of 8 inches (refer to Figure 19). During loading, Instron Partner software continuously recorded load and table displacement directly from the UTM. A National Instruments data acquisition system was also set-up to record load, strain, and displacement during testing. Displacement measurements were taken at the mid-span of specimens using two Duncan 9600 series LVDTs. Photographs taken during testing can be found in Figure 20.

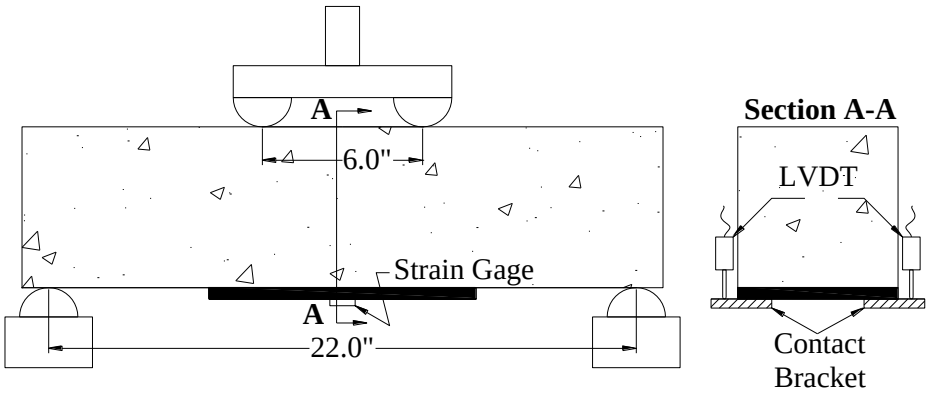

Figure 19. Small-scale Beam Flexure Test Set-up

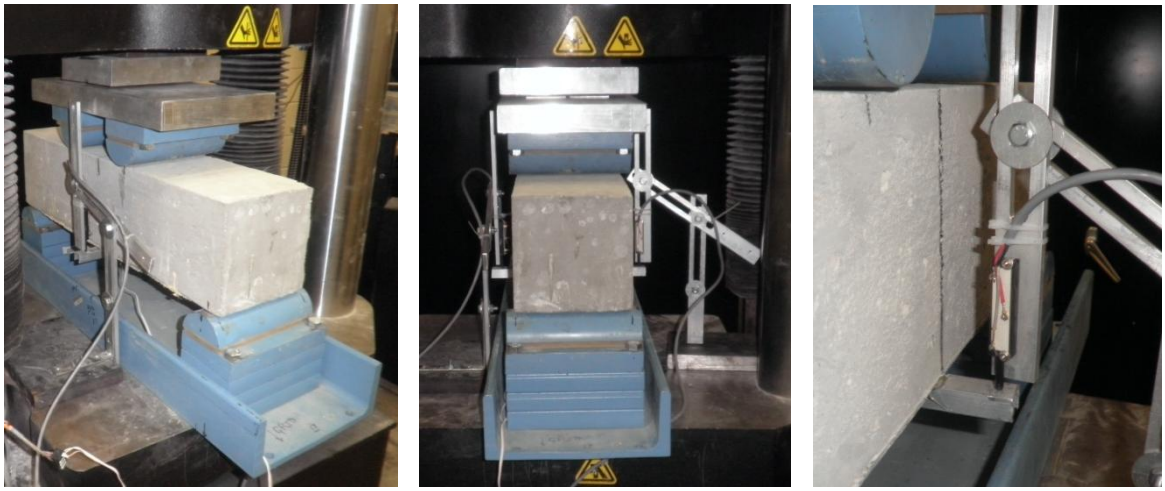

Side View **Front View** **LVDT**

Figure 20. Small-Scale Beam Test Set-up

4.2 Large-scale Beam Specimens

The 12 CFRP strengthened beams were exposed to cyclic loading, environmental conditioning, a combination of cyclic loading and environmental conditioning, and monotonic loading until failure. The following section describes the details and procedures used for experimental testing. Specimens were identified by the composite system used for strengthening and the type of conditioning in which the specimen was exposed. Exposure to cyclic loading and/or environmental conditioning is denoted with an “C” and/or “E”. For example, a polyurethane composite strengthened beam exposed to both cyclic loading and environmental conditioning would be identified as “PU-C-E”.

The first group of specimens to be tested was the strengthened baseline specimens and the unstrengthened control beam. These specimens were not exposed to any type of conditioning. Upon completion of the ultimate loading on baseline specimens, the cyclic loading procedure commenced. During this time, specimens scheduled to receive both cyclic loading and cyclic/thermal conditioning were loaded. Upon completion of cyclic loading, cyclic-only specimens were loaded monotonically to failure. At this point, specimens to receive environmental conditioning were placed in a specially designed environmental chamber to begin conditioning.

4.2.1 Environmental Conditioning

The environmental conditioning phase of the experiment consisted of exposing the selected beams to heating and cooling cycles inside of an environmental conditioning chamber (ECC). Within the chamber, specimens were also exposed to cycling levels of humidity. The purpose of the temperature and humidity cycles was to simulate exposure of the beams to climate conditions similar to that of sub-tropical; typical of southeastern Asia and United States. The chamber was designed to achieve a temperature range between 32 – 130 °F, a maximum humidity of 100%, and to operate continuously. A design schematic of the ECC can be seen in Figure 21. The ECC utilized three main components to produce the desired environment:

1) *Temperature Conditioning Unit* – Temperature conditioning was provided by a 2 ton Goodman AC/Heating Unit (PCK 024-1 HK 50-1); a commercially available packaged unit capable of producing 24,000 Btuh.

2) *Humidifier* – A Honeywell HE160A By-Pass Disk Humidifier was used to provide humidification (commercially available).

3) *Cycle Controller* – A Watlow SD Series controller was used to control the environmental cycles for the chamber.

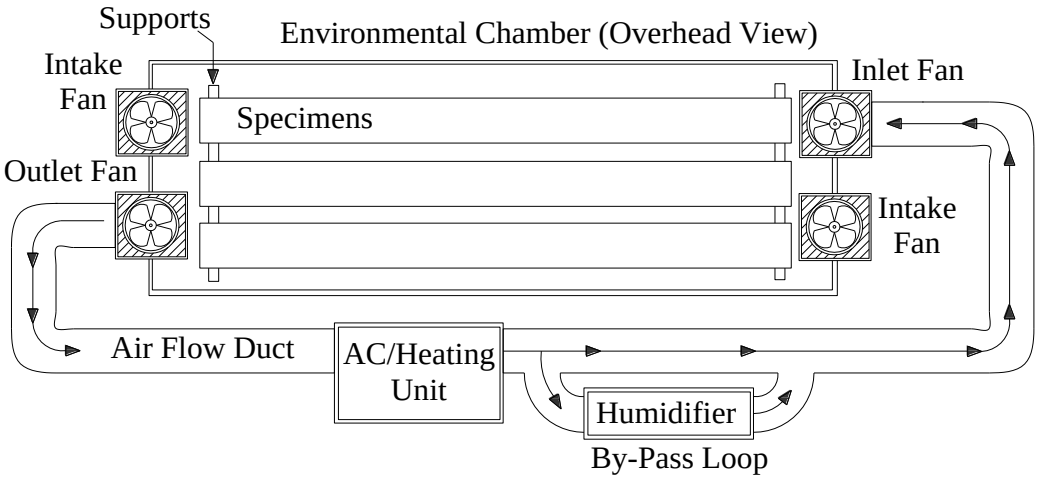

Figure 21. Environmental Conditioning Chamber

The conditioning procedure was comprised of 2 main phases; a heating (high humidity) phase followed by a cooling (low humidity) phase. A full heat-cool cycle took approximately 2 full days to reach completion and conditioned specimens were exposed to 100 full cycles. The thermal conditioning procedure entailed 4 main steps in order to complete a single heat-cool cycle:

1) *Heating/Humidity Ramp-up Period* – The first step in the full cycle was heating and humidification. During this cycle, both the AC unit (heat) and humidifier would be engaged and flow would be introduced into the chamber through the input fan. It was determined that the average input air temperature was approximately 126 °F. The duration of the ramp-up heating cycle was 18hr.

2) *Heat Soak Period* – The second step was a heat soak process. During this phase, it was attempted to maintain the chamber temperature for a duration of 6hr. Exhaust fan were engaged at the conclusion of the heat soak period, expelling air volume, and beginning the cool ramp period.

3) *Cooling Ramp-up Period* – The cooling ramp-up period is similar to the heating/humidity but the AC unit is engaged to provide cold air. It was determined that average input air temperature, for this period, was approximately 39 °F. The cooling ramp-up period lasted for 18hr.

4) *Cool Soak Period* – During this phase, it was attempted to maintain the chamber temperature for a duration of 6hr. Exhaust fan were engaged at the conclusion of the cool soak period, expelling air volume, and beginning the heat/humidity ramp period and completing the full conditioning cycle.

To measure the thermal performance of the conditioning chamber, thermocouples (type-K) were installed on the tension surface of each beam specimen during conditioning, on the top and bottom of the chamber, and outside the chamber (ambient). Temperature and humidity data was acquired continuously during the conditioning period. A multi-day sample of temperature data can be found in Figure 22. It can be observed that the chamber produced internal ambient temperatures between 40 and 115°F and beam surface temperatures between 55 and 100°F. The humidity range achieved was between 19% and 89%.

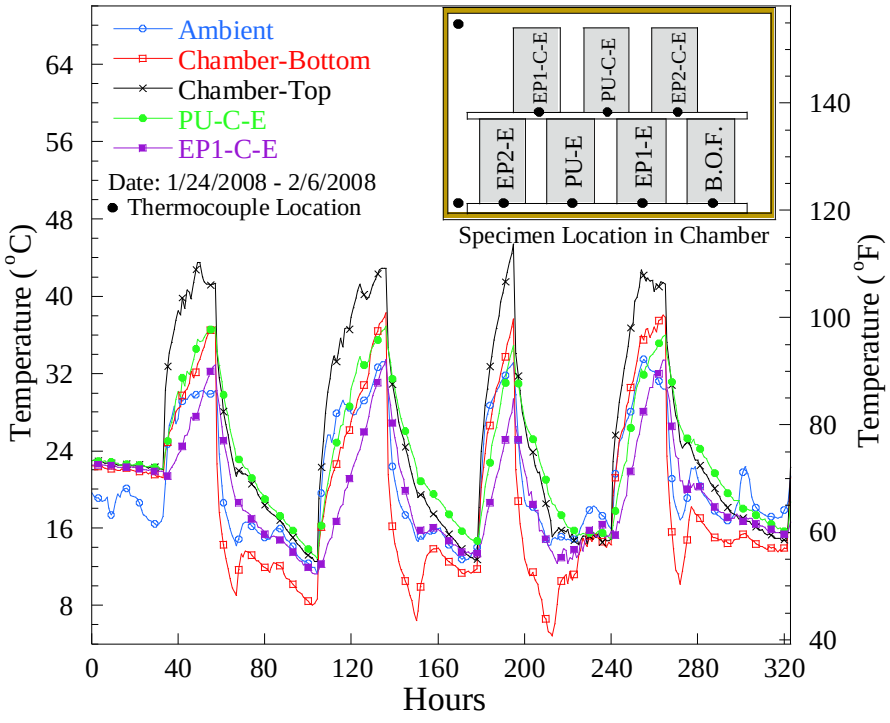

Figure 22. Conditioning Chamber Sample Data

Two important considerations must be taken into account when interpreting the continuity and control of the conditioning process. First, during the time frame in which specimens were being conditioned, the conditioning chamber had intermittent malfunctions with critical components. Therefore, controlled environmental conditioning was not continuous throughout the conditioning portion of this study. Second, all of the beams received some level of uncontrolled ambient environmental conditioning due to the fact that the beams were stored outdoors of the FDOT Structures Research Center (SRC). The beams also received some thermal conditioning when inside of the SRC due to the fact that the facility does not have a climate control system for the testing area. Figure 23 and Figure 24 depict the average monthly precipitation and monthly air temperatures for the duration of time specimens were stored outdoors at the SRC. The temperature and precipitation data was taken from the National Oceanic and Atmospheric Administration (NOAA) archives for the Tallahassee Regional Airport. Although there is a relatively accurate record of the environmental conditions that occurred during the length of this study, there is no way to fully quantify the effect that the ambient environment had on test specimens.

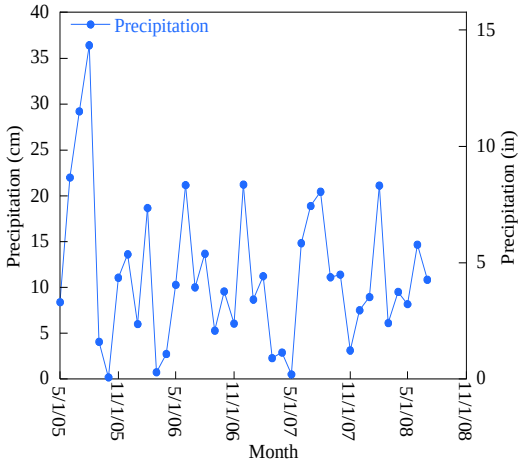

Figure 23. Tallahassee Precipitation Data

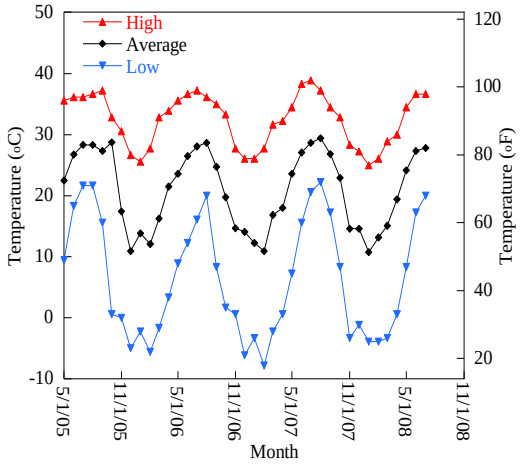

Figure 24.Tallahassee Temperature Data

4.2.2 Mechanical Loading and Data Acquisition

All specimens were loaded using a four-point bending configuration. This configuration was used for both ultimate and cyclic tests that were performed. The supported length for all specimens was 15'; beam supports allowed for rotation. All loading was applied using a 3' spreader beam. During load testing (cyclic and ultimate), steel reinforced neoprene bearing pads were used between load bearing surfaces. All specimens were instrumented with foil-backed resistance strain gauges covered with an environmental coating to protect the gauge. During testing, displacement was measured using either linear variable differential transducers (LVDT) or laser displacement gauges. Displacement measures were taken at both mid-span and support locations. A schematic of gage locations and loading configuration can be found in Figure 25. A photo taken during actual load testing can be found in Figure 26.

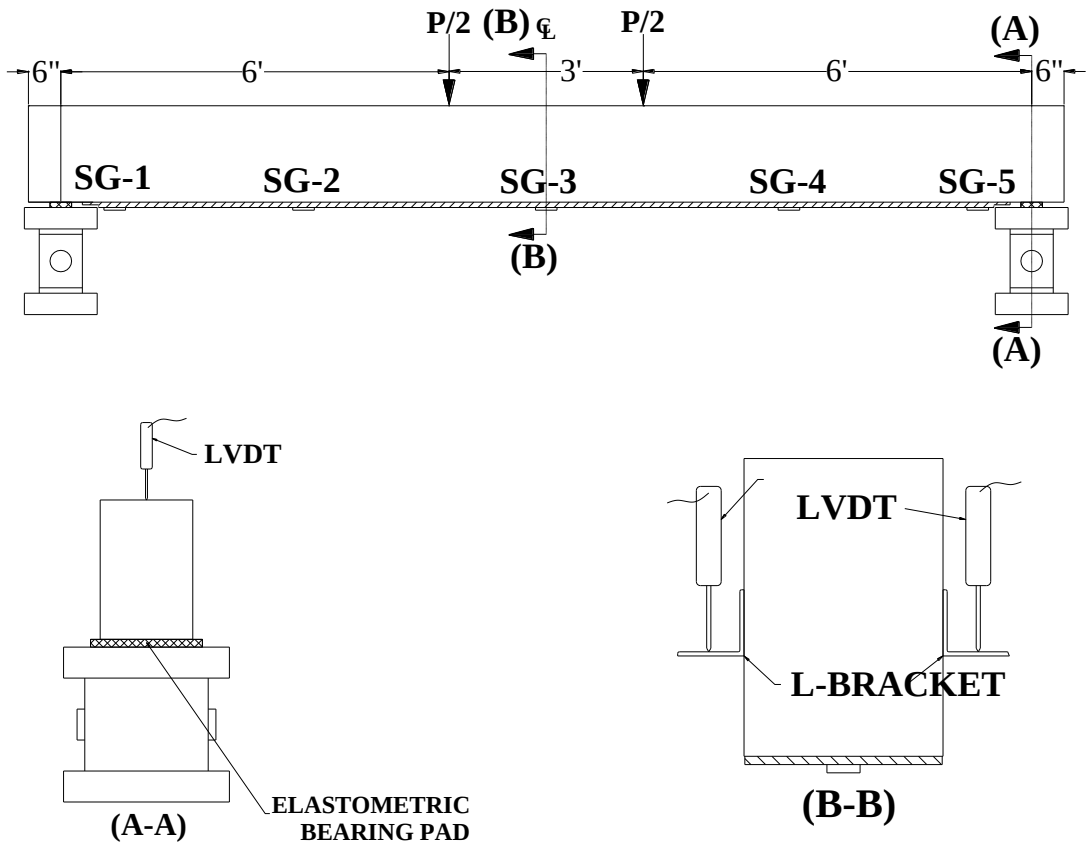

Figure 25. Gage Locations and Loading Configuration

Figure 26. Load Testing

4.2.2.1 Cyclic Loading

The cyclic loading phase of the experiment consisted of subjecting the appropriate specimens to two million cycles of repeated loading at a frequency of 2Hz and a load range of 0.5 kip to 19.2 kip, which induced a calculated change in stress of 23ksi in the tension reinforcement. The load was applied using an MTS servo-controlled actuator. During cycling, load was applied such that the load range remained constant regardless of any reduction in member stiffness. The load level was selected such that tension steel would not yield and such that the stress range within the tension reinforcement would allow for an unlimited fatigue life. During loading the beam displacement and CFRP strains were measured. The strain gauges were calibrated to compensate for the temperature changes that occurred in the lab during the two million cycles. During the cyclic load tests, data was recorded on cycles 1, 1000, 20,000, 100,000 and every 100,000 thereafter until cycle 2 million. The data types recorded were the maximum and minimum of load, displacement, beam temperature, and longitudinal CFRP strains.

4.2.2.2 Monotonic Loading

The ultimate testing phase consisted of loading the specimen until failure. Failure was defined as a drop of at least 50% from the maximum load resisted by the specimen. The loading for the ultimate phase used displacement control to maintain control of the actuator movement during testing. The tests were performed at a rate of 0.1in/min. Load was applied with either an MTS servo-controlled actuator or an Enerpac hydraulic jack. During the ultimate loading procedure, pauses were taken at various points during tests to mark cracks.

4.3 Scanning Electron Microscopy

Scanning electron microscopy (SEM) was used to evaluate whether degradation was occurring at the fiber/matrix integration level. Numerous CFRP laminates samples were taken from small-scale and large-scale beam specimens including samples taken from specimens after 4-pt bending failure. Figure 27 shows a photo of the CFRP samples taken from small-scale beam specimens to be viewed in the SEM.

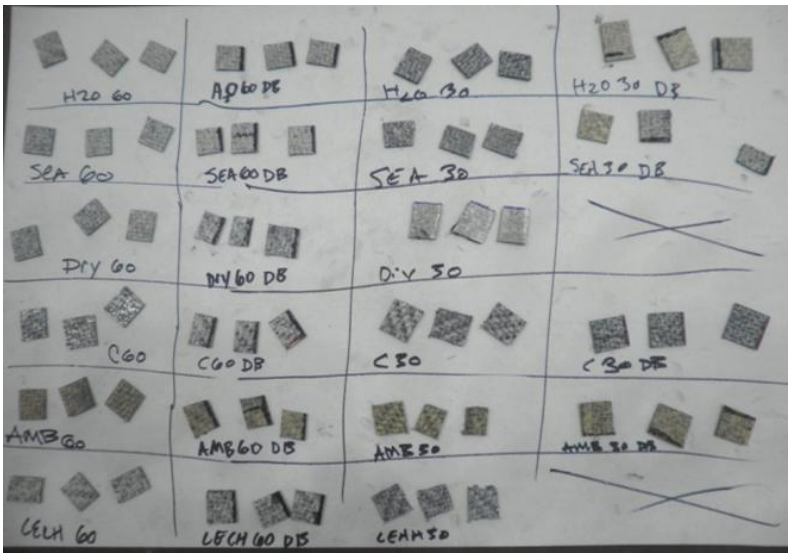

Figure 27. SEM Samples

The scanning electron microscopy (SEM) investigation was performed at the Materials Characterization Facility (MCF), which is a part of the Advanced Materials Processing and Analysis Center (AMPAC), at UCF. High quality images were captured using a Hitachi S-3500N scanning electron microscope (Figure 28). Two primary analysis modes were utilized; the secondary electron detection imaging mode and X-ray energy dispersive spectroscopy. An electron accelerating voltage ranging from 15-20kV was used for all analysis.

Prior to loading CFRP samples in the SEM, all samples were sputter coated with a 1-2A layer of gold palladium (AuPd). This process was utilized to make samples electrically conductive such that they could be viewed in the SEM. The coating device can be seen in Figure 29.

Figure 28. Hitachi S-3500N SEM

Figure 29. Plasma Sputter Coating Machine

5. RESULTS

5.1 Short-term Durability Tests

Prior to testing, small-scale beams were allowed to rest from their respective conditioning environments for at least a week. During this time frame foil backed strain gages were mounted and the specimens were marked for testing. Table 17 indicates the dates in which specimens were removed from respective environments. The following section presents key results from SEM, material tensile tests, and flexural test. Other critical numerical results and photos from tests can be found in the appendix.

Table 17. Conditioning Pull Dates

Exposure Time (days)	H20	LECH	SEA	DRY	AMB
30	11/17/2009	11/29/2009	11/18/2009	11/12/2009	11/12/2009
60	12/16/2009	12/27/2009	12/20/2009	12/14/2009	12/14/2009

5.1.1 Unconditioned Specimens

Initial observations made from SEM micrographs of the unconditioned CFRP laminate indicates good bond between carbon fibers and the surrounding urethane matrix (refer to Figure 30). It was also observed that a significant number of micro-void (Figure 31) existed at the surface of the urethane matrix. This result was confirmed by the manufacturer of the composite system and other research. Micro-voids form during the matrix curing process as CO_2 is released from the urethane matrix.

Unconditioned small-scale beam specimens were tested 12/28/09. Concrete strength for the day of test was experimental determined to be 7897 psi. After testing specimen C-30-3, it was determined that the bonded laminate length was too long for debonding failure to occur. The bond length of the laminate was shortened by 4" to ensure that failure would be caused by debonding. Specimens C-30-1 and C-30-2 both failed via debonding. Load-deflection curves for specimens C-30-1 and C-30-2 can be found in Figure 32. During loading specimens behaved linear-elastic until crack initiation near mid-span. At cracking a significant drop in load was observed followed by a second region of linear-elastic behavior. After loading it was determined that debonding failure occurred within the adhesive layer bonding the laminate to concrete.

The C-60 specimens were load tested on 2/7/2010. Concrete strength for the day of test was experimental determined to be 7936 psi. Behavior similar to that of the C-30 specimens was observed. The load-deflection behavior for C-60 specimens can be found in Figure 33. All C-60 specimens failed via debonding that occurred within that adhesive layer.

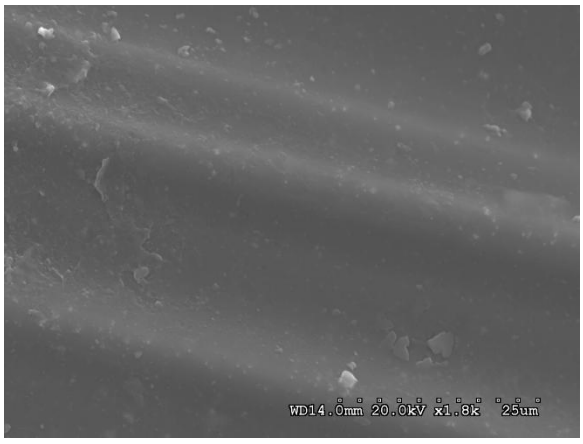

Figure 30. Unconditioned Fibers

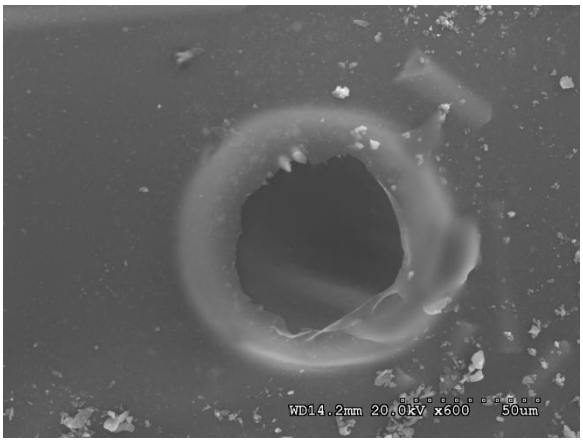

Figure 31. Unconditioned Matrix Void

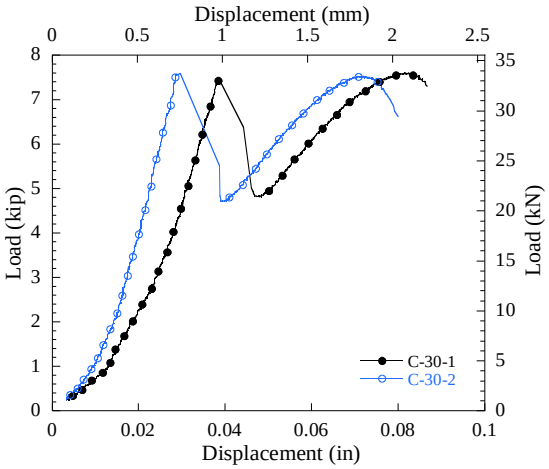

Figure 32. 30 Day Control Load-Deflection Plot

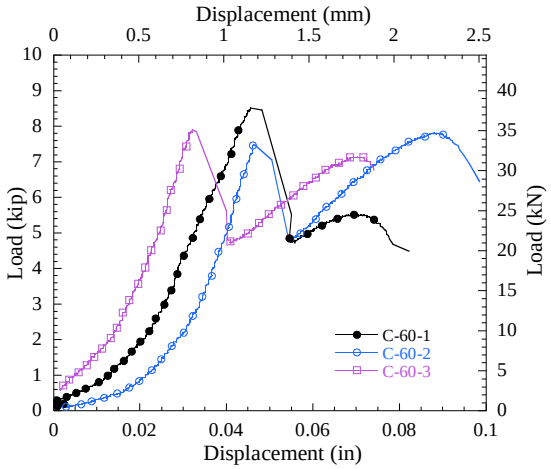

Figure 33. 60 Day Control Load-Deflection Plot

After flexural testing, portions of the debonded CFRP laminate were removed from the unconditioned beam specimens to be inspected with SEM. Although there were areas found where matrix micro-cracking was observed (Figure 35), there was no significant damage observed at the fiber/matrix level (Figure 34). Matrix cracks were not found to bridge between adjacent fibers or voids.

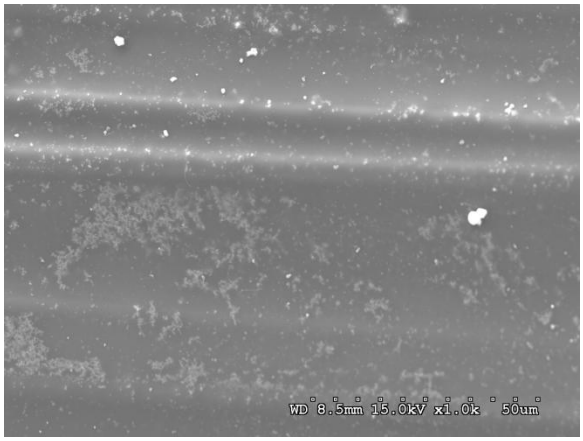

Figure 34. Fibers After Debonding

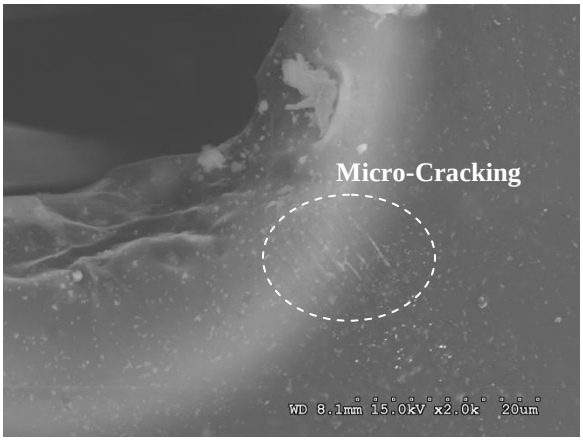

Figure 35. Matrix Void After Debonding

5.1.2 H2O Conditioned Specimens

SEM micrographs of CFRP samples taken from beams exposed to 30 and 60 days of an H_2O solution prior to testing can be seen in Figure 36 and Figure 37. Laminate samples exposed to a 30 day conditioning period showed no signs of fiber or matrix distress. This was not the case with 60 day conditioning samples. There were multiple locations where bond degradation was observed to have occurred between reinforcing fibers and the urethane matrix. There were no signs of distress observed at or around matrix void locations.

Tensile test results for elastic modulus and ultimate strength can be seen in Figure 38 and Figure 39 respectively. Plots reflect degradation of material properties with respect to duration of environmental exposure; error bars shown depict a single standard deviation. The number of coupons tested for 30 and 60 day test was 8 and 7 coupons respectively. An increase in both tensile modulus and ultimate strength was observed for the 30 day tests. It is hypothesized that the initial increase is due to the fact that H_2O aids the curing reaction of the urethane matrix. Although an initial increase was observed, 60 day tests indicate decreases in both elastic modulus and ultimate strength by 14.3% and 10.3% respectively.

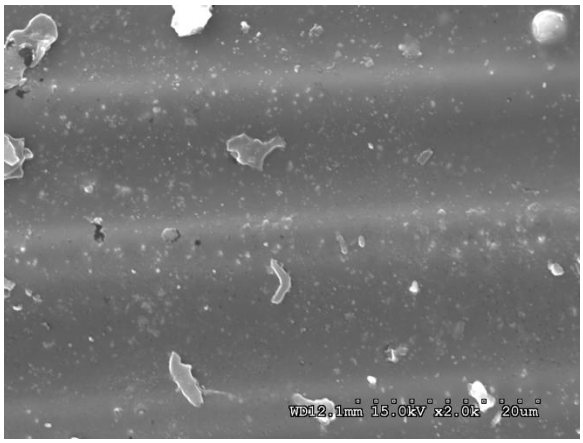

Figure 36. 30 Day H_20 Fibers

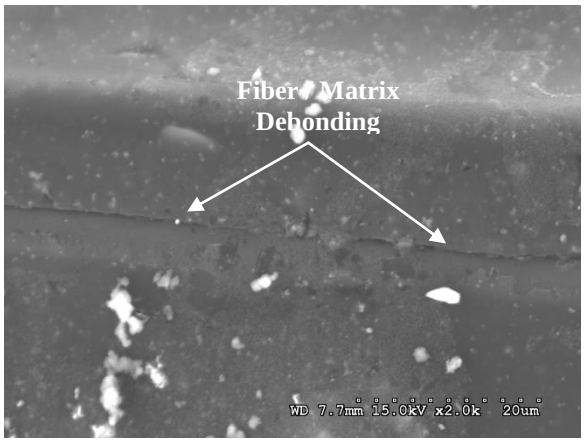

Figure 37. 60 Day H_20 Fibers

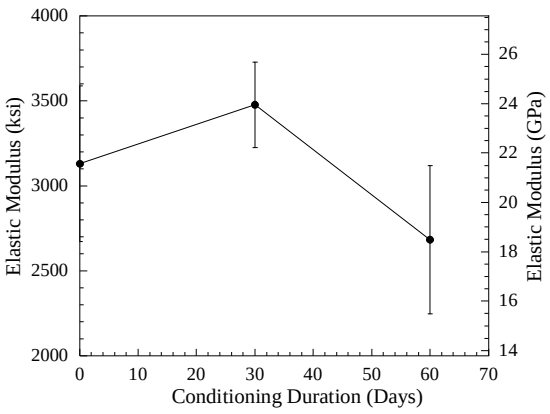

Figure 38. H_2O Elastic Modulus Degradation Plot

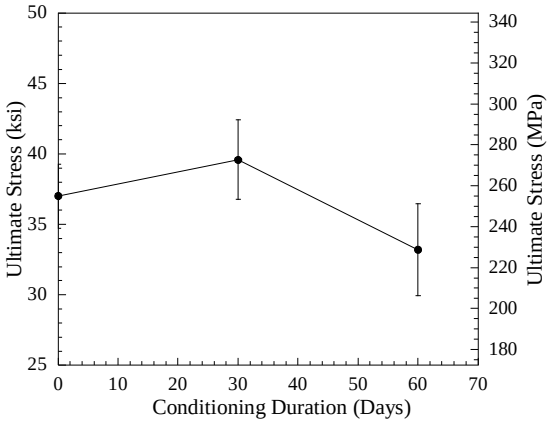

Figure 39. H_2O Ultimate Strength Degradation Plot

30 day beam specimens where tested on 12/28/09. Conditioned concrete strength for the day of test was experimental determined to be 7683psi. A plot of the load deflection behavior of 30 day specimens can be found in Figure 40. All H_2O-30 beam specimens failed via laminate debonding. Similar to the unconditioned specimens, it was determined that debonding failure occurred within the adhesive layer for all specimens.

60 day beam specimens where tested on 2/6/10. Conditioned concrete strength for the day of test was experimental determined to be 7810psi. A plot of the load deflection behavior of 60 day specimens can be found in Figure 41. Specimens H_2O-60-2 and 3 both failed via debonding (within the adhesive layer) similar to that of the unconditioned specimens. The H_2O-60-1 did not however fail by laminate debonding. Failure in the H_2O-60-1 specimen was caused by initiation of a flexural crack outside of that laminate region. The first load drop depicted in Figure 41 for specimen H_2O-60-1 correlates with a flexural crack that originated at mid-span.

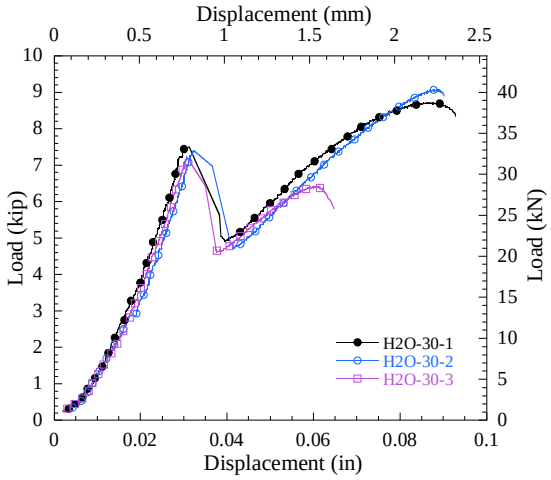

Figure 40. 30 Day H2O Load-Deflection Plot

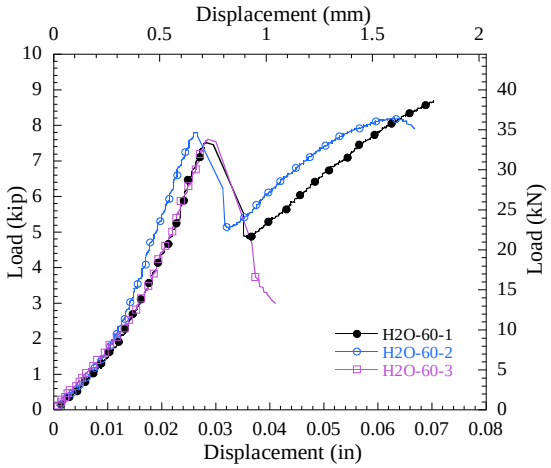

Figure 41. 60 Day H_2O Load-Deflection Plot

The load bearing capacity at cracking and ultimate are plotted verse duration of H_2O conditioning in Figure 42. Load at cracking tends to remain stable with increase in conditioning period; approximately a 1% increase in load at cracking for 60 days of H_2O exposure. Stability of the cracking load is more than likely due to the increase in concrete strength and slight decrease of the CFRP elastic modulus. After 60 days of conditioning, the average ultimate load bearing capacity of specimens was found to increase by 11.6% compared to control specimens. Indicating minimal degradation to bond caused by H_2O exposure.

Figure 43 depicts a plot of pre- and post-cracking flexural stiffness verses conditioning period. A consistent increase can be observed in the average pre-cracking flexural stiffness. Furthermore, little scatter was found to occur in both pre- and post-cracking stiffness specimens. The post-cracking stiffness mainly indicates the contribution of CFRP to the flexural response of the specimen. It was observed that at 60 days of conditioning that average flexural stiffness of specimens decreased by 8%. This result is in correlation with the slight degradation observed to occur in conditioned tensile coupons (refer to Figure 38).

The average ultimate deflection of specimens verses duration of conditioning can be found in Figure 44. There is an obvious trend in the data that indicates an inverse relationship between duration of conditioning and ultimate deflection. That is, as the duration of conditioning increases the average ultimate deflection decreases.

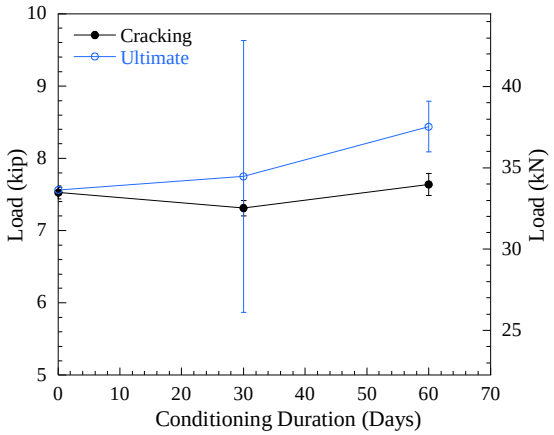

Figure 42. H_2O Load Bearing Capacity Degradation Plot

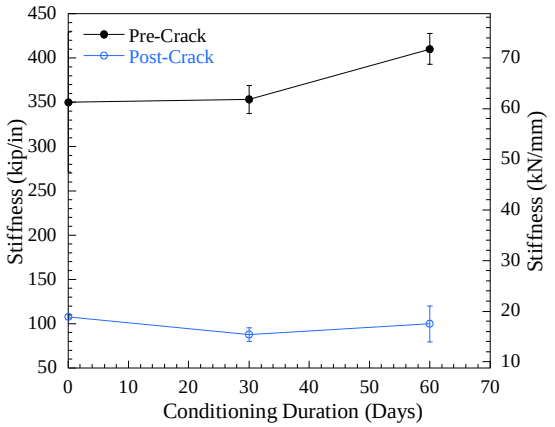

Figure 43. H_2O Stiffness Degradation Plot

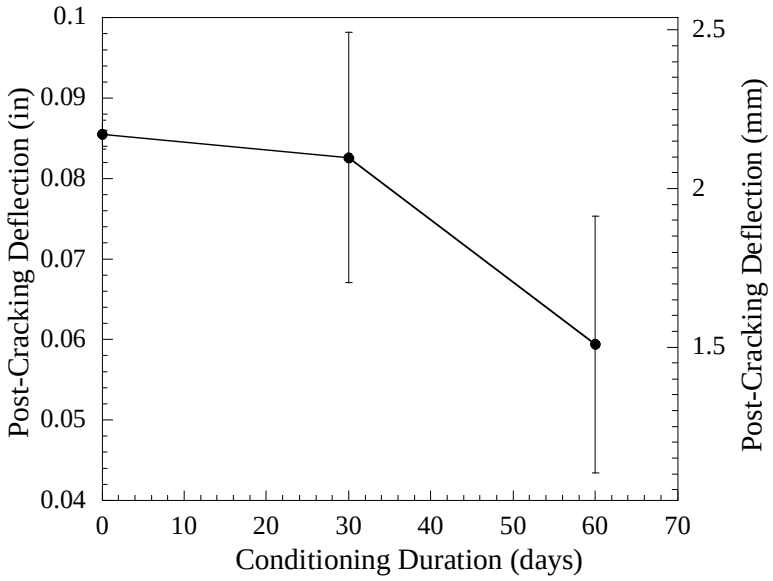

Figure 44. H2O Deflection Degradation Plot

SEM investigation of samples taken from 60 day conditioned beams revealed that a substantial amount of damage had accumulated at or around the fiber/matrix interface. Figure 45 and Figure 46 are micrographs taken of debonded laminate. Both figures depict examples of the surface morphology found on tested 60 day laminate samples removed form beams.

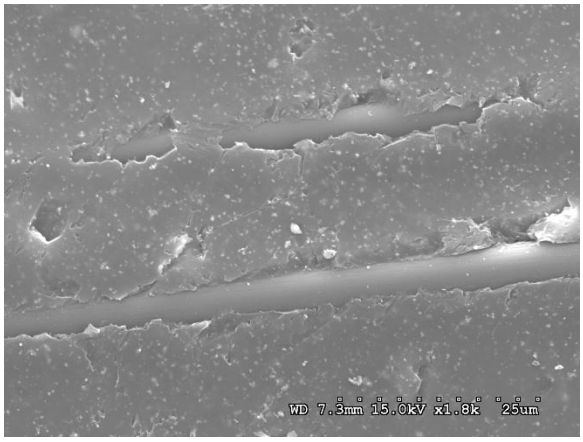

Figure 45. Fibers After Beam Failure – 60 Day

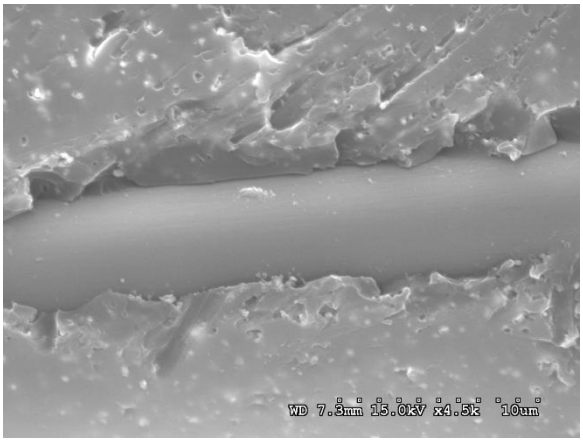

Figure 46. Single Fiber After Beam Failure – 60 Day

5.1.3 Concrete Leachate Conditioned Specimens

SEM micrographs of CFRP samples taken from beams exposed to 30 and 60 days of a concrete leachate solution prior to testing can be seen in Figure 47, Figure 48, Figure 49, and Figure 50. In both 30 day and 60 day samples there was no obvious degradation in the PU matrix or of the fiber/matrix bond. There was a significant amount of debris seen on the surface of leachate conditioned laminates. X-ray detection was used to determine the chemical nature of the crystal-like debris. Figure 51 and Figure 52 depict the characteristic X-ray and the corresponding detection location. The X-ray count indicates that this debris is merely calcium crystals that have formed on the surface of the composite laminate. The count plot also indicates other trace elements such as silicon, magnesium, and aluminum.

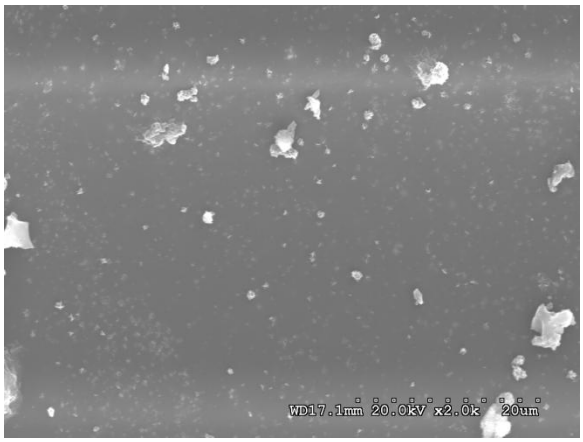

Figure 47. 30 Day Concrete Leachate Fibers

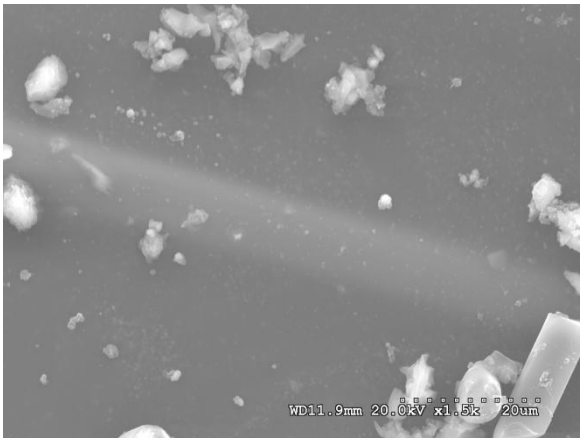

Figure 48. 60 Day Concrete Leachate Fibers

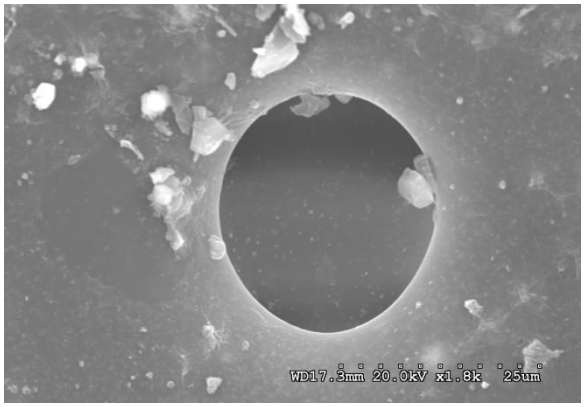

Figure 49. 30 Day Concrete Leachate Void

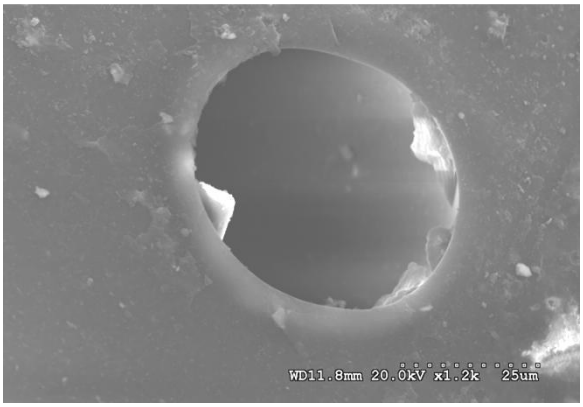

Figure 50. 60 Day Concrete Leachate Void

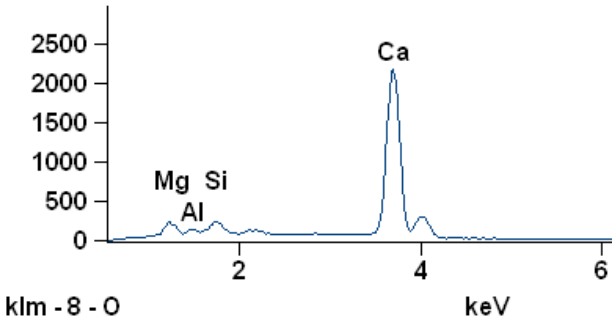

Figure 51. Characteristic X-ray Count

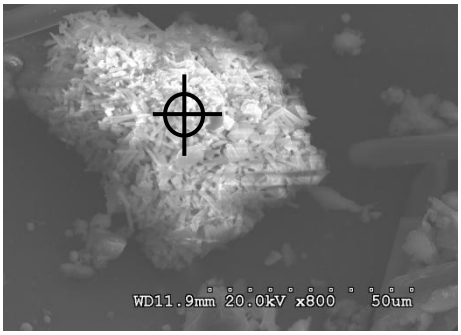

Figure 52. Detection location

In order to evaluate the material performance of the PU CFRP system under high pH exposure, 7 tensile coupons were tested for both 30 and 60 day conditioning periods. Figure 53 and Figure 54 depict the relationships between tensile modulus and ultimate tensile strength with regard to conditioning duration respectively. The tensile modulus tends to decrease initially by 21.2% at 30 day but recover slightly by 60 days (total decrease of 9.2%). Furthermore, there is a large amount of scatter that can be observed in 60 day specimens. It can be seen in Figure 54 that there is an obvious decreasing trend in the ultimate tensile strength with respect to increase in conditioning period. Reductions in ultimate strength for 30 and 60 tests were found to 11.6% and 15.4% respectively.

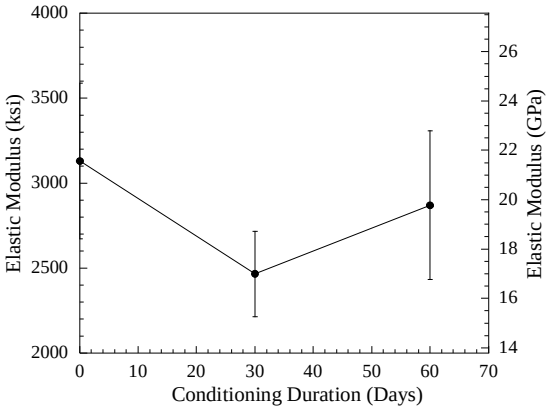

Figure 53. Concrete Leachate Elastic Modulus Degradation Plot

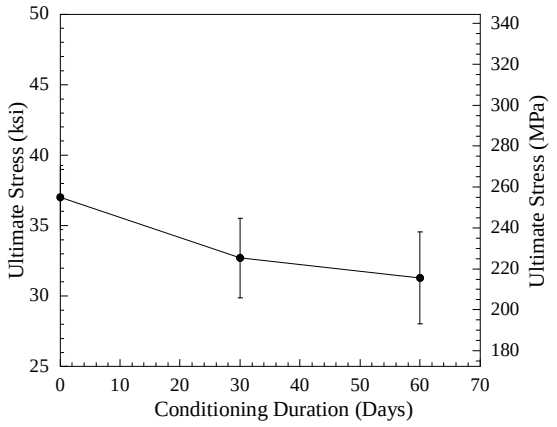

Figure 54. Concrete Leachate Ultimate Strength Degradation Plot

Unlike other conditioning environments, there were only 2 specimens for both 30 and 60 day concrete leachate tests. This was due to lack of space for conditioning the extra two specimens. 30 day beam specimens where tested on 12/31/09. Conditioned concrete strength for the day of test was experimental determined to be 8037 psi. A plot of the load deflection behavior of 30 day specimens can be found in Figure 55. Both 30 day specimens failed via laminate debonding. Specimen LECH-30-2 exhibited failure within the adhesive layer while specimen LECH-30-1 failure occurred partially within the adhesive and partially within the concrete substrate. Furthermore, the LECH-30-1 specimen failed immediately after crack formation.

60 day beam specimens where tested on 2/6/10. Conditioned concrete strength for the day of test was experimental determined to be 7610 psi. A plot of the load deflection behavior of 60 day specimens can be found in Figure 56. Both 60 day specimens failed by debonding that originated by rupture of the PU adhesive layer

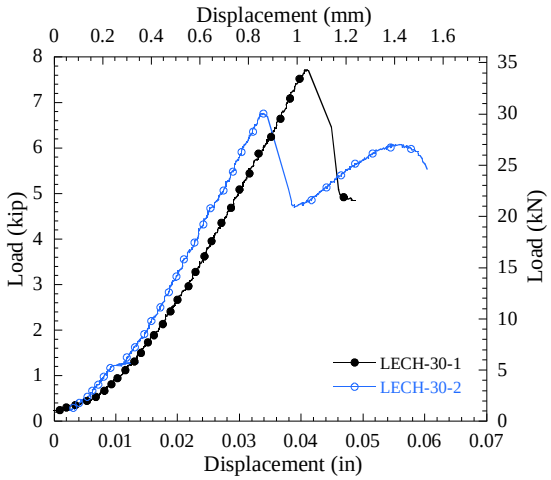

Figure 55. 30 Day Concrete Leachate Load-Deflection Plot

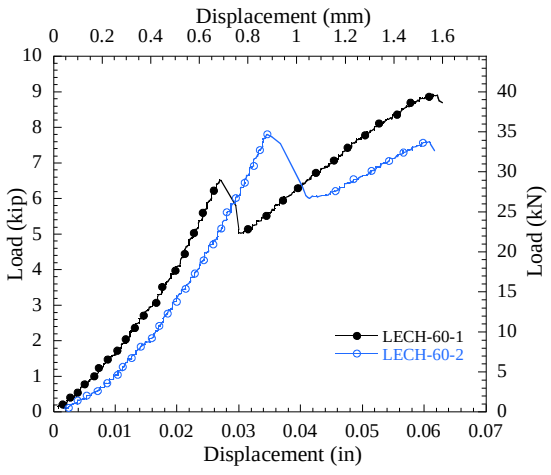

Figure 56. 60 Day Concrete Leachate Load-Deflection Plot

The relationship between flexural behavior and conditioning period can be seen in Figure 57 and Figure 58. There are no error bars shown for 30 day specimen post-cracking load bearing capacity and stiffness because failure occurred in specimen LECH-30-1. It can be observed in Figure 57 that there is a significant initial decrease in capacity (19.7%). Yet, at 60 days of conditioning, the average leachate specimen load bearing capacity had increased by 9.3% above the average baseline. With the increase, there was also a significant increase in data scatter observed.

Figure 58 depicts the pre- and post-cracking member stiffness. As observed with specimens bearing capacity, there is a significant initial decrease in post-cracking of 36.7% for the 30 day tests. Yet, at 60 days, the average post-cracking stiffness value was found to be 110 kip/in (1.8% increase from baseline). The flexural stiffness results are in good correlation with tensile test results. It should be noted that 30 days results are not as reliability due to the number of specimens considered.

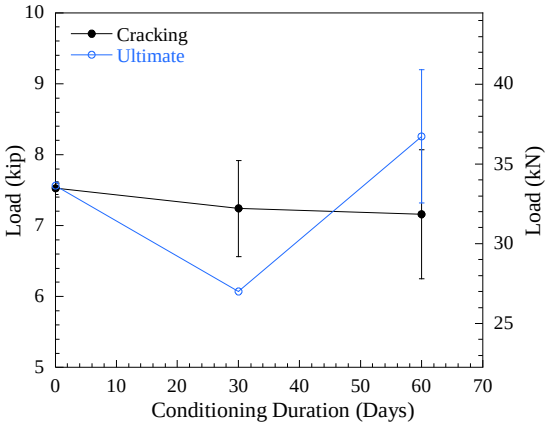

Figure 57. Concrete Leachate Load Bearing Capacity Degradation Plot

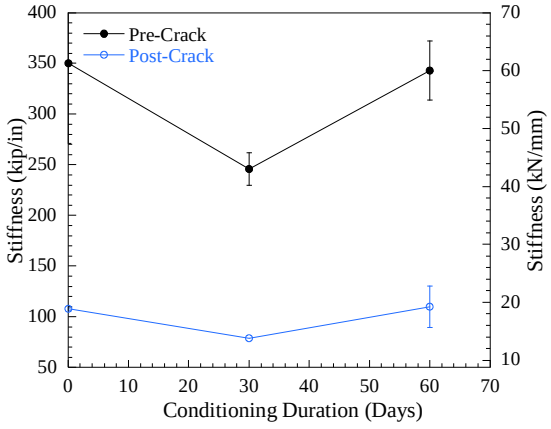

Figure 58. Concrete Leachate Stiffness Degradation Plot

Average ultimate deflection verses duration of conditioning can be found in Figure 59. There is an obvious trend in the data that indicates an inverse relationship between duration of conditioning and ultimate deflection. That is, as the duration of conditioning increases the average ultimate deflection decreases. Although, there is a significant decrease in ultimate deflection at 30 days, the difference in deflection at 60 days, when compared to the 30 day tests, is not that significant.

After completion of flexural testing, portions of the CFRP laminate were removed to be viewed using SEM. Micrographs shown at different magnifications can been seen in Figure 60 and Figure 61. There is a substantial amount of matrix damage present. This is especially noticed near reinforcing fibers. It can be observed in Figure 61 that some debonding has occurred near the laminate surface.

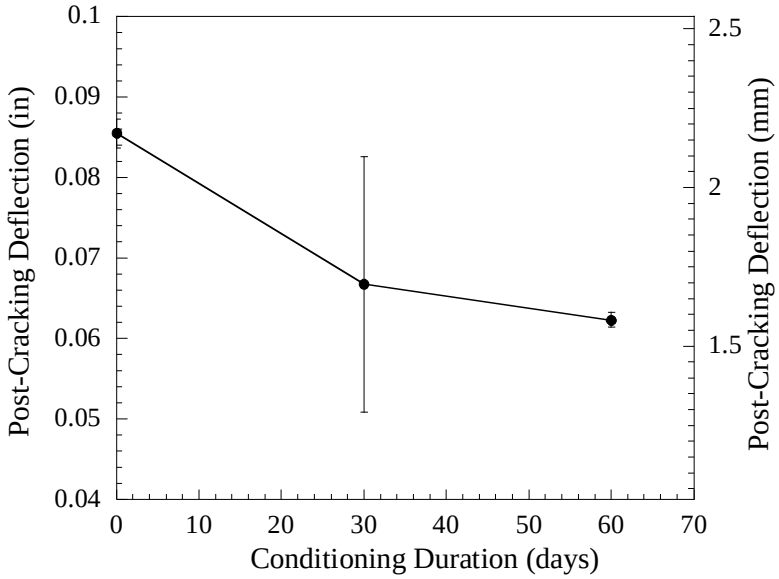

Figure 59. Concrete Leachate Deflection

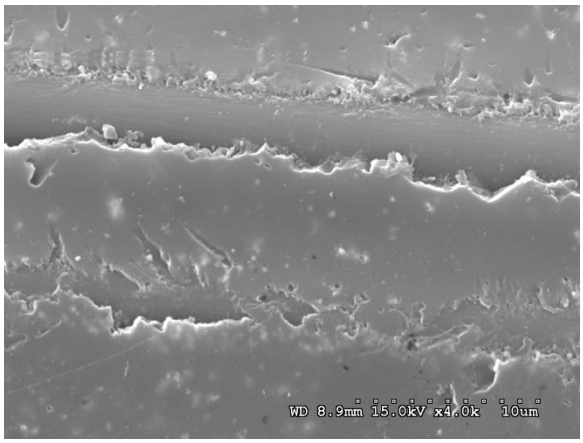

Figure 60. Post-fail 60 Day Leachate Fibers (x4,000)

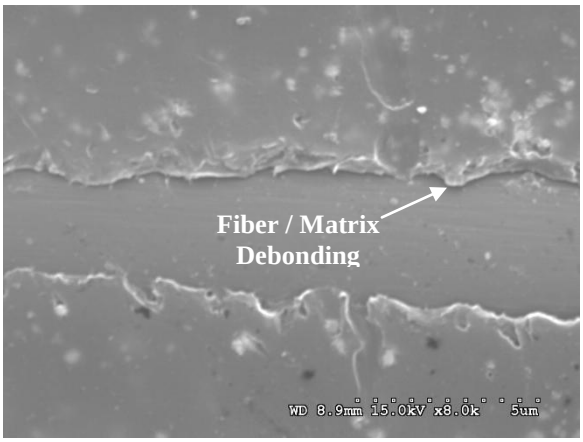

Figure 61. Post-fail 60 Day Leachate Fibers (x8,000)

5.1.4 Seawater Conditioned Specimens

Prior to testing, samples of seawater conditioned CFRP laminates were inspected using SEM. The initial inspection of 30 day sample was not beneficial for the surface of the composites was almost entirely covered with crystal growth (refer to Figure 63). Using X-ray detection (Figure 62), it was determined that the crystals mainly consisted of sodium, chlorine, and calcium. Therefore prior to proceeding with any further scanning, new samples were prepared by cleaning that composite surface and sputter coating with AuPd.

Micrographs taken of 60 day samples can been seen in Figure 64, Figure 65, and Figure 66. It is very clear that surface morphological changes in the PU matrix. The majority of these changes were observed near matrix micro-voids in the form of small pits and openings. There was also some debonding that was found to have occurred between the reinforcing fibers and the PU matrix

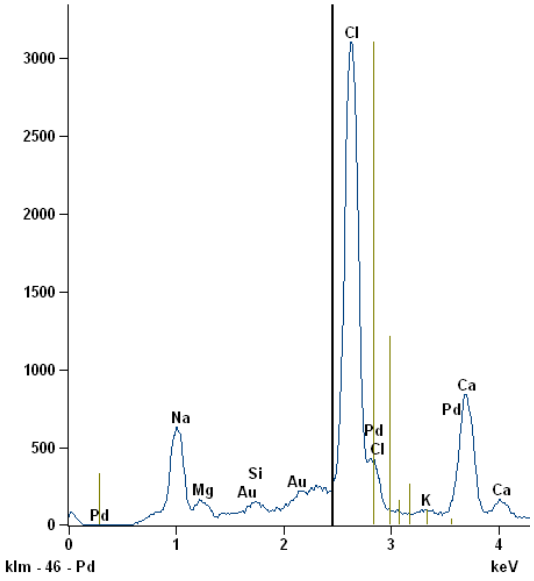

Figure 62. X-ray Detection Count

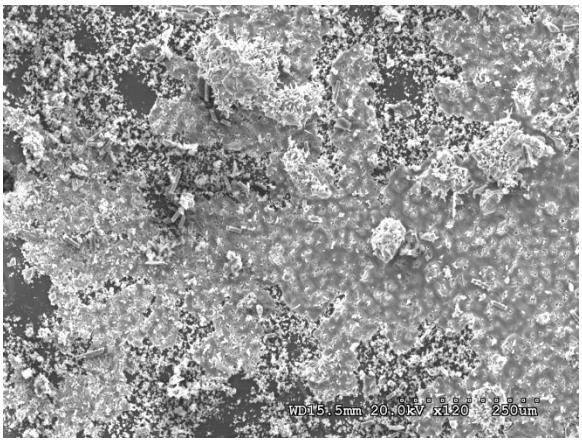

Figure 63. SEA-30 Sample Surface

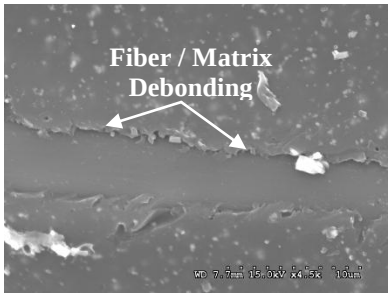

Figure 64. 60 Day Seawater Fibers

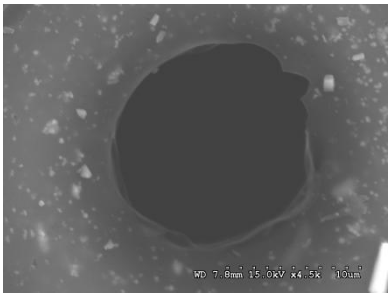

Figure 65. 60 Day Seawater Void

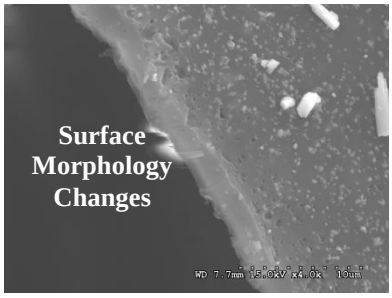

Figure 66. 60 Day Seawater Void Wall

Eight tensile coupons were tested for each conditioning period. It was found that conditioned specimens showed minimal to zero degradation of average tensile properties. Figure 67 shows how the tensile modulus changed with conditioning duration. It was determined that there was negligible change (± 1%) with respect to conditioning period. The only significant change observed was increase in data scatter. The ultimate tensile strength of conditioned specimens increased 4.1% for both 30 and 60 days of seawater exposure.

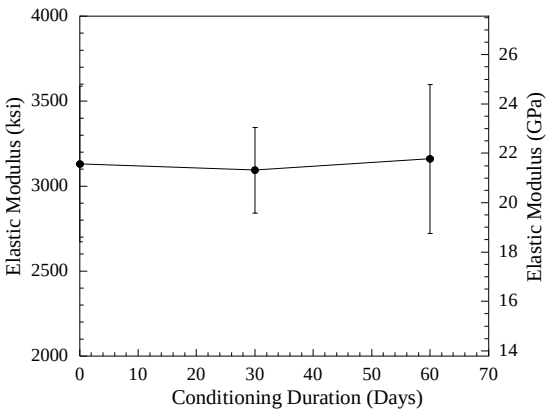

Figure 67. Seawater Elastic Modulus Degradation Plot

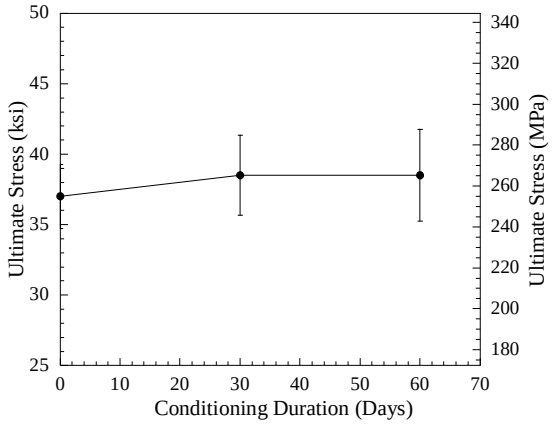

Figure 68. Seawater Ultimate Strength Degradation Plot

30 day beam specimens where tested on 12/28/09. Conditioned concrete strength for the day of test was experimental determined to be 7902 psi. A plot of the load deflection behavior of 30 day specimens can be found in Figure 69. Specimens SEA-30-1 and SEA-30-3 both failed via laminate debonding caused by rupture of the PU adhesive. Specimen SEA-30-2 did not fail in this manner, but in flexure when a second flexure crack developed outside the laminate span. Although this result is not consistent with other specimens, it does indicate substantial bond integrity after conditioning

60 day beam specimens where tested on 2/6/10. Conditioned concrete strength for the day of test was experimental determined to be 7781 psi. A plot of the load deflection behavior of 60 day specimens can be found in Figure 70. All 60 day specimens failed in different manners. During loading, specimen SEA-60-1 developed 2 flexural cracks prior to failure. Ultimate failure of specimen SEA-60-1 occurred by the formation of a third flexural crack and resulted in debonding of the CFRP laminate. Failure of specimen SEA-60-2 occurred similar to that of SEA-30-2 that is by the formation of a flexural crack outside of the laminate span. Finally, SEA-60-3 failed by CFRP debonding.

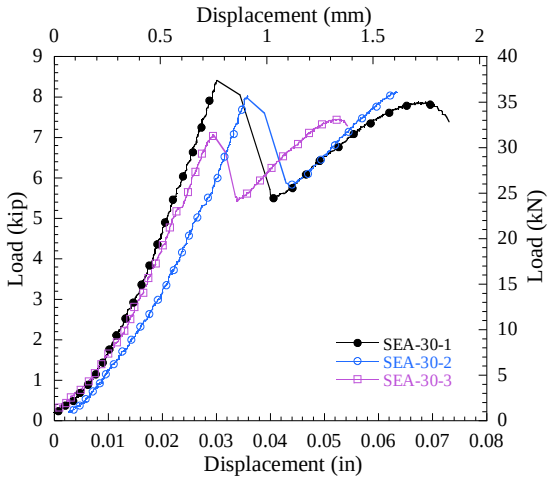

Figure 69. 30 Day Seawater Load-Deflection Plot

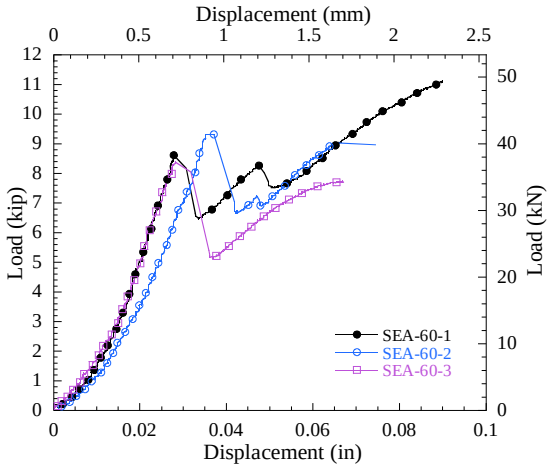

Figure 70. 60 Day Seawater Load-Deflection Plot

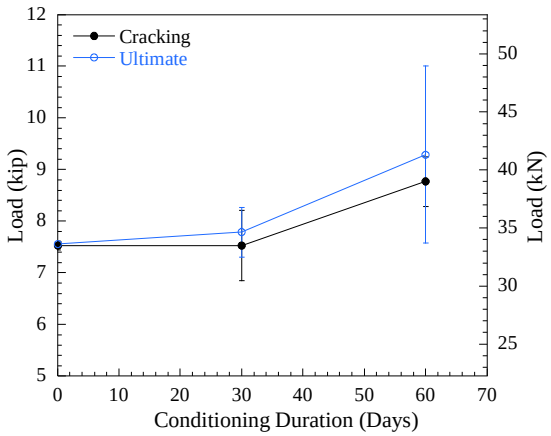

Figure 71. Seawater Load Bearing Capacity Degradation Plot

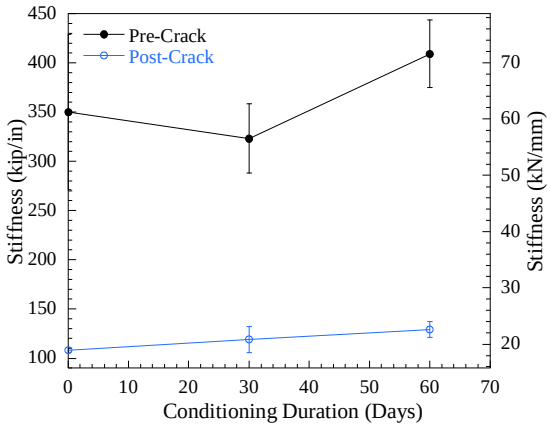

Figure 72. Seawater Stiffness Degradation Plot

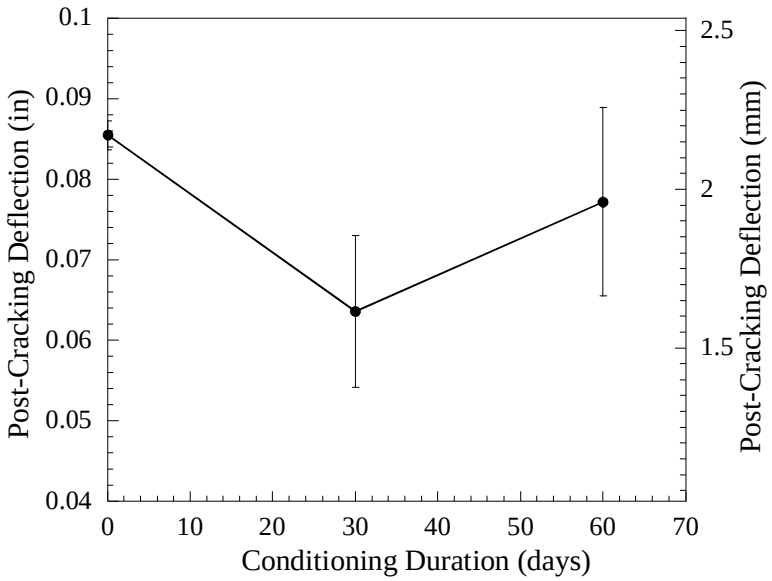

Figure 73. Seawater Deflection

Samples of CFRP laminate were removed from beams that failed though laminate debonding for inspection under SEM. Micrographs taken from 30 day samples can be found in Figure 74, Figure 75, and Figure 76. It can be observed that there was some bond loss at the fiber-matrix interface. Although bond loss was found, it was not continuous along fibers. The degradation that was found prior to testing around micro-voids seemed to become more severe after mechanical loading (refer to Figure 75 and Figure 76). Similar results were found in 60 day specimens in terms of fiber-matrix bond and the increased localized damage near matrix micro-voids (shown in Figure 77, Figure 78, and Figure 79). Yet, the damage found in the 60 day case was much more significant.

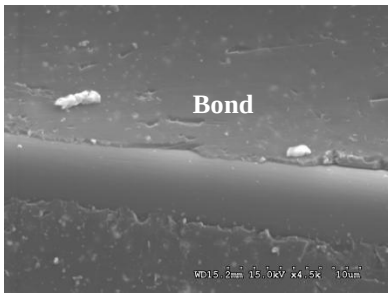

Figure 74. Fiber After Beam Failure – 30 Day

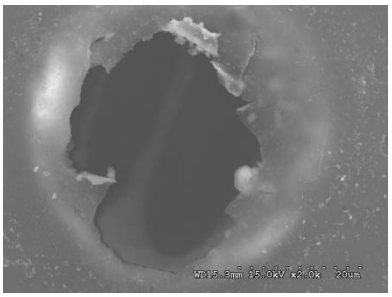

Figure 75. Void After Beam Failure – 30 Day

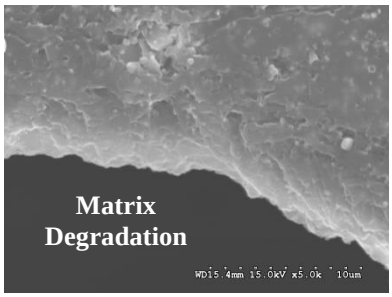

Figure 76. Void Wall After Beam Failure – 30 Day

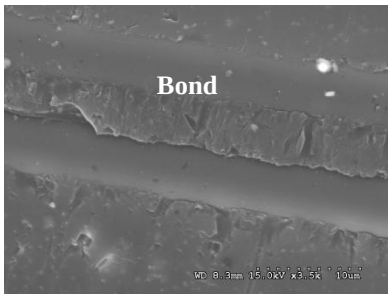

Figure 77. Fiber After Beam Failure – 60 Day

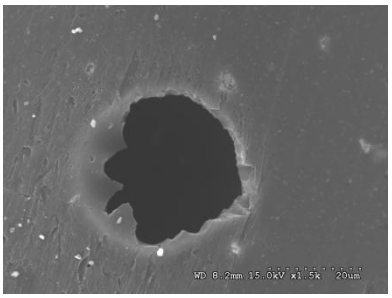

Figure 78. Void After Beam Failure – 60 Day

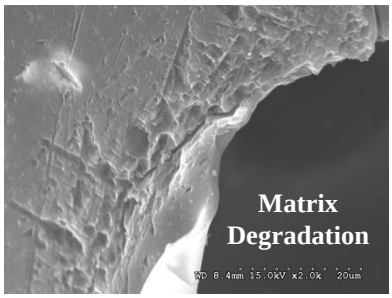

Figure 79. Void Wall After Beam Failure – 60 Day

5.1.5 Dry Heat Conditioned Specimens

Specimens were conditioned in a industrial oven set at 120 °F for periods of 30 and 60 days. Figure 80 and Figure 81 show micrograph taken using SEM of the CFRP composite conditioned for 60 days. It can be observed that there is no apparent degradation of the PU matrix, reinforcing fibers, of locations were fiber/matrix debonding can be seen. This indicates that short term dry heat conditioning does not cause physical damage to PU matrix CFRP laminate.

Seven tensile coupons were tested for both 30 and 60 day conditioning periods. The plot shown in Figure 82 depicts the relationship between elastic modulus and conditioning period. Results indicate that the elastic modulus of the PU system tended to increase with conditioning during. Increases of 9% and 13.1% were observed for 30 and 60 day conditioning duration respectively. Furthermore, the same trend can be observed with coupon ultimate strength. Figure 83 depicts the relationship between ultimate tensile strength and conditioning duration. Compared to control coupons, increases of 11% and 15.1% were observed for 30 and 60 day conditioning periods respectively. The increase in both tensile modulus and ultimate strength could be attributed to an increased level of laminate cure. The cure rate of many polymeric matrices is significantly increased with addition of heat. Although scatter increased significantly with conditioning period, tensile specimen failure modes were observed to be very consistent compared to those subjected to other conditioning environments.

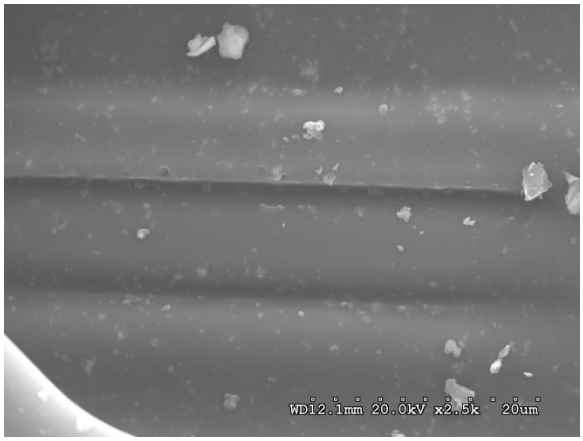

Figure 80. 60 Day Dry Heat Fibers

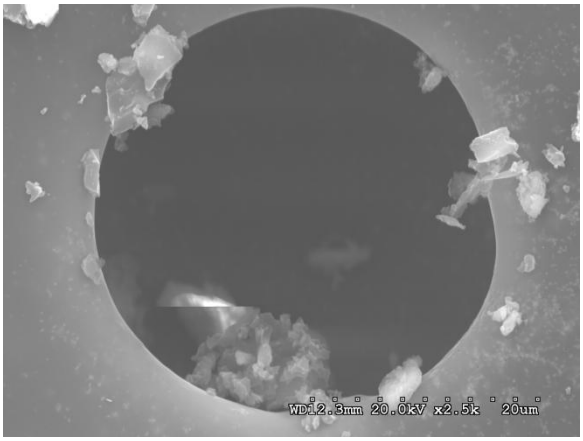

Figure 81. 60 Day Dry Heat Micro-void

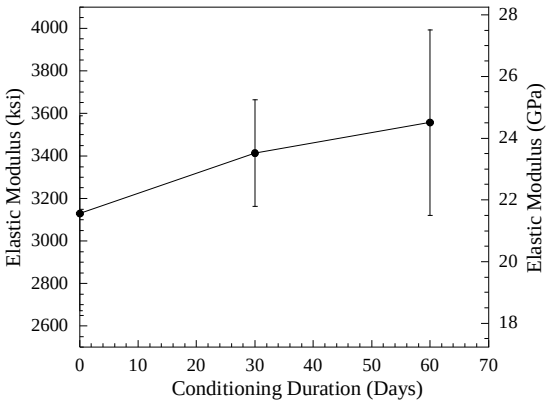

Figure 82. Dry Heat Elastic Modulus Degradation Plot

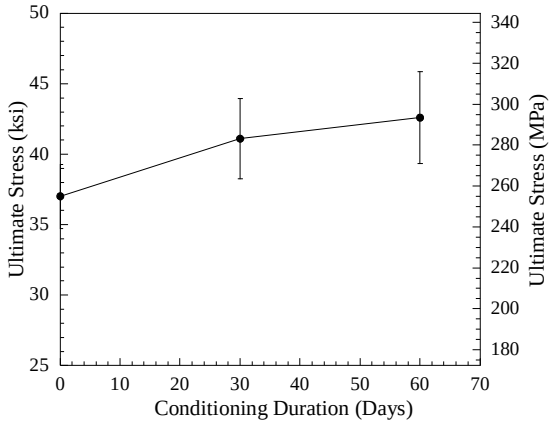

Figure 83. Dry Heat Ultimate Strength Degradation Plot

30 day beam specimens where tested on 12/31/09. Conditioned concrete strength for the day of test was experimental determined to be 5979 psi. A plot of the load deflection behavior of 30 day specimens can be found in Figure 84. The observed load-deflection behavior and failure mode for 30 day dry heat conditioned specimens was consistent. All specimens displayed load-deflection similar to that of the unconditioned control specimens. Furthermore, all 3 30 day specimens failed debonding of the CFRP laminate; failure occurring within the adhesive layer.

60 day beam specimens where tested on 2/6/10. Conditioned concrete strength for the day of test was experimental determined to be 6060 psi. A plot of the load deflection behavior of 60 day specimens can be found in Figure 85. The 60 day specimen load-deflection behavior was also similar to that of the unconditioned specimens. Moreover, failure mode was also similar to unconditioned specimens. All 60 day beams failed via laminate debonding initiated by rupture within the adhesive layer.

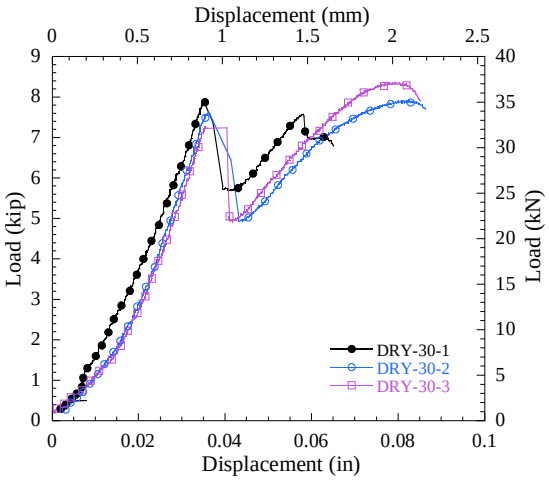

Figure 84. 30 Day Dry Heat Load-Deflection Plot

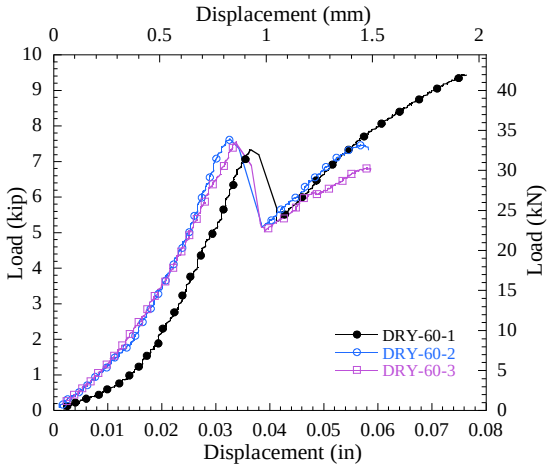

Figure 85. 60 Day Dry Heat Load-Deflection Plot

The relationship between ultimate flexural capacity and conditioning duration can be found in Figure 86. It can be observed that the ultimate flexural capacity of dry heat conditioned specimens tended to increase with conditioning duration. At 60 days, there was an increase of flexural capacity, compared to baseline, of 4.5%. The increase in flexural capacity would indicate stability of the PU adhesive bond under continuous exposure to heat. Although an increase is observed, there was also a significant increase in measurement scatter.

Figure 87 depicts the relationship between member flexural stiffness and exposure duration. It was found that member post-cracking stiffness tended to increase, without increase in data scatter, as the duration of conditioning increased. This result is supported by those found in tensile test results. A total increase in post-cracking stiffness of 5.6 % was observed from experimental result.

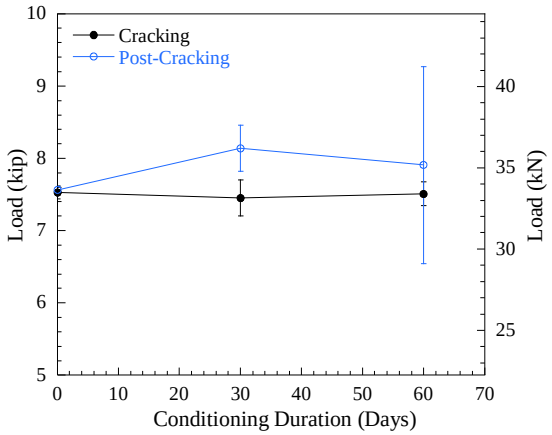

Figure 86. Dry Heat Load Bearing Capacity Degradation Plot

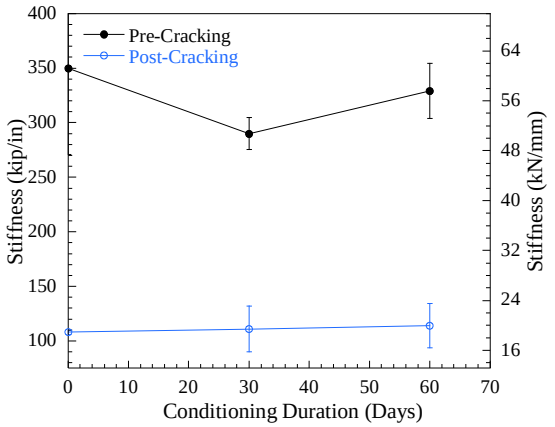

Figure 87. Dry Heat Stiffness Degradation Plot

Figure 88 shows how the member post-cracking ultimate deflection was effected by conditioning duration. It can be observed that as conditioning duration increases, there is a decrease in deflection at failure. At 60 days, average deflection was found to have decreased by 24.2%

After specimens were tested, portions of the CFRP laminate were removed from one of the 60 day specimens. Samples were viewed using SEM to identify if damage caused by loading differed from that of unconditioned specimens. Micrographs taken at different magnifications can be found in Figure 89 and Figure 90. Micrographs show that there is no excess damage that has been induced by dry heat conditioning.

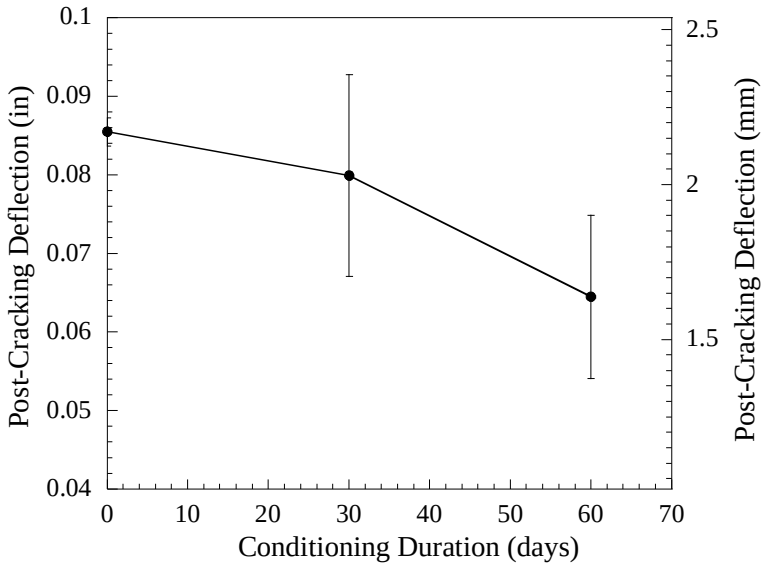

Figure 88. Dry Heat Deflection

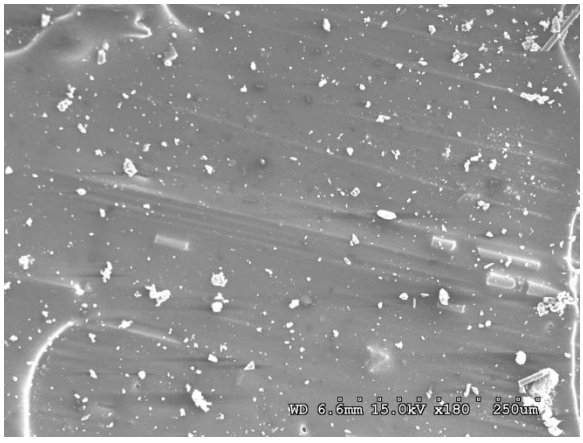

Figure 89. Dry Heat Fibers after Beam Failure – 60 Day (x180)

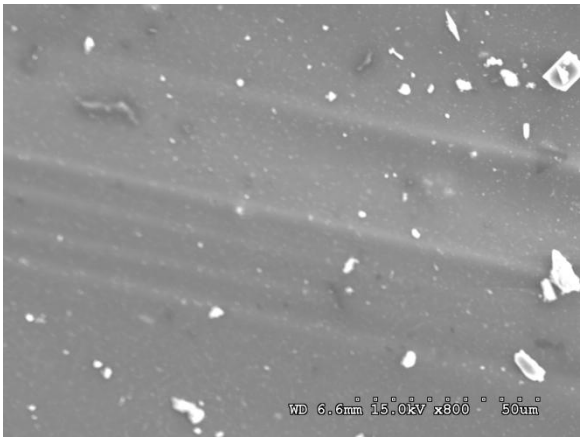

Figure 90. Dry Heat Fibers after Beam Failure – 60 Day (x800)

5.1.6 Ambient Outdoor Conditioned Specimens

Specimens subjected to the ambient outdoor environment where left undisturbed on the roof of the UCF College of Engineering and Computer Science Building II. There specimens were exposed to UV, continuous temperature change, high levels of humidity, and rain. Specimens were inspected weekly to document visual changes. On the 7^{th} day of conditioning, it was found that the urethane matrix had begun to change in color from a whitish-tan to a greenish-yellow. Figure 91 and Figure 92 are photos taken of the CFRP laminate surface prior to conditioning and after 30 days of ambient exposure respectively. There is a very discernable difference in color between the two laminate samples.

SEM Inspection of conditioned samples revealed that a significant amount of cracking had occurred within the bulk polyurethane matrix and at the fiber/matrix interface. Figure 93 shows cracks that have developed at the fiber/matrix interface along with those that propagate transversely to the fiber. The crack formation seen in Figure 93 was identified in both 30 day and 60 day laminate samples (Figure 94). The other cracking pattern found in both 30 and 60 day samples was that illustrated in Figure 95 and Figure 96. Cracks were found to develop at matrix micro-voids and propagate in the radial direction. The possible concern with such crack formation at the micro-voids is that, under minimal mechanical loading, cracks will join between voids. Such a mechanism, if found extensively within a laminate, could result in significant changes in the characteristic material properties such as elastic modulus and breaking strength.

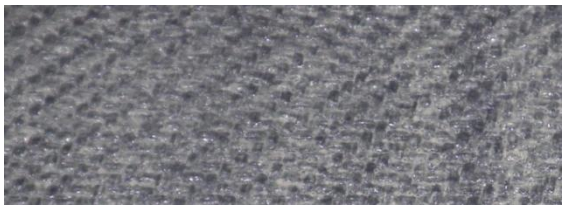

Figure 91. Control Laminate

Figure 92. 30 Day Ambient Environment Laminate

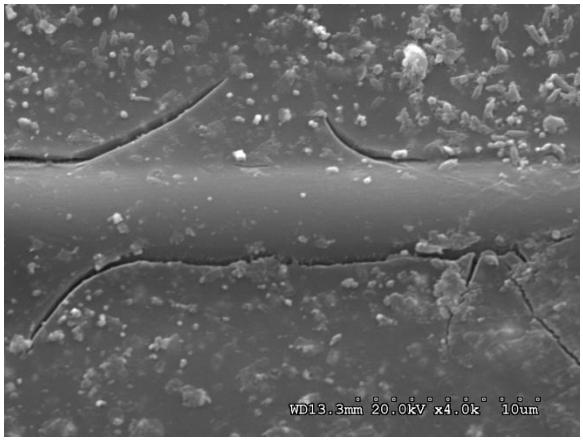

Figure 93. 30 Day Ambient Environment Fibers

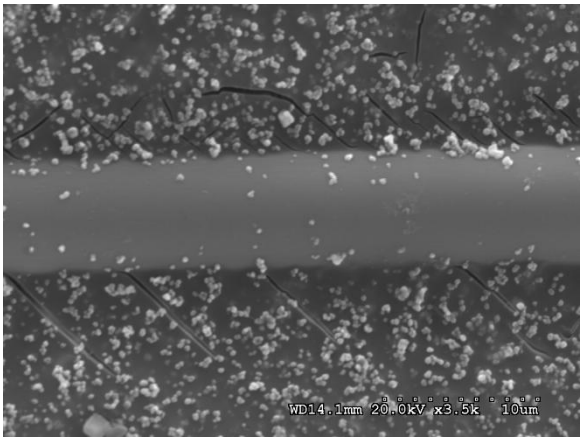

Figure 94. 60 Day Ambient Environment Fibers

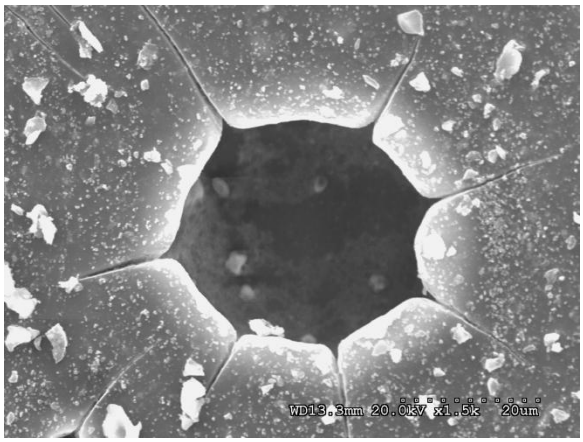

Figure 95. 30 Day Ambient Environment Void

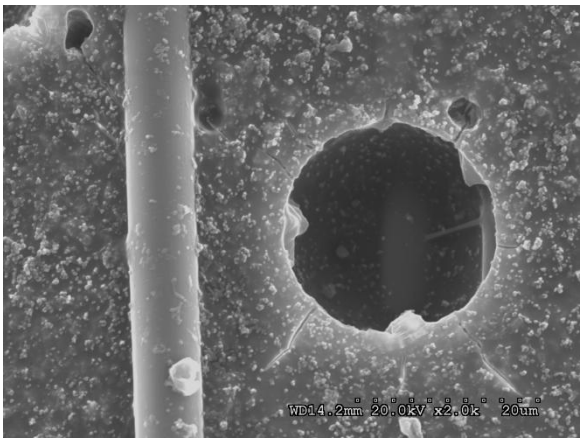

Figure 96. 60 Day Ambient Environment Void

Figure 97 and Figure 98 represent the evolution of elastic modulus and ultimate strength for tensile specimens tested. For 30 day and 60 day conditioning periods, a total of 5 and 4 tensile coupons were tested. Although test results indicated an initial decrease in elastic modulus, 60 day results indicated an overall increase in modulus of 4.9%. It can also be observed that there was also more scatter present in the 60 day results compared to that of the 30 day results. There was no significant change in the breaking strength with respect to duration of conditioning; data scatter was also consistent. Such results would indicate that although SEM micrographs show the presence of crack formation within the matrix that this degradation did not seem to have a significant impact on behavior of the macro-mechanical behavior of the composite.

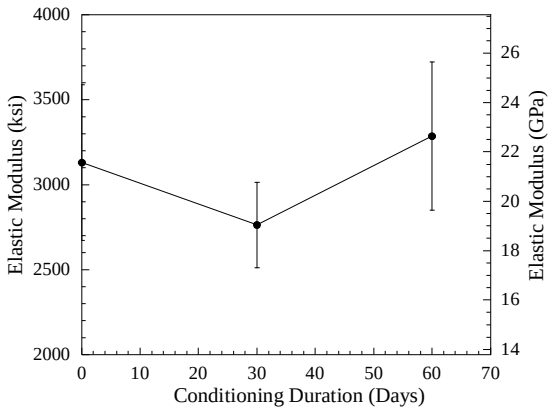

Figure 97. Ambient Environment Elastic Modulus Degradation Plot

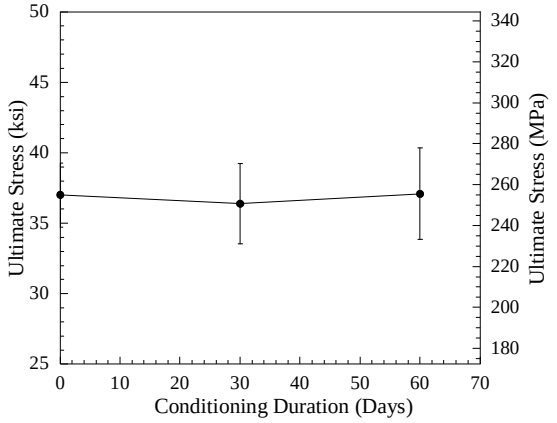

Figure 98. Ambient Environment Ultimate Strength Degradation Plot

30 day beam specimens where tested on 12/28/09. Conditioned concrete strength for the day of test was experimental determined to be 7673psi. A plot of the load deflection behavior of 30 day specimens can be found in Figure 99. All AMB-30 specimens exhibited load-deflection behavior similar to that of the unconditioned specimens. AMB-30 specimens failed via debonding of the CFRP laminate. In all cases, debonding was initiated by rupture within the BP-1 adhesive layer.

60 day beam specimens where tested on 2/6/10. Conditioned concrete strength for the day of test was experimental determined to be 8348psi. A plot of the load deflection behavior of 60 day specimens can be found in Figure 100. Specimen AMB-60-1 was the only beam to behave similar to unconditioned specimens. AMB-60-2 and 3 both failed soon after the initiation of the first mid-span flexural crack. Hence, both specimens show little to no post-cracking behavior. Nevertheless, all three specimens failed by laminate debonding within the adhesive layer.

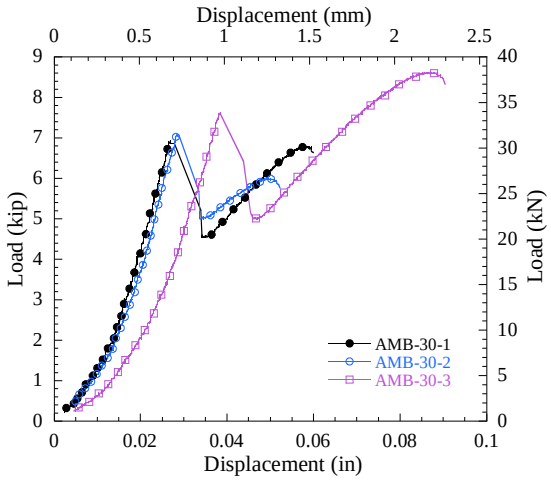

Figure 99. 30 Day Ambient Environment Load-Deflection Plot

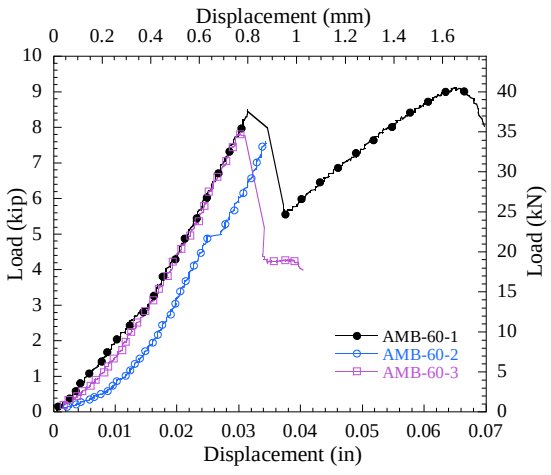

Figure 100. 60 Day Ambient Environment Load-Deflection Plot

Figure 101 depicts the evolution of load bearing capacity at cracking and ultimate for specimens exposed to ambient conditioning. At 30 days the load to induce cracking tends to decrease slightly but recovers by 60 days and exceeds that of the unconditioned specimens. Furthermore, data scatter is nominal for cracking loads at 30 and 60 days. These cases are not seem with specimen ultimate capacity, rather there exists a decreasing tend as conditioning time increases. Scatter of data for 30 day tests is quite significant for ambient exposure specimens. It should be noted that only a single 60 day specimen (AMB-60-1) was used for the plot shown in Figure 101. This was because the other specimens failure immediately after cracking.

The effect of conditioning on flexural stiffness can be observed in Figure 102. The trend seen in the post-cracking stiffness correlates to the initial decline at 30 day and recovery at 60 day of the elastic modulus.

The average ultimate deflection of specimens verses duration of conditioning can be found in Figure 103. There is an obvious trend in the data that indicates an inverse relationship between duration of conditioning and ultimate deflection. That is, as the duration of conditioning increases the average ultimate deflection decreases. Yet, this trend does not seem substantial due to the exclusion of specimens AMB-60-2 and 3.

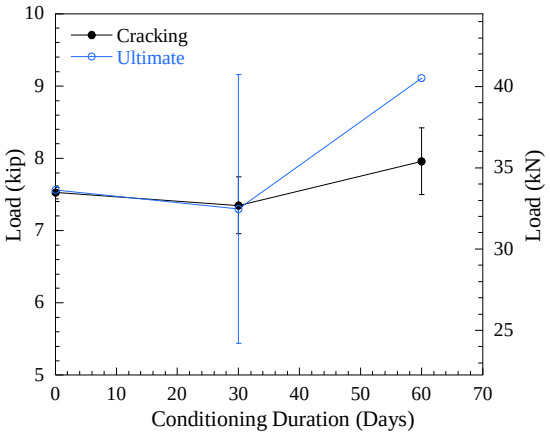

Figure 101. Ambient Environment Load Bearing Capacity Degradation Plot

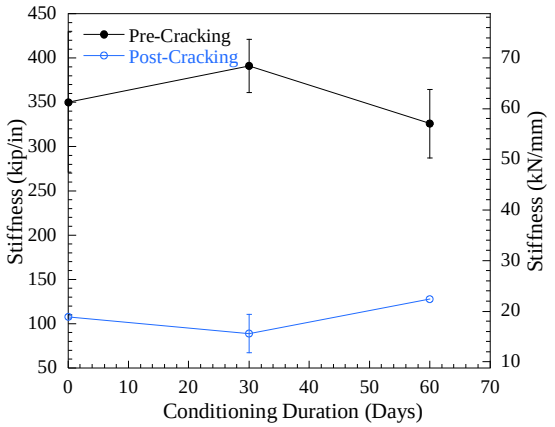

Figure 102. Ambient Environment Stiffness Degradation Plot

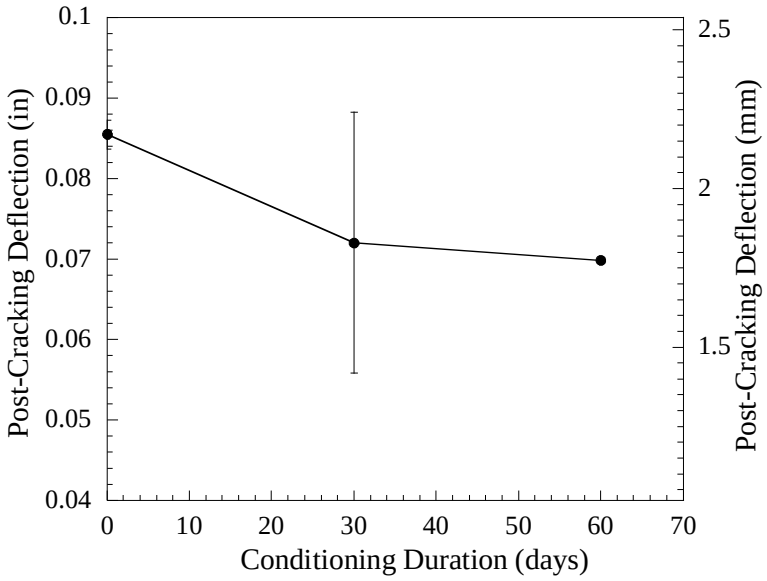

Figure 103. Ambient Environment Deflection

Samples of debonded laminate were taken for 30-day specimens and viewed under the SEM. Representative micrographs are shown in Figure 104 and Figure 105 at different magnifications. It can be observed that matrix cracks propagated within close proximity of adjacent matrix micro-voids. Furthermore, a number of free-standing cracks also developed within the bulk urethane matrix. In comparison with

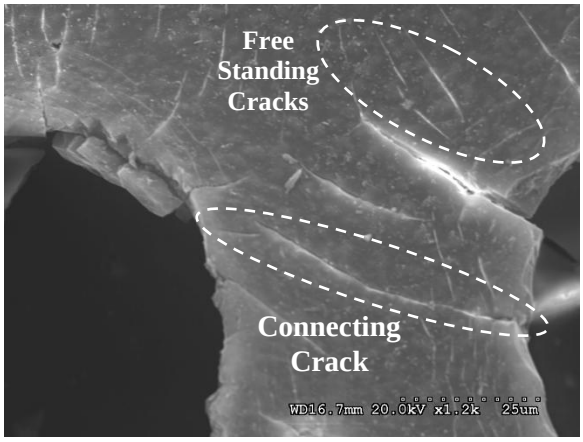

Figure 104. Ambient Environment Laminate After Beam Failure – 30 Day (x80)

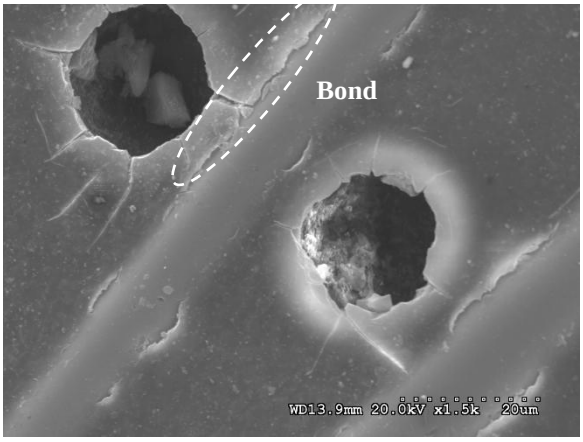

Figure 105. Ambient Environment Laminate After Beam Failure – 30 Day (x1500)

5.2 Large-scale Beam Specimens

Large-scale beams were tested on different days depending on the conditioning. Details regarding test dates, cure times, and specimen compressive strengths can be found in Table 18.

Table 18. Large-scale Test Dates and Compressive Strengths

Batch No.	Pour Date	Test Date	Cure Time (days)	Beam ID	Compressive Strength	
					psi	*MPa*
1	5/11/2005	5/30/2008	1115	1 & 2	8203	56.6
2	5/18/2005	11/7/2008	1269	3 & 4	9530	65.7
3	6/1/2005	5/30/2008	1094	5 & 6	9684	66.8
4	6/8/2005	11/7/2008	1248	7 & 8	8237	56.8
5	6/15/2005	11/7/2008	1241	9 & 10	8589	59.2
6	6/22/2005	5/30/2008	1073	11	9836	67.8
	6/22/2005	11/7/2008	1234	12	9356	64.5
8	8/31/2005	11/7/2008	1164	15[2] & 16	9668	66.7

[1]Under Strength [2]Damaged [3]Excluded

5.2.1 Baseline Flexural Tests

5.2.1.1 Unstrengthened Control Beam

The control beam for this project was tested to failure on 2/6/2007. Loading was paused at 20.3, 30.5, and 40.6kip to mark cracks. The control beam failed in a progressive manner; first with concrete cracking, steel yielding, and finally concrete crushing. The ultimate load obtained by the control beam was 52.2kip (Δ=2.63”).

5.2.1.2 PU Baseline Beam

The PU baseline specimen was tested to failure on 2/6/2007. During the load testing, there were no observed problems with DAQ or the test set-up. Therefore the load test was completed in a single run. Loading was paused at 26.3, 39.5, and 52.6 kips for cracks to be marked. Failure of the PU baseline specimen ultimately occurred at 74.3 kips (Δ=1.82”). The failure mode was determined to be CFRP rupture followed by laminate debonding. During the final three minutes of the load test, a video was recorded to capture the beam’s failure. Figure 106 shows two frames from the video taken. The first frame where failure was evident (initial CFRP rupture) is denoted to have a time interval of *t = 0sec* for reference. The initial ruptured occurred approximately 50” from the north support (between SG2 and SG3). Immediately after the CFRP rupture, laminate debonding occurred. It should be noted that debonding failure occurred within the urethane adhesive layer. Figure 107 shows a close-up picture of the debonding surface. It can be observed that a whitish colored layer of material (urethane) remains on the concrete substrate, supporting the conclusion of cohesive failure within the adhesive layer.

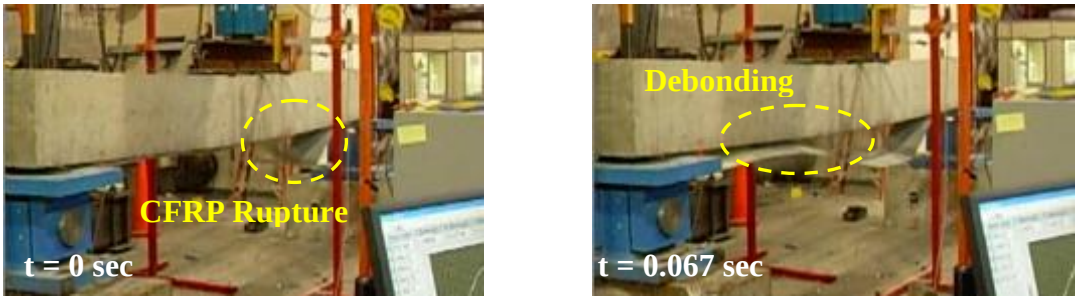

Figure 106. PU Baseline at Failure: Video Frame Shots

Figure 107. PU Baseline CFRP Rupture Plane

5.2.1.3 EP1 Baseline Beam

The EP1 baseline specimen was tested to failure on 2/6/2007. During the load testing, there were no observed problems with DAQ or the test set-up. Loading was paused at 25.5, 38.3, and 51.1 kips for cracks to be marked. The EP1 baseline specimen failed at a load of 70.3kip (Δ=1.56”). The dominate mode of failure was CFRP debonding. Figure 108 was taken from a video, taken during the time of testing, that shows the initiation of CFRP debonding occurring the North end of the specimen. It was observed that during the debonding failure longitudinal splitting of the CFRP composite and concrete cover separation occurred. Figure 108 shows a photo taken after failure occurred. It can be observed that both light and dark colored portions exist on the concrete tensile face. The lighter colored areas indicate the removal of concrete substrate during debonding; this implies a sound interface between CFRP and concrete. The darker colored areas indicate that debonding occurred at the CFRP-to-concrete interface; this could indicate poor wetting of the fiber surface.

Figure 108. EP-Baseline Failure

5.2.1.4 EP2 Baseline Beam

EP2 baseline specimen was tested on 2/6/2007. During the load testing, there were no observed problems with DAQ or the test set-up. Loading was paused at 25.5, 38.3, and 51.1 kips for cracks to be marked. Recall that during the application of the CFRP sheets to the EP2 baseline specimen, there were problems with premature gelling of the epoxy resin. A number of the following results shown are more than likely a result of this issue. The EP2 baseline specimen failed at a load of 71.5 kip (Δ=1.61”). The dominating mode of failure was debonding originating from the north end of the specimen. When debonding failure occurred, only one half of the laminate separated from the concrete substrate (refer to Figure 109). During debonding, the north plate-end of the CFRP also ruptured via interlaminar shear (refer to Figure 109). The most interesting result to be seen was in the post-fail inspection of the debonded CFRP and respective concrete surface. If was found that a significant number of areas on the debonded plate did have adequate or any matrix saturation of the reinforcing fiber. Moreover, these areas showed signs of little or no adhesion to the concrete substrate (see Figure 109). Figure 110 depicts a close-up picture of the post-fail tensile concrete surface. Three distinct regions can be identified:

1) Region 1 (R1): Area where plate debonding occurred within the concrete substrate indicting sound FRP-to-concrete bonding.

2) Region 2 (R2): Area where plate debonding occurred at the FRP-to-concrete interface indicting poor bonding.

3) Region 3 (R3): Area of poor fiber saturation/wetting. R3 areas could have resulted from, as mentioned earlier, premature gelling of the resin.

It should be noted that the small area shown in Figure 110 was typical for the debonding surface found on the EP2 specimen.

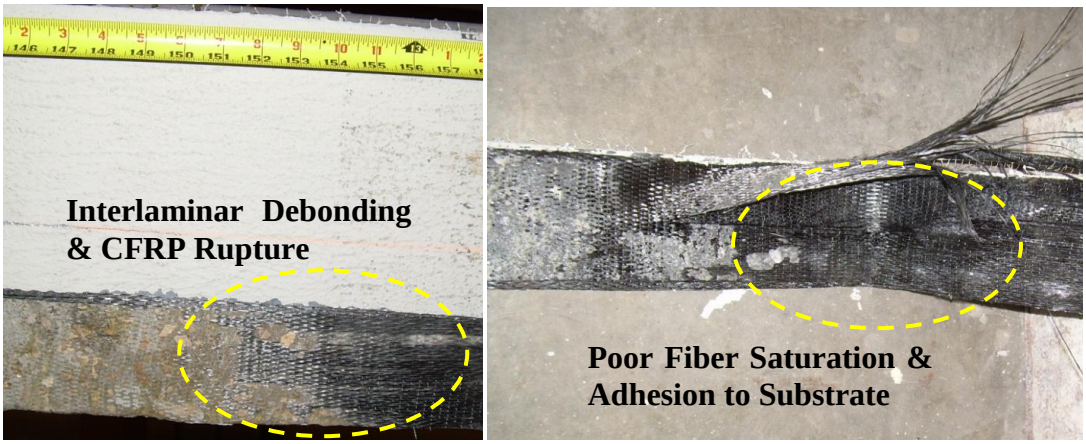

Figure 109. EP2 Baseline at Failure

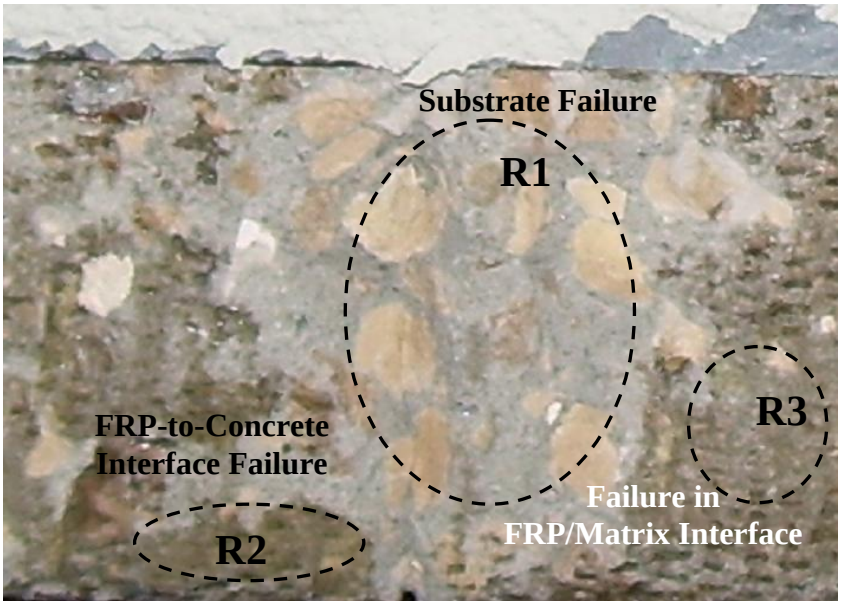

Figure 110. EP2 Baseline Concrete Substrate Post-fail

5.2.1.5 Baseline Beam Comparative Results

Figure 111 shows the load-deflection behavior of all strengthened baseline specimens along with the control beam. This figure shows that all strengthened specimens significantly increase (34.7-42.3%) the load bearing capacity of the control member. Yet, this increase in capacity comes at the cost of decreased ductility (losses of 48-60%). It can be observed that the all specimens show no significant stiffness increases in the pre- and post-cracking stages of loading. This is more than likely due to the initial steel reinforcement ratio (ρ=0.01) and the small amount of CFRP added to the member. Yet, there is a noticeable post-yield stiffness increase with all strengthened specimens compared to the control beam. The polyurethane baseline specimen exhibited the greatest ultimate load-bearing capacity, deflection, and post-yielding ductility (followed by the EP2 and EP1 type specimens respectively.

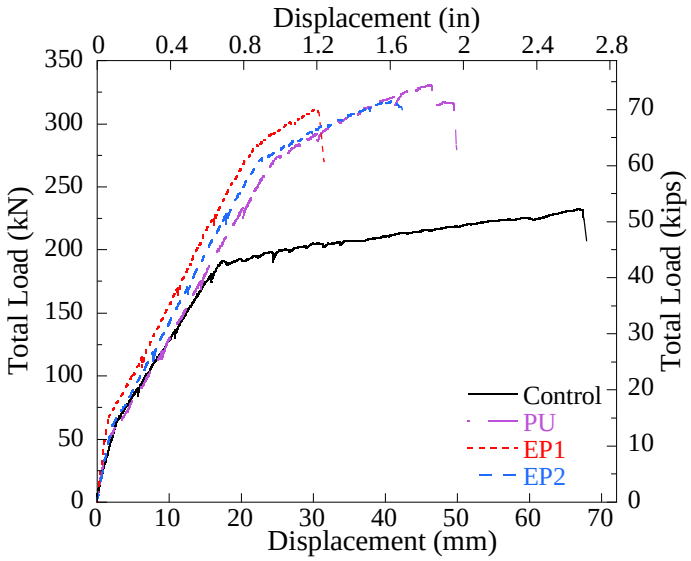

Figure 111. Baseline Specimen Load-Deflection Results

5.2.1.6 Failure Modes and Bond

CFRP strengthened beam specimens were inspected after failure in order to gather more information regarding the governing mode of debonding failure. Four modes of debonding failure were identified:

Mode 1) Cover Delamination: Failure caused when the bonded CFRP laminate ruptures the mechanical bond between concrete and tension reinforcement. Ultimately, separation between concrete and tension reinforcement is caused.

Mode 2) Type-1 Laminate Debonding: Failure mode caused by rupture of the concrete substrate within the bond-line region of the tension soffit (refer to Figure 112). This failure mode can be identified by a thin layer of concrete that remains on the separated CFRP sheet.

Mode 3) Type-2 Laminate Debonding: Failure caused by simultaneous rupture within the concrete substrate, adhesive layer, and CFRP laminate (refer to Figure 112). Failure at interface layers also occurs.

Mode 4) Type-3 Laminate Debonding: Failure caused by rupture within the adhesive layer (refer to Figure 112).

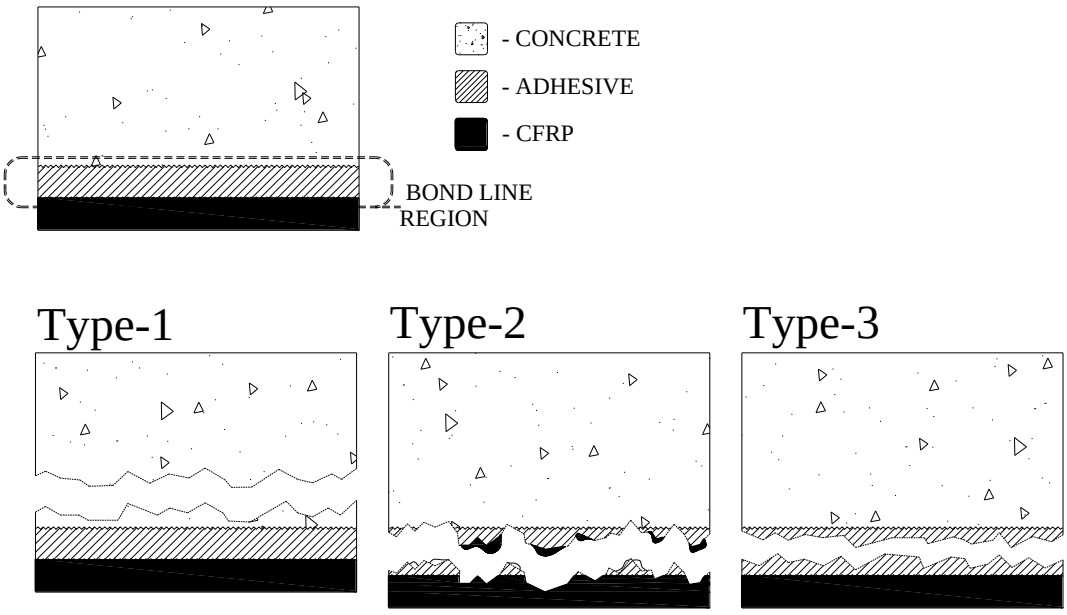

Figure 112. Bond-line Failure Mode

In this study, the CFRP systems utilizing epoxy matrices displayed combinations of failure modes 1-3. This result is considered to by typical for epoxy matrix/adhesive systems (Buyukozturk & Yu, 2006). The PU system displayed Mode 4 debonding failure. Although, this mode is debonding in nature it is fundamentally different than those the literature considers normal for externally bonded FRP strengthened concrete.

In order to confirm the mechanism by which debonding failure occurred, samples of CFRP laminate were viewed using SEM. Micrographs were taken of portion of the laminate that was bonded to the concrete substrate. Figure 113 and Figure 114 depict micrographs taken of CFRP utilizing the EP1 matrix system. It can be observed in Figure 113 that rupture occurred mainly within the FRP-to-concrete interface and within the FRP/adhesive interface. Figure 114 shows rupture within the adhesive layer and within the concrete substrate. Figure 115 and Figure 116 are micrograph taken from of CFRP samples utilizing the PU matrix/adhesive system. It can be observed in both figures that rupture occurred within the adhesive layer confirming visual inspection

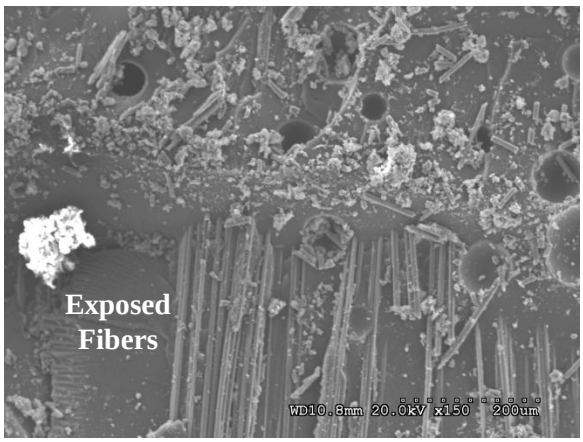

Figure 113. EP1 Debonded Laminate (x150)

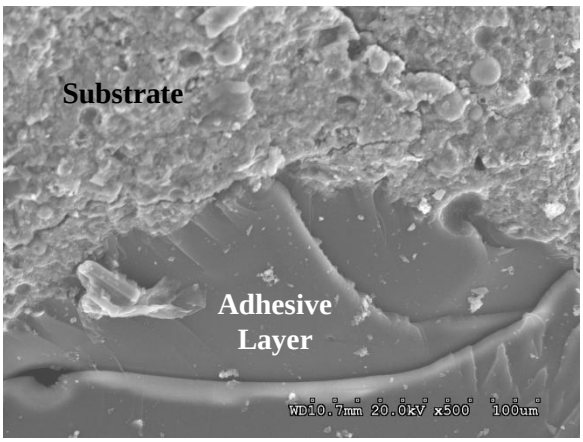

Figure 114. EP1 Debonded Laminate (x500)

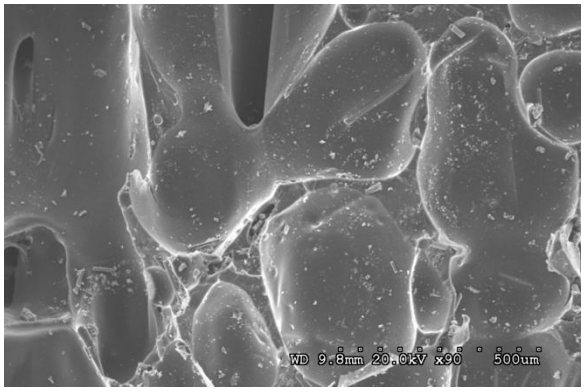

Figure 115. PU Debonded Laminate (x90)

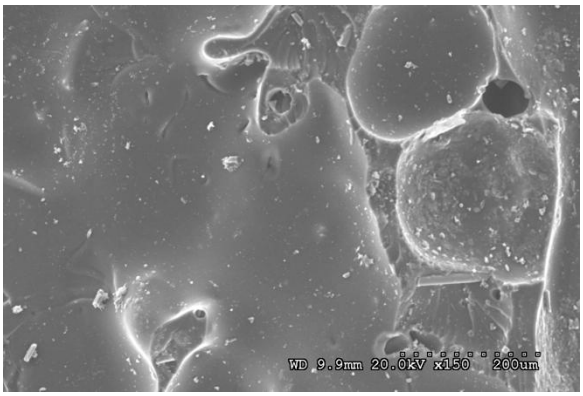

Figure 116. PU Debonded Laminate (x150)

5.2.1.7 Flexural Cracking

Along with differences in failure mode and bond behavior, the epoxy-type and polyurethane specimens possessed slightly different cracking patterns at failure. Crack patterns observed during testing can be found in Figure 117, Figure 118, Figure 119, and Figure 120. It was observed that the polyurethane specimen had a higher concentration of flexural cracks along the beam profile compared to epoxy-type specimens. Moreover, the polyurethane specimen exhibited increased propagation of cracks throughout the member cross-section. The increased presence of cracks in the polyurethane specimens could be attributed to the stiffness of the urethane primer layer used to adhere the CFRP laminate to concrete. That is, the urethane primer layer is significantly less stiff than either epoxy resin used. This would result in larger stress transfer lengths and reduced section stiffness.

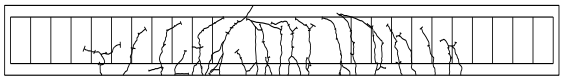

Figure 117. Unstrengthened Control Beam Crack Pattern

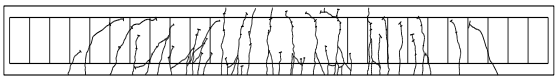

Figure 118. PU Strengthened Beam Crack Pattern

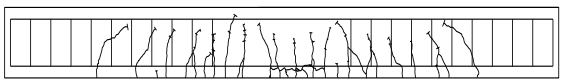

Figure 119. EP1 Strengthened Beam Crack Pattern

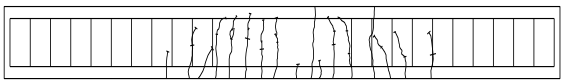

Figure 120. EP2 Strengthened Beam Crack Pattern

5.2.2 Cyclic Loading Results

A total of 6 beams were subjected to 2 million loading cycles; three of which would also receive controlled thermal conditioning. Figure 121 presents the displacement measurements acquired during the loading period. It should be noted that displacement results for the PU-C-E specimen are not shown. It was determined that a significant amount of sensor drift occurred during testing. Hence, these results have been omitted. Measurements reflect displacements recorded at the minimum (0.5 kip) and maximum (19.2 kip) load points; measurements account for settlement and softening of bearing pads.

All specimens endured the full 2 million cycles without failure. During loading, all epoxy matrix specimens exhibited a similar trend with increase in cycle number. During the first 100,000 load cycles the maximum deflection progressively increased. After the 100,000 cycle mark, the maximum deflections of epoxy-based specimens tend to converge to limiting values. The EP-type specimens exhibited consistent increases in total fatigue induced deflection compared to the initial cycle measurement. Total measured deflection increase ranged from 19.5% to 22.4% for EP-type specimens. Compared to the epoxy-type specimens, the initial deflection (cycle 1) of the PU-C specimen was higher. Yet, with an increasing number of load cycles, the mid-span deflection tended to increase only slightly; 3.8% increase from the first load cycle.

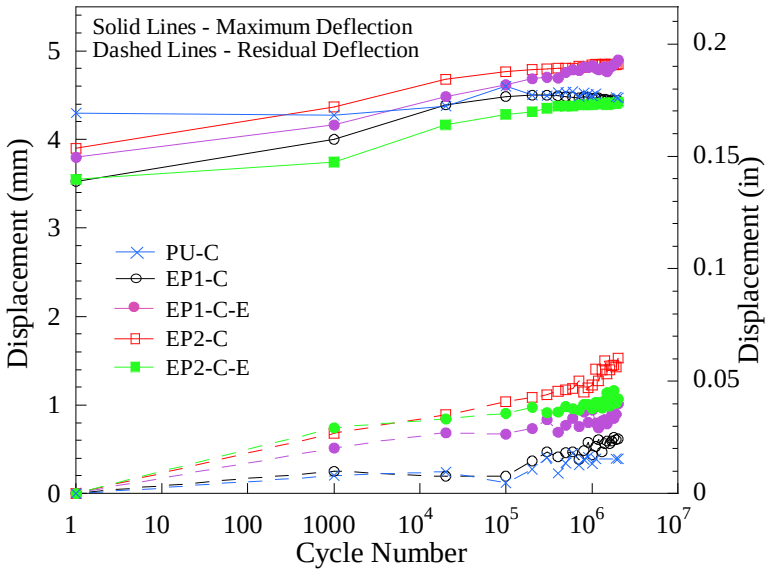

Figure 121. Mid-span Displacement History Plot

The residual deflections recorded during the cyclic loading procedure seemed to steadily accumulate with increasing number of load cycles. This steady increase was more dominant in the EP1-C-E specimen and both EP2 specimens. This would indicate that either concrete is undergoing creep/softening due to repeated loading or the bond is deteriorating with cycle number. Either one of these actions would lead to reduced deflection recovery after the load cycle reached maximum load. Yet, bond degradation is believed to be governing cause for the PU-C specimen, because the specimen displayed only a slight increase in maximum and residual deflection during the full cyclic loading procedure. If excess deflection were governed by concrete's tendency to creep and soften under repeated loading, the PU-C specimen would have displayed behavior similar to that of the EP-type specimens

The results presented in Figure 122-Figure 124 correspond to axial CFRP strain measurements recorded during the fatigue loading procedure; the maximum recorded strains are shown (solid lines). Gage positions 2, 3, and 4 are shown left to right respectively. Due to an error that occurred with the data acquisition system, data for the PU-C specimen was lost.

It is evident from Figure 122-Figure 124 that all specimens exposed to cyclic loading experienced increase in maximum mid-span strains (SG3 location) by the end of 2 million cycles, relative to the initial load cycle. Epoxy-based specimens showed a more continuous increase in mid-span strain with increase in cycle number; the rate of strain increase was also more significant in epoxy-based specimens. It was observed that epoxy-based specimens experienced maximum mid-span strain increases of 37.7%-45.3% from initial values. The converse can be observed for the polyurethane specimen (PU-F-T). The initial maximum mid-span strain value recorded was significantly higher than those recorded for epoxy specimens. Yet, the increase in strain over time, relative to the initial cycle, was much lower (8.5%).

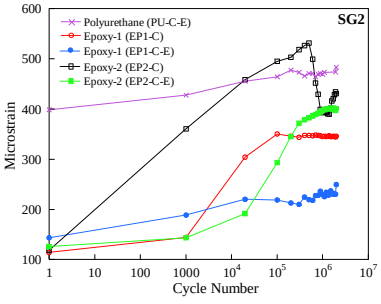

Figure 122. Strain Gage 2 History Plot

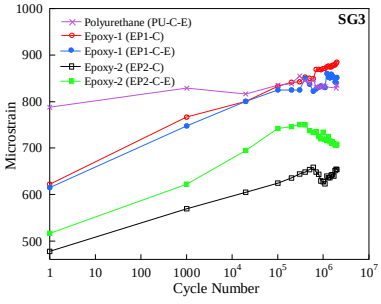

Figure 123. Strain Gage 3 History Plot

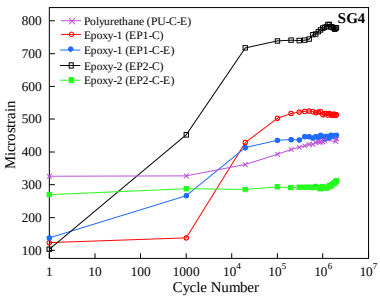

Figure 124. Strain Gage 4 History Plot

The maximum strains recorded at the quarter-span locations (SG2 and SG4) begin at relatively low values for all epoxy-based specimens. Yet, as the cycle number increases, some epoxy specimens experienced abrupt increases in strain values at quarter-span locations. Previous to conducting monotonic load tests, all specimens were inspected for areas of debonding on the CFRP laminate. Inspection was conducted using coin tapping and approximate debonding regions were marked and plotted (Figure 125). A correlation can be observed between specimens that experienced abrupt jumps in quarter-span strain and approximate debonding locations. The EP2-C specimen underwent the most significant increase in maximum quarter-span strain and was found to have a considerable amount of debonding in the vicinity of the quarter-span gages. This same result was observed at the SG2 and SG4 locations for the EP2-C-E and EP1-C specimens respectively. Although maximum quarter-span strains were initially higher than epoxy specimens, the polyurethane specimen (PU-C-E) only sustained 21.1% and 34.7% strain increases at the SG2 and SG3 locations respectively after 2 million fatigue cycles.

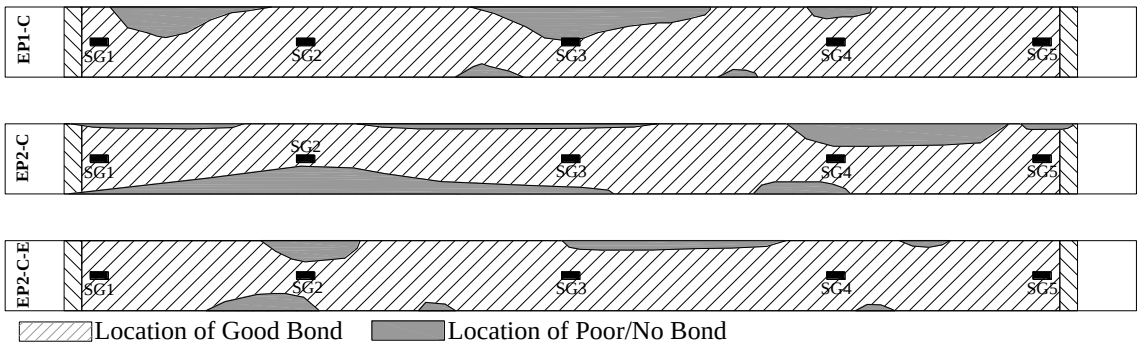

Figure 125. Approximate Debonding Locations

5.2.3 Ultimate Loading of Conditioned Specimens

Although the load-bearing capacity for all three specimens increased, the EP1-C and EP2-C specimens displayed a considerable reduction in deflection capacity at failure (refer to Figure 126). Furthermore, both epoxy based specimens achieved yield as failure occurred (EP2-C) or just previous to failure (EP1-C). There was also a significant decrease in the maximum achieved strain in the CFRP laminate for the epoxy based systems (refer to Table 19). The decrease in maximum strain, at the time of failure, indicates inefficient use of the CFRP in term of strength.

Cyclic loading seemed to have little effect of the polyurethane based CFRP system. Compared to the urethane baseline specimen, exposure to cyclic loading only caused a 4.4% reduction in load bearing capacity and a 14.5% reduction in ultimate deflection.

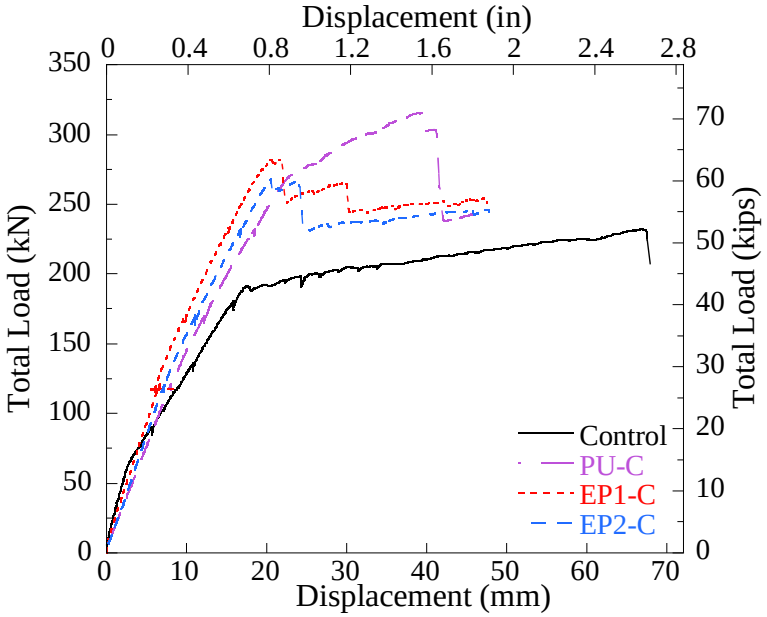

Figure 126. Ultimate Load-Displacement Plot - Cyclic Loading Specimens

There was not a considerable difference in the load-deflection behavior (Figure 127) between any of the specimens subjected to environmental conditioning. There was only a 11% difference between the ultimate deflections for the PU-E and EP2-E specimens; these specimens had the lowest and highest ultimate deflections respectively. Furthermore, the difference between the minimum and maximum observed ultimate loads was found to be 5.9%. Therefore there was no one CFRP system that significantly outperformed any other in term of post-conditioning flexural performance. It should be noted that the EP2 system achieved a considerable level of mid-span strain failure. Moreover, all specimens performed comparably or out performed baseline ultimate load, deflection, and strain achieved at failure (refer to Table 19).

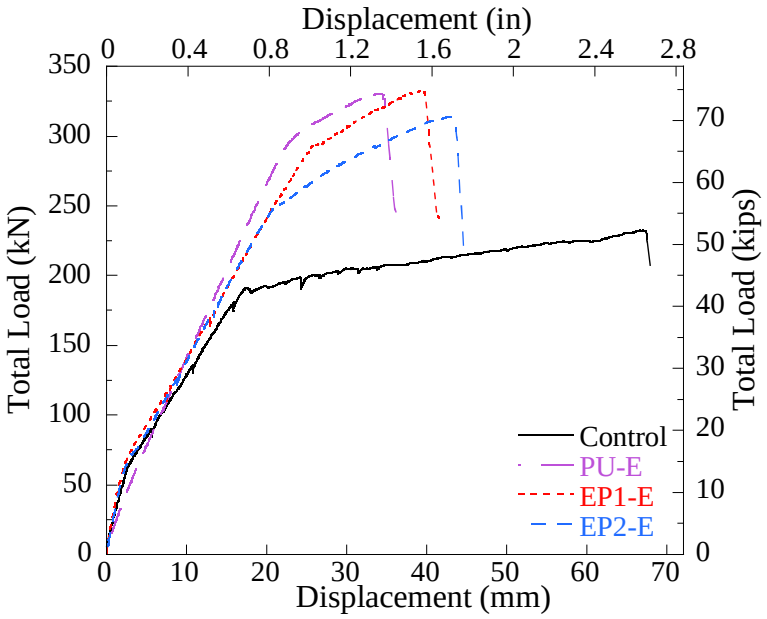

Figure 127. Ultimate Load-Displacement Plot – Environmentally Conditioned Loading Specimens

It can be observed form load-deflection results (Figure 128) of the C-E specimen types that there is no significant difference between the PU and EP1 strengthened beams. Although, the EP2-C-E specimen showed significant decreases in deflection, ultimate load, and mid-span strain achieved at failure (refer to values in Table 19).

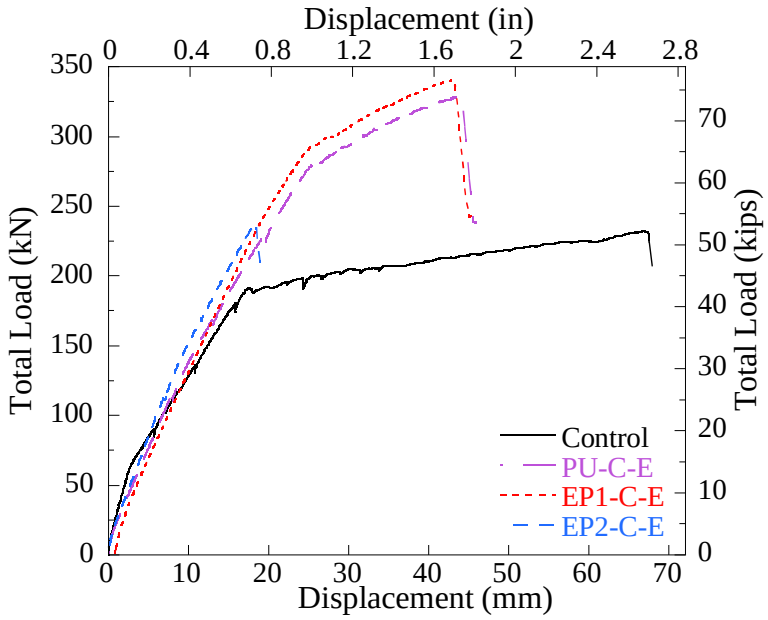

Figure 128. Ultimate Load-Displacement Plot - Cyclic Loading & Env. Conditioning Specimens

Table 19. Results Summary

Specimen ID	Yielding			Ultimate			Ductility Index	Failure Mode
	Load (kip)	*Deflection (in)*	*Mid-span Strain in CFRP (με)*	*Load (kip)*	*Deflection (in)*	*Mid-span Strain in CFRP (με)*		
Control	41.7	0.7	N/A	52.2	2.6	N/A	4.02	cc
PU	61.0	1.0	3669	74.3	1.8	3904	1.88	rup/db
EP1	63.2	0.8	3135	70.3	1.2	5382	1.44	db
EP2	60.9	0.9	3474	71.4	1.6	6829	1.81	db
PU-C	61.9	0.9	3408	71.0	1.6	5637	1.78	rup/db
EP1-C	63.4	0.8	3235	63.5	0.9	3403	1.06	db
EP2-C	60.2	0.8	3187	60.3	0.8	3194	1.00	db
PU-E	66.6	0.9	3269	74.3	1.4	5139	1.56	db
EP1-E	65.4	1.0	3176	74.8	1.5	6072	1.58	db
EP2-E	56.2	0.8	3505	70.5	1.7	7676	2.15	db
PU-C-E	63.1	1.0	3328	73.9	1.7	6174	1.73	db
EP1-C-E	65.2	0.9	3217	76.6	1.7	6785	1.76	db
EP2-C-E	-	-	-	53.1	0.7	2273	-	db

By examining the differences in flexural performance measures between conditioned and non-conditioned specimens, trends can be identified and conclusions can be drawn. Figure 129 depicts the percentage retention of strain, deflection, and ultimate load at failure compared to baseline results. Three key results can be identified:

- The PU system specimen performed consistently with changes in conditioning type. This was a result not observed in the epoxy-based systems.

- Fatigue loading appears to have a pronounced effect on flexural performance. This is mostly observed with the GE system specimens.

- Thermal conditioning does not appear to have an adverse effect on flexural performance.

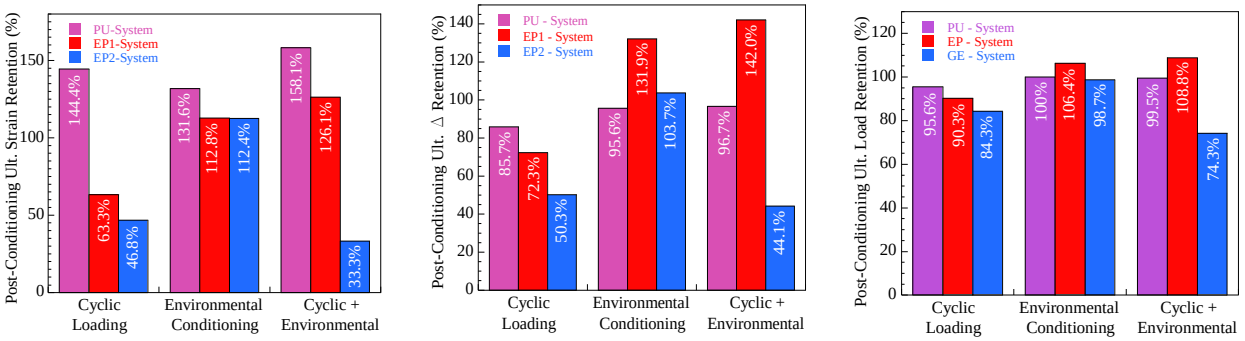

(a) Strain Retention % **(b) Deflection Retention %** **(c) Ultimate Load Retention %**

Figure 129. Quantitative Results

5.2.4 Scanning Electron Microscopy

Upon completion of thermal conditioning and cyclic/ultimate loading procedures, samples of debonded CFRP were taken from the EP1-C-E and PU-C-E specimens to be examined via SEM. The objective of SEM investigation was to detect viable degradation at the fiber/matrix level along with detailed observations of the composite surface that was bonded to concrete. Results were compared to respective samples that had been exposed to ambient air for the duration of this study.

Figure 130 and Figure 131 depict virgin samples of the EP1 CFRP laminate. In both figures it can be observed that there is good bond between the surrounding matrix and reinforcing fibers. Also the bulk epoxy matrix is seen to be very smooth. This is not that case in the micrographs seen in Figure 132 and Figure 133 which were taken from the EP1-C-E beam specimen. It is apparent that degradation occurred at the fiber/matrix level. Furthermore, there is a discernable difference in matrix morphology. The same type of degradation can be observed between Figure 134/Figure 135 and Figure 136/Figure 137 which depict the PU laminate type.

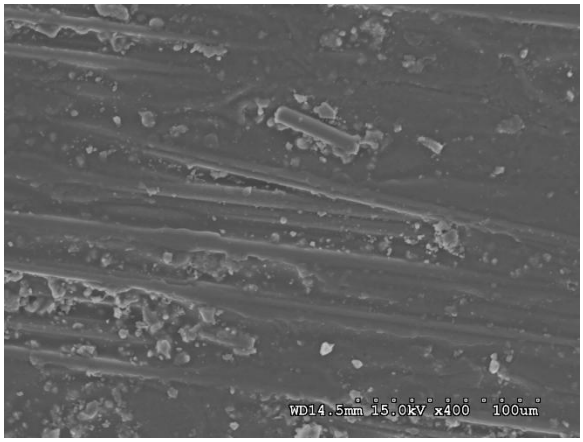

Figure 130. Unconditioned EP1 Fibers (x400)

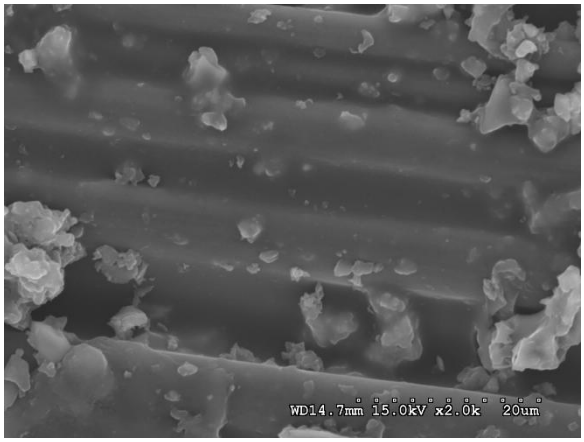

Figure 131. Unconditioned EP1 Fibers (x2000)

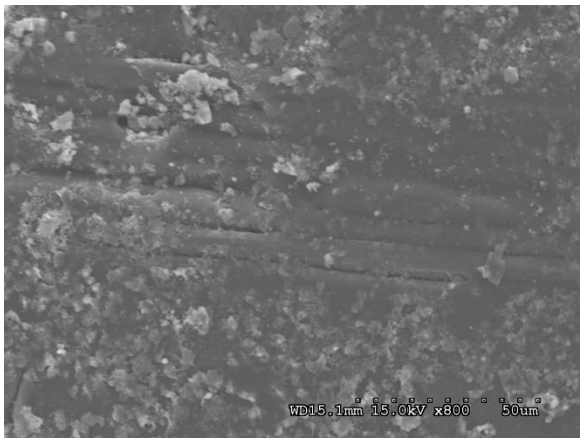

Figure 132. Conditioned EP1-C-E Fibers (x800)

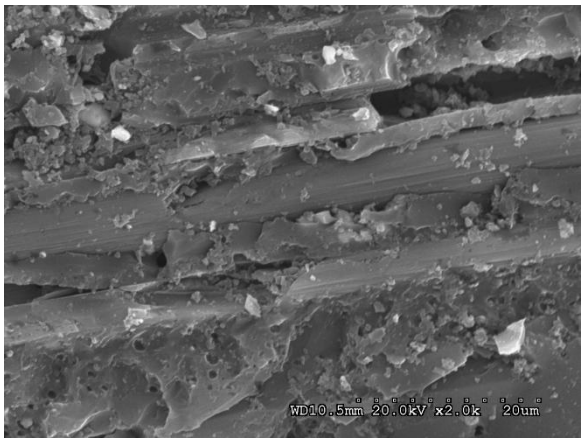

Figure 133. Conditioned EP1-C-E Fibers (x2000)

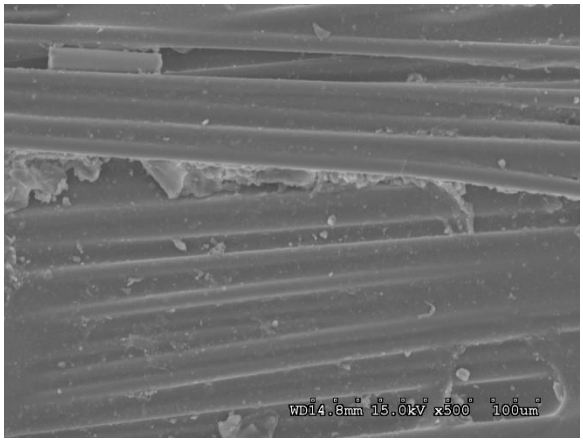

Figure 134. Unconditioned PU Fibers (x500)

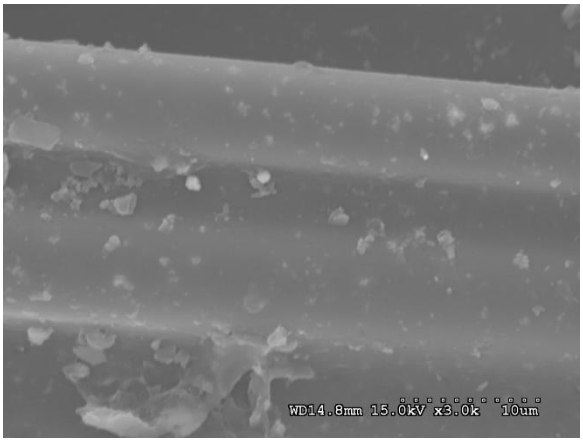

Figure 135. Unconditioned PU Fibers (x3000)

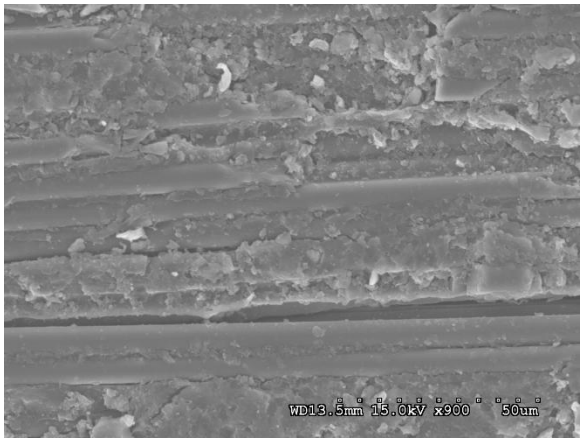

Figure 136. Conditioned PU-C-E Fibers (x900)

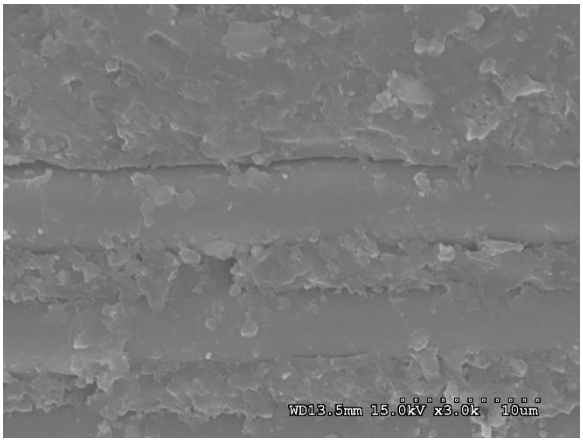

Figure 137. Conditioned PU-C-E Fibers (x3000)

5.2.5 Bond Pull-off Tests

Upon completion of the conditioning period, bond pull-off test locations were prepared and tested. Pull-off testing was performed using a James Instruments Inc. *007 James Bond Tester* fixture. This fixture conforms to the current ASTM standard for such a test.

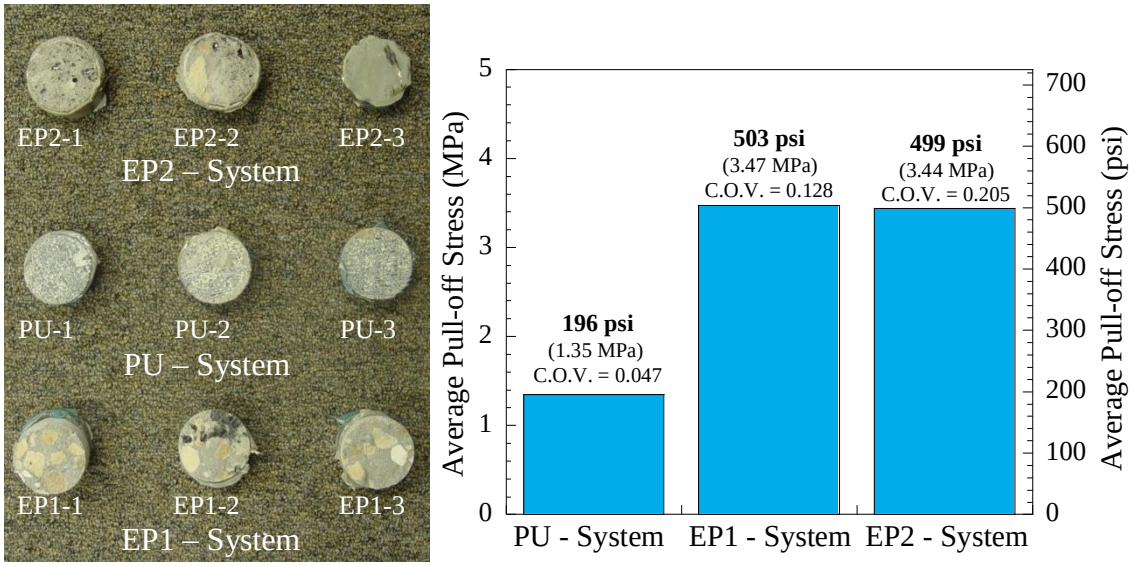

(a) Failure Surfaces (b) Average Pull-off Stress

Figure 138. FDOT Bond Pull-off Results

The dominant mode of failure observed, in the epoxy-based systems, was rupture of disc specimen within the concrete layer. This indicates a good bond between FRP and concrete, that is a sound FRP/concrete interface layer. Specimen A3 was observed to fail in the top epoxy layer of the pull-off specimen. This means that the testing disc was pulled from the CFRP substrate leaving the CFRP material remaining adhered to concrete. Based on the results from specimens A1 and A2, pull-off specimen A3 was either not prepared properly or that poor bond existed between the test disc and the CFRP substrate.

All PU specimens exhibited a cohesive failure mode occurring within the urethane adhesive layer. The pull-off stress at failure, although low compared to the epoxy systems, and the failure surface for this matrix system were very consistent compared to the epoxy based systems.

6. CONCLUSIONS AND RECOMMENDATIONS

This thesis presented experimental results related to the characterization of polyurethane matrix carbon fiber composites for strengthening reinforced concrete structures. There were two main groups of specimens tested; small-scale and large-scale specimens. Small-scale specimens were used to investigate both component and bond durability. Large-scale tests were used to characterize the system response of beams strengthened with PU composite laminates and how they compared to epoxy matrix/adhesive composites.

The conclusions are drawn from experimental tests will be presented in three groups: small-scale test conclusions (or durability performance conclusions), large-scale test conclusions, and general conclusions. Based on the conclusions, design recommendations will be made along with installation recommendations. Finally, insight will given as to where further investigation on the use of PU composites for strengthening concrete should be concentrated.

6.1 Conclusions on Durability

Based on results from environmentally conditioned tensile coupons and small-scale beams, the following conclusions can be drawn:

- Given pre- and post-test SEM results, the polyurethane matrix system appeared to be sensitive to the aqueous conditioning environments i.e. H_2O, seawater, and the concrete leachate.

- The dry heat conditioning environment did not have any adverse effect on the PU composite system; average elastic modulus and ultimate strength actually tended to increase with duration of conditioning.

- Ambient exposure (UV) caused a significant amount of damage at the fiber/matrix level. Damage was typically found in the form of mirco-cracking at the fiber/matrix bondline and crack initiation from micro-voids. Yet, average tensile properties (at 60 days) did not seem to be deviate substantially from baseline results.

- Although some degradation was observed in material properties, conditioning did not alter the primary debonding failure mechanism (shear rupture within the adhesive layer) of strengthened beams.

- The polyurethane adhesive was not significantly affected by environmental conditioning other than that of the ambient outdoor environment. Degradation is attributed to exposure to UV light.

6.2 Conclusions on System Performance

- Members strengthened with the PU composite system displayed a considerable level of consistency in the following areas:

1. Ductility (although reduced from the RC control)

2. Load bearing capacity at failure

3. Failure mode

4. Post-conditioning bond integrity

- The consistency of results with the PU system indicates that both the cyclic loading and environmental conditioning had little or no adverse effect on the strengthening ability of this system.

- Due to a softer adhesive interface, flexural members strengthened with CFRP laminates bonded with PU adhesives are expected to undergo an increased cracking.

6.3 General Conclusions

- The governing mode of flexural failure for members strengthen with the PU systems was debonding occurring within the adhesive layer

- Mirco-cracking in the PU matrix radiating from micro-voids formed during curing tends to propagate and connect under applied stress.

6.4 Design and Construction Recommendations

- Upon removing the PU system from the sealed package, the polyurethane matrix begins catalyzing with moisture in the air. Therefore careful consideration must be taken during installation to incorporate the relative humidity of the application environment.

- During the matrix hardening process of the polyurethane system, carbon dioxide is released as a reaction byproduct. Therefore periodic rolling of the fiber after installation must be done to avoid formation of voids in the laminate.

6.5 Recommendation for Future Work

Significant attention should be paid to the bond behavior of PU adhesives to concrete. The work presented in this thesis showed that fundamental debonding mechanism of externally bonded PU-CFRPs is via shear rupture of the PU adhesive interface. Therefore it is recommended that the shear bond strength of PU adhesives to concrete be investigated along with the development of a bond model to predict bond failure. Further study of the material and system performance of PU-CFRPs should also be investigated for resistance to mechanical and environmental loading.

APPENDIX A - TENSILE SPECIMENS

A1 H20 Conditioning Tensile Specimens

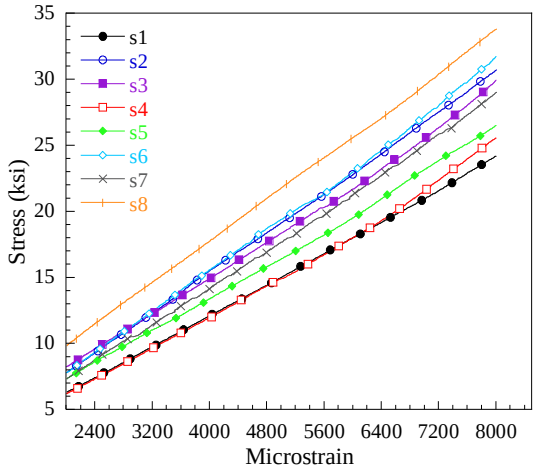

Figure 139. H2O-30 Tensile Samples – Stress/Strain Behavior

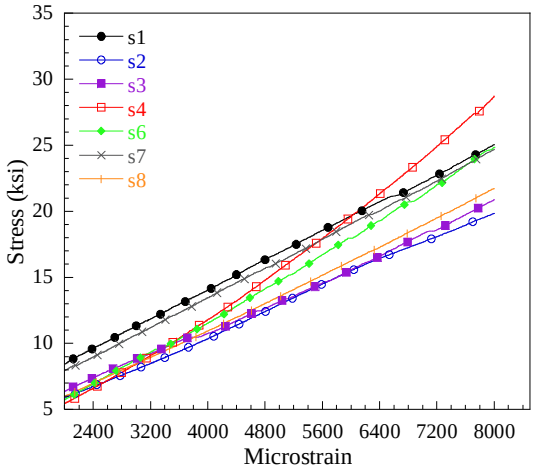

Figure 140. H2O-60 Tensile Samples – Stress/Strain Behavior

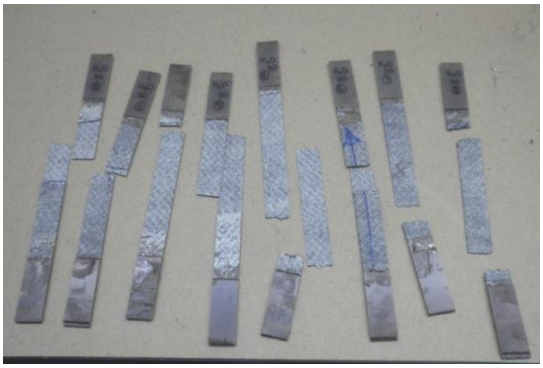

Figure 141. H2O-30 Tensile Samples – Test Photos

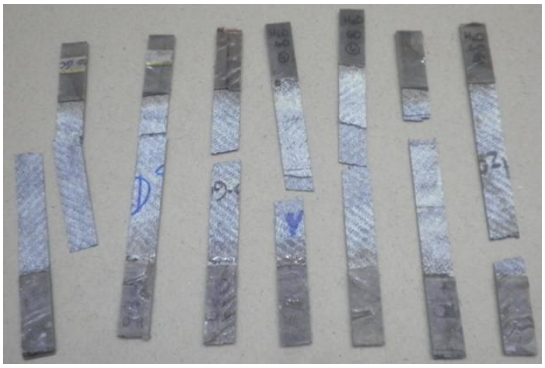

Figure 142. H2O-60 Tensile Samples – Test Photos

Table 20. H2O-30 Tensile Samples – Results Summary

Sample ID	Max Stress (ksi)	Max Load (kip)	E (ksi)
S1	35.9	2.4	2961
S2	35.9	2.1	3787
S3	36.7	2.3	3512
S4	37.7	2.4	3149
S5	39.8	2.5	3893
S6	43.6	2.4	3557
S7	47.8	2.5	3940
Average	39.6	2.4	3476
SD	4.62	0.155	296

Table 21. H2O-60 Tensile Samples – Results Summary

Sample ID	Max Stress (ksi)	Max Load (lbs)	E (ksi)
S1	39.9	2.6	2746
S2	34.8	2.5	2394
S3	28.7	2.3	2352
S6	29.5	2.3	3150
S7	33.1	2.4	2778
S8	33.1	2.6	2612
Average	33.2	2.4	2684
SD	4.03	0.138	293

A2 Leachate (LECH) Conditioned Tensile Specimens

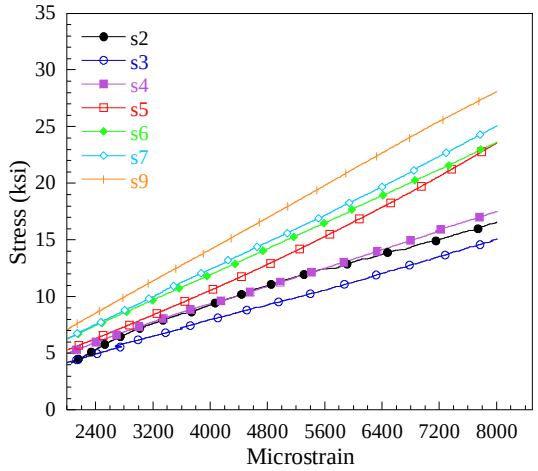

Figure 143. LECH-30 Tensile Samples – Stress/Strain Behavior

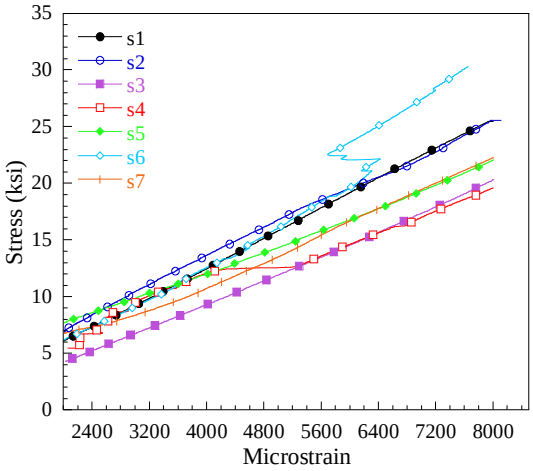

Figure 144. LECH -60 Tensile Samples – Stress/Strain Behavior

Figure 145. LECH -30 Tensile Samples – Test Photos

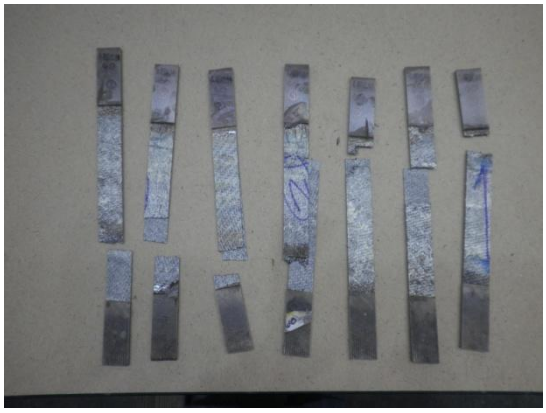

Figure 146. LECH -60 Tensile Samples – Test Photos

Table 22. LECH -30 Tensile Samples – Results Summary

Sample ID	Max Stress (ksi)	Max Load (kip)	E (ksi)
S2	23.1	1.7	2021
S3	23.3	1.8	1771
S4	30.6	2.2	2042
S5	33.8	2.3	3017
S6	35.1	2.1	2878
S7	42.3	2.5	3067
S9	40.5	2.4	3528
Average	32.7	2.2	2466
SD	7.60	0.314	666

Table 23. LECH -60 Tensile Samples – Results Summary

Sample ID	Max Stress (ksi)	Max Load (kip)	E (ksi)
S1	30.4	2.2	3295
S2	33.3	2.3	3028
S3	35.3	2.5	2629
S4	26.3	1.9	2491
S5	33.3	2.5	2363
S6	32.4	2.5	3417
S7	28.4	2.2	2735
Average	31.3	2.3	2871
SD	3.12	0.207	404

A3 Seawater (SEA) Conditioned Tensile Specimens

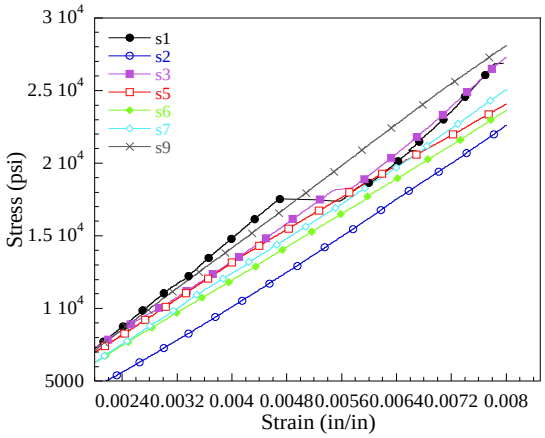

Figure 147. SEA-30 Tensile Samples – Stress/Strain Behavior

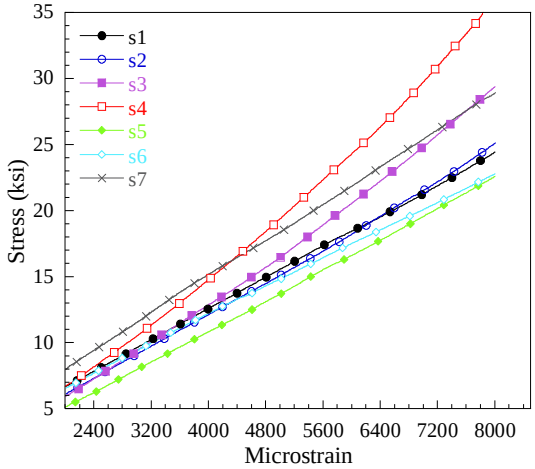

Figure 148. SEA-60 Tensile Samples – Stress/Strain Behavior

Figure 149. SEA-30 Tensile Samples – Test Photos

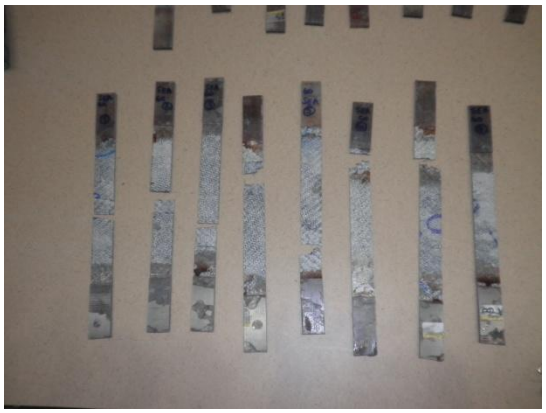

Figure 150. SEA-60 Tensile Samples – Test Photos

Table 24. SEA-30 Tensile Samples – Results Summary

Sample ID	Max Stress (ksi)	Max Load (kip)	E (ksi)
S1	35.4	2.3	2989
S2	25.6	1.6	3024
S3	39.2	2.4	3237
S5	38.1	2.3	2856
S6	35.1	2.1	2878
S7	42.3	2.5	3083
S9	40.5	2.4	3518
Average	36.6	2.2	3084
SD	5.50	0.312	230

Table 25. SEA-60 Tensile Samples – Results Summary

Sample ID	Max Stress (ksi)	Max Load (kip)	E (ksi)
S1	37.3	2.5	2930
S2	34.3	2.1	3114
S3	38.4	2.5	3875
S4	35.0	2.1	4836
S5	42.6	2.7	2898
S6	36.5	2.3	2683
S7	42.2	2.5	3459
Average	38.0	2.4	3399
SD	3.26	0.220	748

A4 Dry Heat (DRY) Conditioned Tensile Specimens

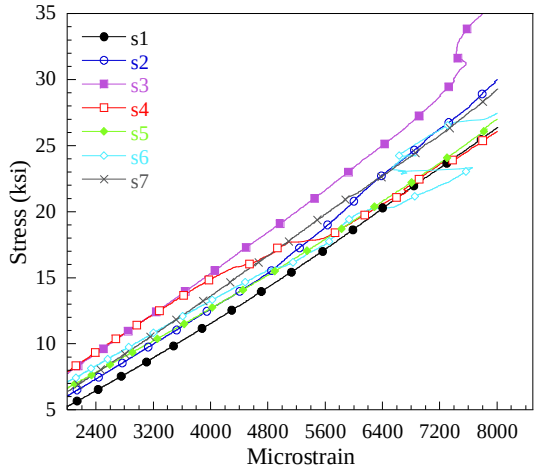

Figure 151. DRY-30 Tensile Samples – Stress/Strain Behavior

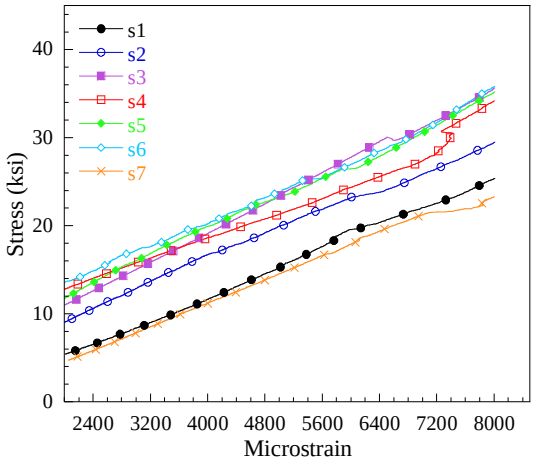

Figure 152. DRY-60 Tensile Samples – Stress/Strain Behavior

Figure 153. DRY-30 Tensile Samples – Test Photos

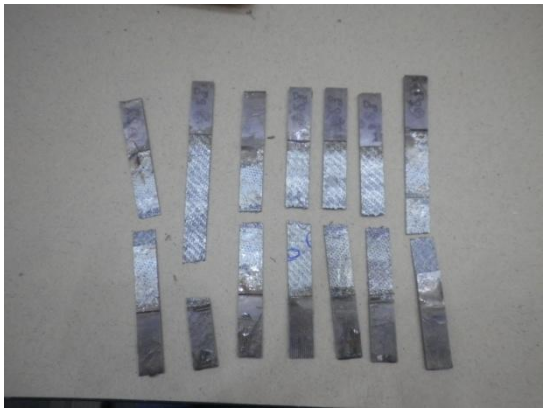

Figure 154. DRY-60 Tensile Samples – Test Photos

Table 26. DRY-30 Tensile Samples – Results Summary

Sample ID	Max Stress (ksi)	Max Load (kip)	E (ksi)
S1	44.8	2.7	3521
S2	45.7	2.8	3959
S3	39.4	2.5	3959
S4	40.1	2.5	2833
S5	39.4	2.3	3317
S6	38.7	2.6	2898
S7	39.7	2.3	3777
Average	41.1	2.5	3414
SD	2.86	0.186	471

Table 27. DRY-60 Tensile Samples – Results Summary

Sample ID	Max Stress (ksi)	Max Load (kip)	E (ksi)
S1	41.7	2.6	3411
S2	46.2	2.6	3312
S3	40.8	2.7	4097
S4	39.1	2.6	3285
S5	44.4	2.7	3694
S6	45.6	2.6	3545
S7	40.2	2.6	3233
Average	42.6	2.6	3557
SD	2.80	0.072	304

A5 Ambient (AMB) Conditioning Tensile Specimens

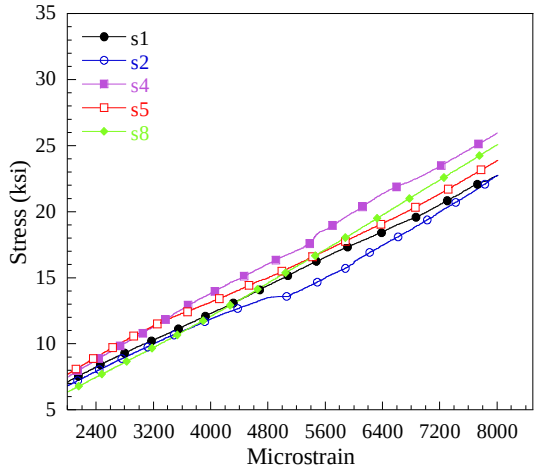

Figure 155. AMB-30 Tensile Samples – Stress/Strain Behavior

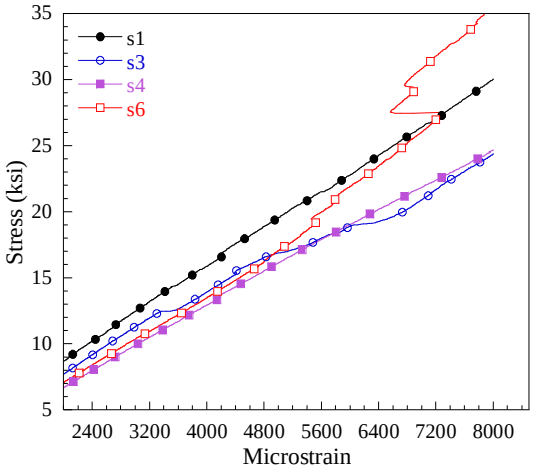

Figure 156. AMB-60 Tensile Samples – Stress/Strain Behavior

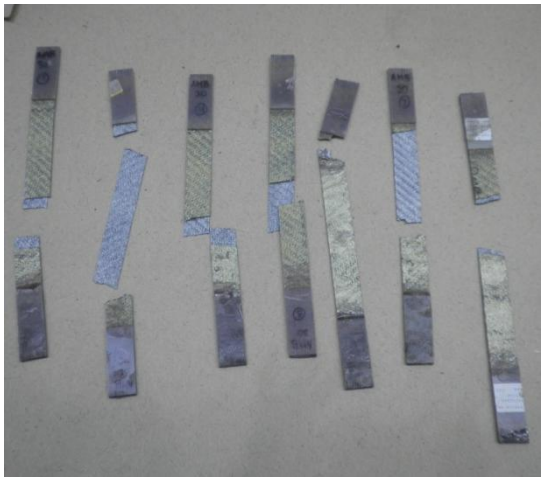

Figure 157. AMB-30 Tensile Samples – Test Photos

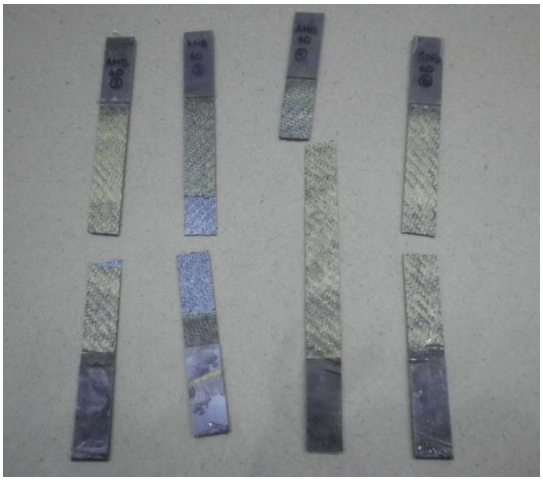

Figure 158. AMB-60 Tensile Samples – Test Photos

Table 28. AMB-30 Tensile Samples – Results Summary

Sample ID	Max Stress (ksi)	Max Load (kip)	E (ksi)
S1	38.0	2.5	2578
S2	33.8	2.5	2486
S4	38.6	2.6	3062
S5	35.7	2.6	2561
S8	35.7	2.7	3126
Average	36.4	2.6	2763
SD	1.96	0.089	305

Table 29. AMB -60 Tensile Samples – Results Summary

Sample ID	Max Stress (ksi)	Max Load (kip)	E (ksi)
S1	36.7	2.4	3504
S3	39.8	2.5	2809
S4	34.0	2.2	3002
S6	37.8	2.5	3828
Average	37.1	2.4	3286
SD	2.41	0.157	465

APPENDIX B - SMALL-SCALE BEAM SPECIMEN DATA AND PHOTOS

B1 Unconditioned Control Beam Specimens

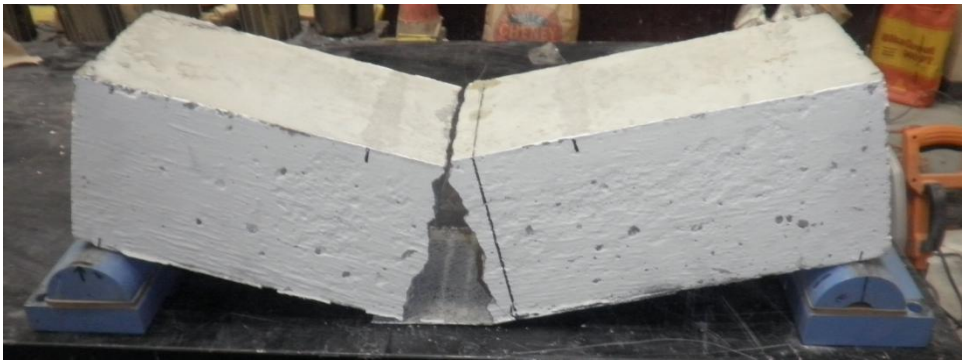

(a) Specimen at Failure

(b) Concrete Substrate

(c) Debonded Fiber

Figure 159. Beam C-30-1

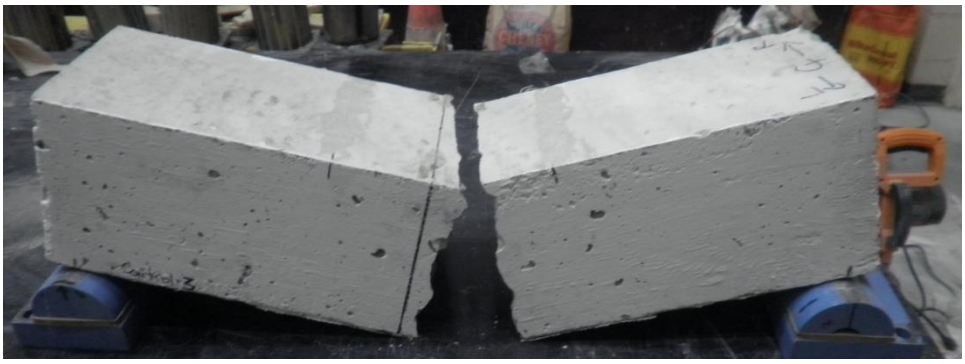

(a) Specimen at Failure

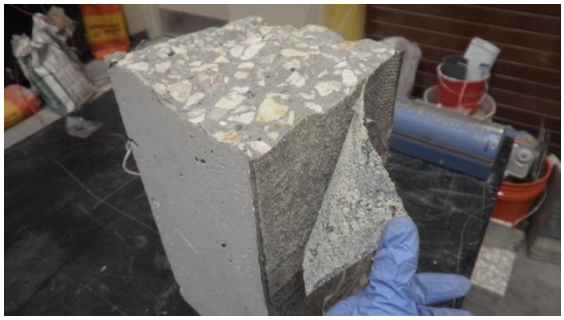

(b) Concrete Substrate **(c) Debonded Fiber**

Figure 160. Beam C-30-2

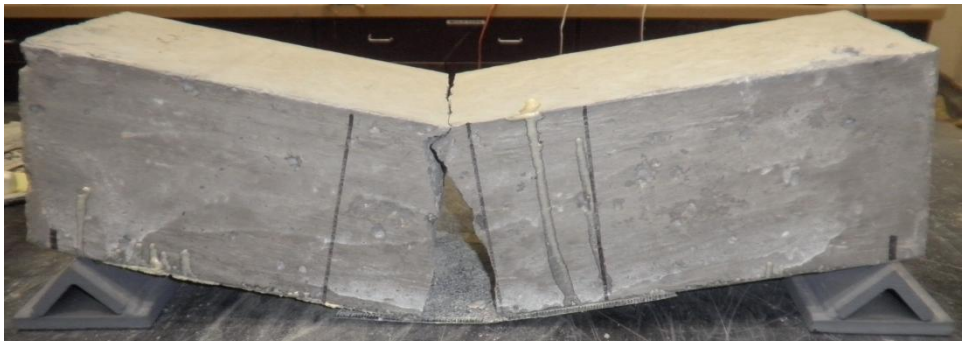

(a) Specimen at Failure

(b) Concrete Substrate **(c) Debonded Fiber**

Figure 161. Beam C-60-1

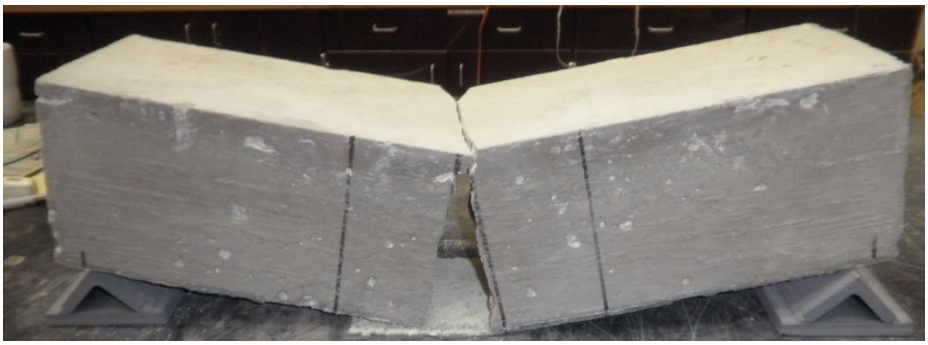

(a) Specimen at Failure

(b) Concrete Substrate

(c) Debonded Fiber

Figure 162. Beam C-60-2

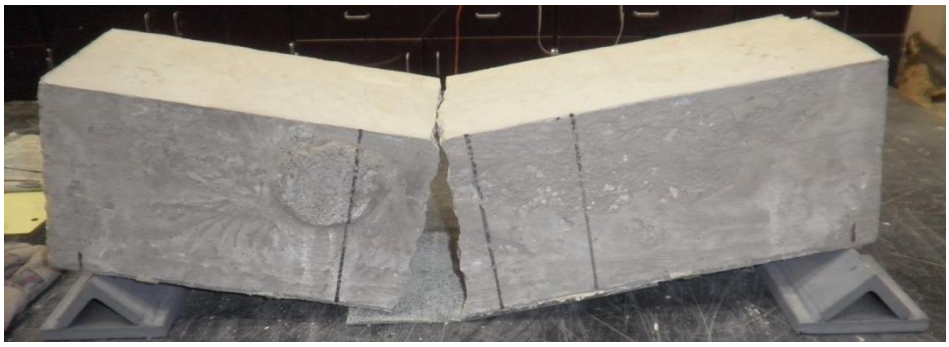

(a) Specimen at Failure

(b) Concrete Substrate

(c) Debonded Fiber

Figure 163. Beam C-60-3

B2 H_2O Conditioning Beam Specimens

Table 30. H2O-30 Beam Test Results Summary

ID	Cracking Load (kip)	Pre-crack Stiffness (kip/in)	Post-crack Load (kip)	Post-crack Deflection (in)	Post-crack Stiffness (kip/in)	Max Strain
H2O-30-1	7.50	370	8.71	0.093	92	6787
H2O-30-2	7.39	348	9.07	0.090	93	8924
H2O-30-3	7.23	339	6.42	0.065	79	2633
Average	7.37	353	8.07	0.08	88	6115
Standard Dev.	0.133	16.0	1.440	0.016	7.99	3199
C.O.V.	0.0180	0.0453	0.1786	0.1877	0.0907	0.5232

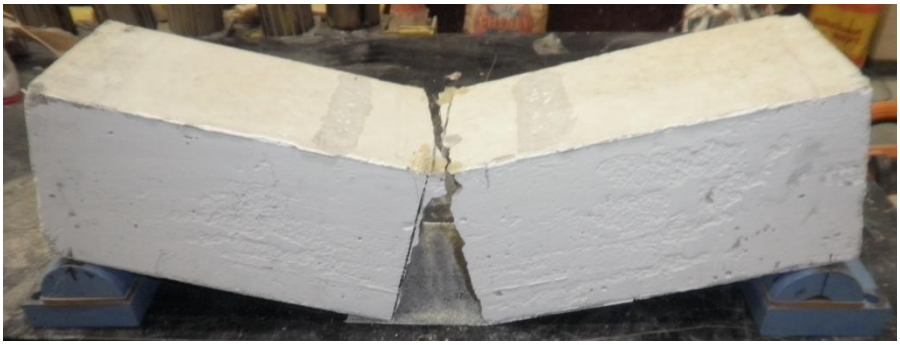

(a) Specimen at Failure

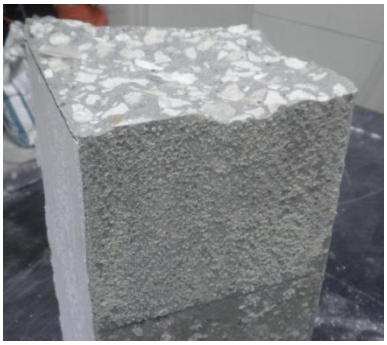

(b) Concrete Substrate

(c) Debonded Laminate

Figure 164. Beam H2O-30-1

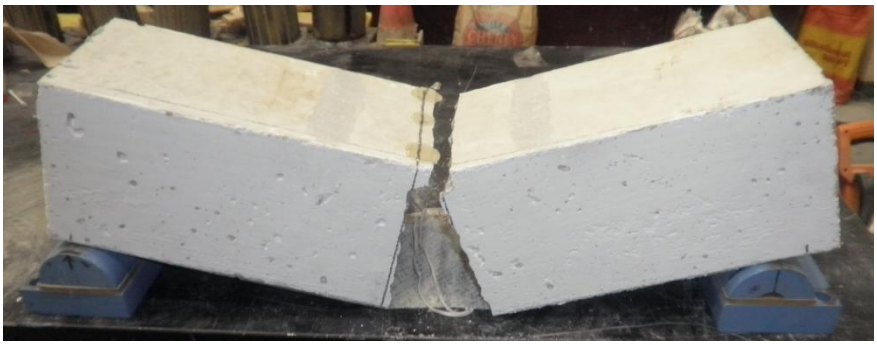

(a) Specimen at Failure

(b) Concrete Substrate

(c) Debonded Laminate

Figure 165. Beam H2O-30-2

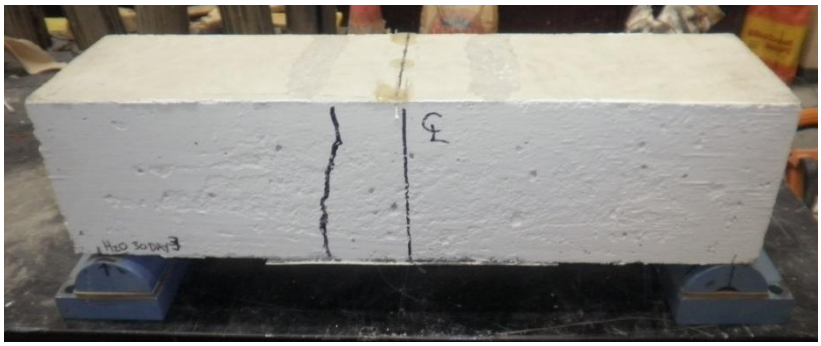

(a) Specimen at Failure

(b) Concrete Substrate

(c) Debonded Laminate

Figure 166. Beam H2O-30-3

Table 31. H2O-60 Beam Test Results Summary

Specimen ID	Cracking Load (kip)	Pre-crack Stiffness (kip/in)	Post-crack Load (kip)	Post-crack Deflection (in)	Post-crack Stiffness (kip/in)	Max Strain
H2O-60-1	7.52	429	8.69	0.070	114	9634
H2O-60-2	7.80	403	8.20	0.067	86	7894
H2O-60-3	7.61	396	n/a	0.041	n/a	908
Average	7.64	410	8.44	0.06	100	6145
SD	0.146	17.3	0.348	0.016	20.17	4619
COV	0.0191	0.0423	0.0412	0.2686	0.2020	0.7516

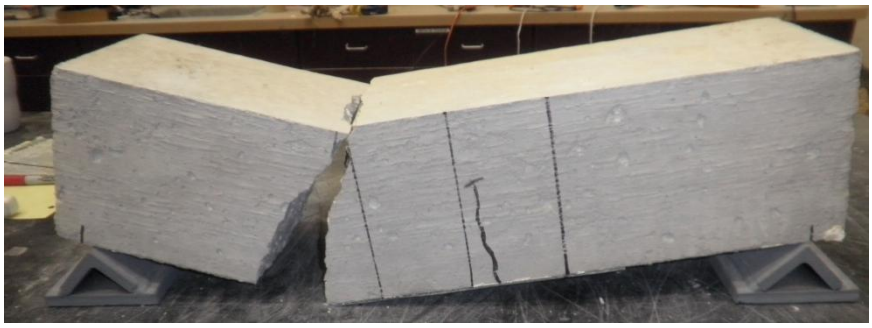

Figure 167. Beam H2O-60-1

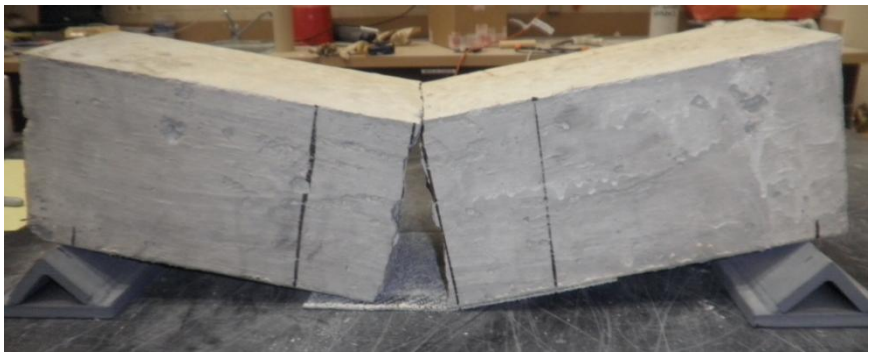

(a) Specimen at Failure

(b) Concrete Substrate

(c) Debonded Laminate

Figure 168. Beam H2O-60-2

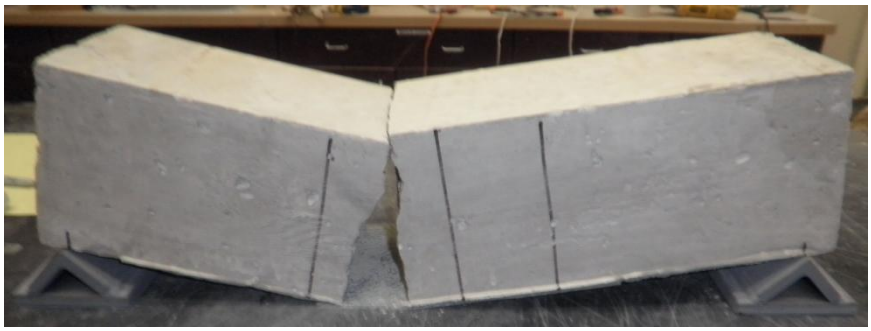

(a) Specimen at Failure

(b) Concrete Substrate

(c) Debonded Laminate

Figure 169. Beam H2O-60-3

B3 Concrete Leachate (LECH) Conditioning Beam Specimens

Table 32. LECH-30 Beam Test Results Summary

ID	Cracking Load (kip)	Pre-crack Stiffness (kip/in)	Post-crack Load (kip)	Post-crack Deflection (in)	Post-crack Stiffness (kip/in)	Max Strain
LECH-30-1	7.72	235	4.93	0.056	N/A	164
LECH-30-2	6.76	258	6.07	0.078	79	1745
Average	7.24	246	5.50	0.07	79	955
Standard Dev.	0.679	15.9	0.810	0.016	N/A	1118
C.O.V.	0.0938	0.0645	0.1473	0.2374	N/A	1.1713

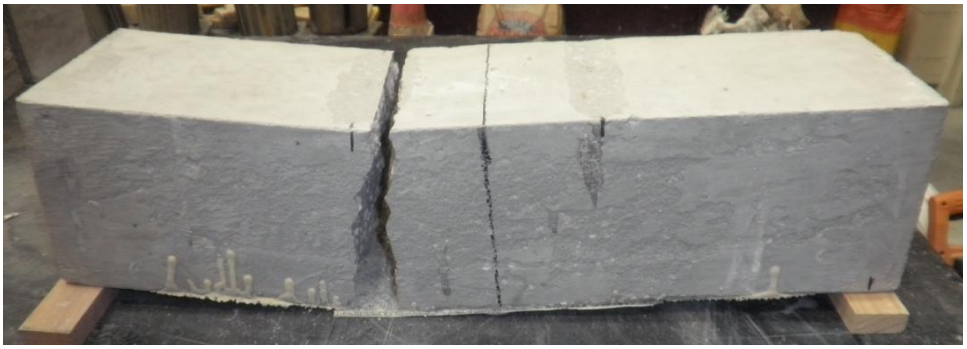

(a) Specimen at Failure

(b) Concrete Substrate

(c) Debonded Laminate

Figure 170. Beam LECH-30-1

(a) Specimen at Failure

(b) Concrete Substrate

(c) Debonded Laminate

Figure 171. Beam LECH-30-2

Table 33. LECH-60 Beam Test Results Summary

Specimen ID	Cracking Load (kip)	Pre-crack Stiffness (kip/in)	Post-crack Load (kip)	Post-crack Deflection (in)	Post-crack Stiffness (kip/in)	Max Strain
LECH-60-1	6.52	363	8.92	0.063	124	4984
LECH-60-2	7.81	322	7.59	0.062	95	5565
Average	7.16	343	8.26	0.06	110	5274
SD	0.912	29.0	0.940	0.062	20.31	411
COV	0.1273	0.0845	0.1138	0.9948	0.1849	0.0779

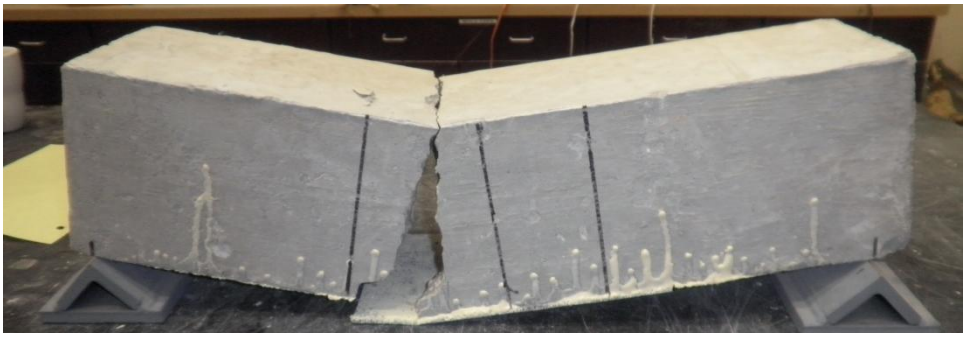

(a) Specimen at Failure

(b) Concrete Substrate

(c) Debonded Laminate

Figure 172. Beam LECH-60-1

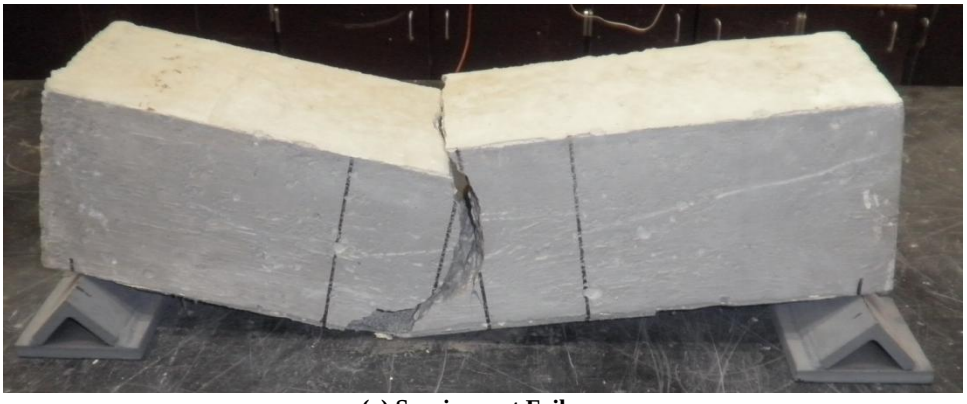

(a) Specimen at Failure

(b) Concrete Substrate

(c) Debonded Laminate

Figure 173. Beam LECH-60-2

B4 Seawater (SEA) Conditioning Beam Specimens

Table 34. SEA-30 Beam Test Results Summary

ID	Cracking Load (kip)	Pre-crack Stiffness (kip/in)	Post-crack Load (kip)	Post-crack Deflection (in)	Post-crack Stiffness (kip/in)	Max Strain
SEA-30-1	8.41	364	7.87	0.073	104	6860
SEA-30-2	8.01	304	8.13	0.063	127	4133
SEA-30-3	7.05	302	7.45	0.054	126	1906
Average	7.83	323	7.82	0.06	119	4299
Standard Dev.	0.698	35.2	0.344	0.009	13.25	2481
C.O.V.	0.0892	0.1089	0.0440	0.1475	0.1113	0.5771

(a) Specimen at Failure

(b) Concrete Substrate

(c) Debonded Laminate

Figure 174. Beam SEA-30-1

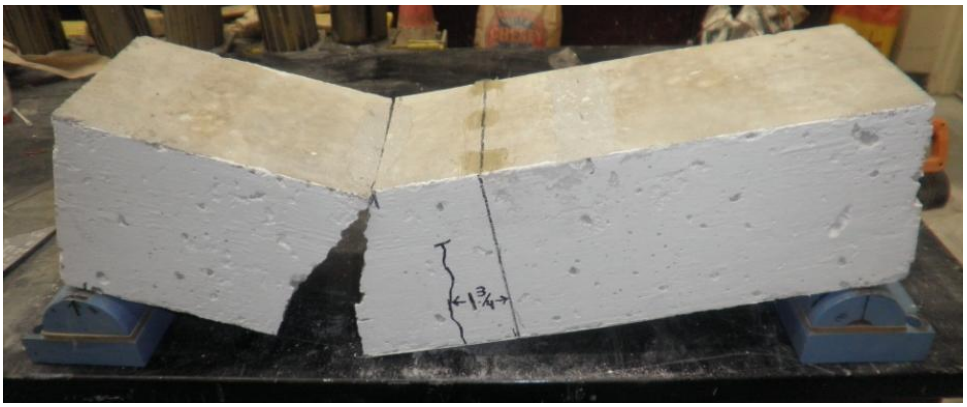

(a) Specimen at Failure

Figure 175. Beam SEA-30-2

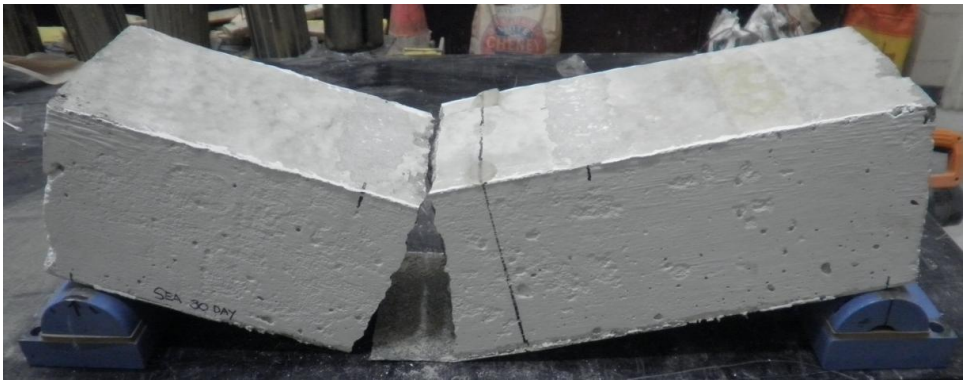

(a) Specimen at Failure

(b) Concrete Substrate

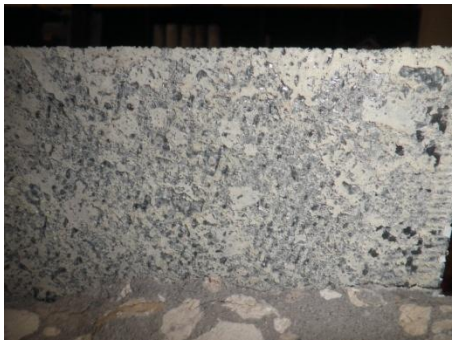

(c) Debonded Laminate

Figure 176. Beam SEA-30-3

Table 35. SEA-60 Beam Test Results Summary

Specimen ID	Cracking Load (kip)	Pre-crack Stiffness (kip/in)	Post-crack Load (kip)	Post-crack Deflection (in)	Post-crack Stiffness (kip/in)	Max Strain
SEA-60-1	8.62	444	11.12	0.090	136	11168
SEA-60-2	9.31	376	9.03	0.074	128	2534
SEA-60-3	8.38	406	7.73	0.067	121	5227
Average	8.77	409	9.29	0.08	129	6310
Standard Dev.	0.484	34.1	1.710	0.012	7.90	4418
C.O.V.	0.0551	0.0834	0.1840	0.1514	0.0615	0.7001

Figure 177. Beam SEA-60-1

Figure 178. Beam SEA-60-2

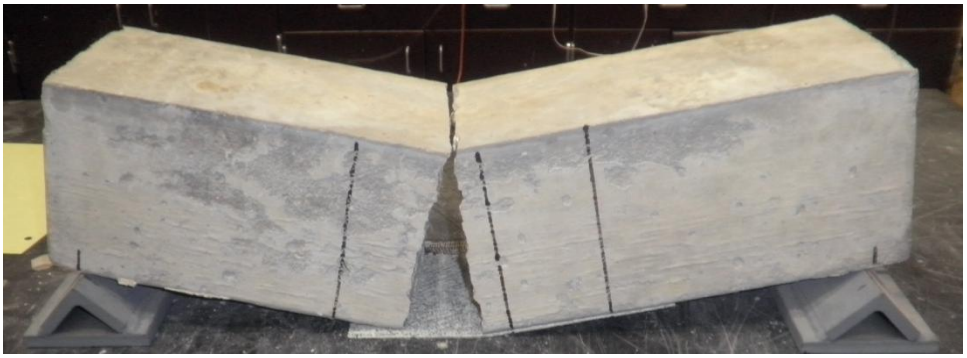

(a) Specimen at Failure

(b) Concrete Substrate

(c) Debonded Laminate

Figure 179. Beam SEA-60-3

B5 Dry Heat (DRY) Conditioning Beam Specimens

Table 36. DRY-30 Beam Test Results Summary

ID	Cracking Load (kip)	Pre-crack Stiffness (kip/in)	Post-crack Load (kip)	Post-crack Deflection (in)	Post-crack Stiffness (kip/in)	Max Strain
DRY-30-1	7.87	278	7.57	0.065	131	5837
DRY-30-2	7.62	307	7.91	0.086	89	5512
DRY-30-3	7.27	286	8.36	0.088	114	5873
Average	7.59	290	7.95	0.08	111	5741
Standard Dev.	0.301	14.8	0.396	0.013	21.06	199
C.O.V.	0.0397	0.0510	0.0498	0.1607	0.1893	0.0346

(a) Specimen at Failure

(b) Concrete Substrate

(c) Debonded Laminate

Figure 180. Beam DRY-30-1

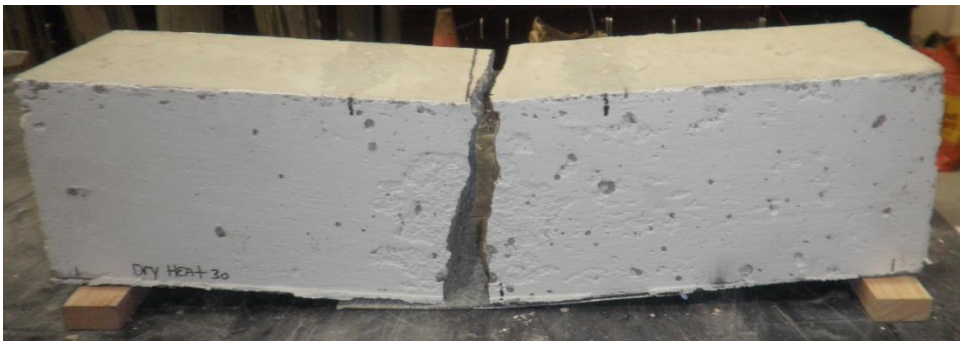

(a) Specimen at Failure

(b) Concrete Substrate

(c) Debonded Laminate

Figure 181. Beam DRY-30-2

(a) Specimen at Failure

(b) Concrete Substrate

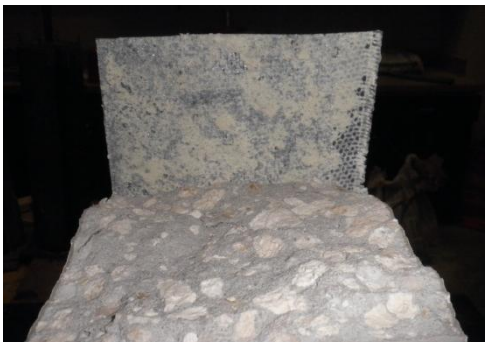

(c) Debonded Laminate

Figure 182. Beam DRY-30-3

Table 37. DRY-60 Beam Test Results Summary

ID	Cracking Load (kip)	Pre-crack Stiffness (kip/in)	Post-crack Load (kip)	Post-crack Deflection (in)	Post-crack Stiffness (kip/in)	Max Strain
DRY-60-1	7.33	325	9.43	0.076	119	9546
DRY-60-2	7.63	356	7.47	0.058	131	3278
DRY-60-3	7.56	306	6.81	0.059	92	2431
Average	7.51	329	7.91	0.06	114	5085
Standard Dev.	0.155	25.2	1.364	0.010	20.40	3886
C.O.V.	0.0207	0.0766	0.1725	0.1607	0.1790	0.7643

(a) Specimen at Failure

(b) Concrete Substrate

(c) Debonded Laminate

Figure 183. Beam DRY-60-1

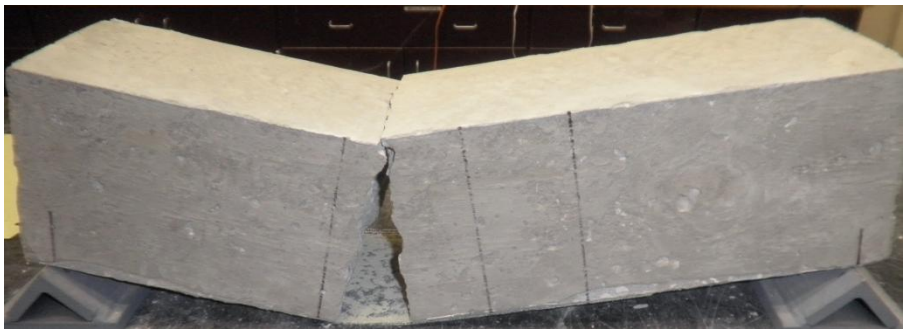

(a) Specimen at Failure

(b) Concrete Substrate

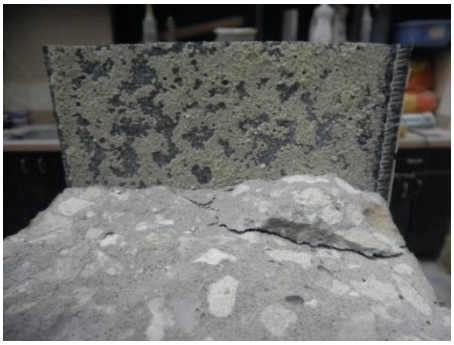

(c) Debonded Laminate

Figure 184. Beam DRY-60-2

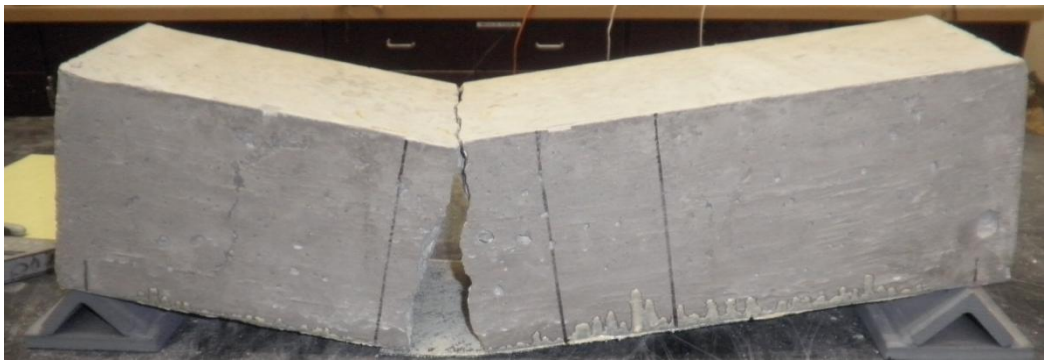

(a) Specimen at Failure

(b) Concrete Substrate

(c) Debonded Laminate

Figure 185. Beam DRY-60-3

B.6 Ambient (AMB) Conditioning Tensile Specimens

Table 38. AMB-30 Beam Test Results Summary

ID	Cracking Load (kip)	Pre-crack Stiffness (kip/in)	Post-crack Load (kip)	Post-crack Deflection (in)	Post-crack Stiffness (kip/in)	Max Strain
AMB-30-1	6.91	399	6.78	0.060	104	5622
AMB-30-2	7.08	416	5.99	0.066	64	1443
AMB-30-3	7.62	357	8.61	0.090	99	6969
Average	7.20	391	7.13	0.07	89	4678
Standard Dev.	0.375	30.1	1.346	0.016	21.58	2881
C.O.V.	0.0521	0.0771	0.1888	0.2252	0.2424	0.6159

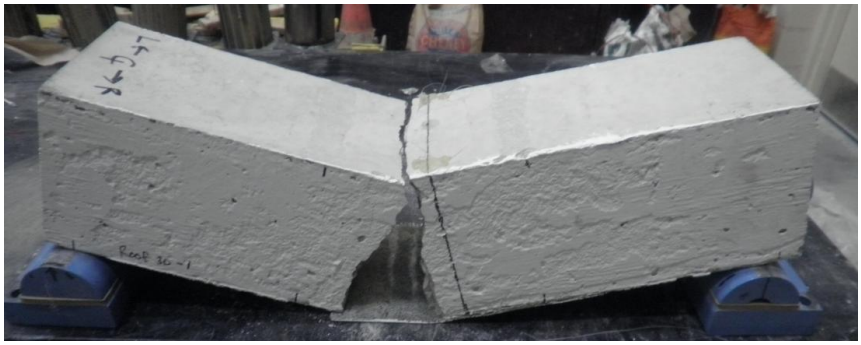

(a) Specimen at Failure

(b) Concrete Substrate

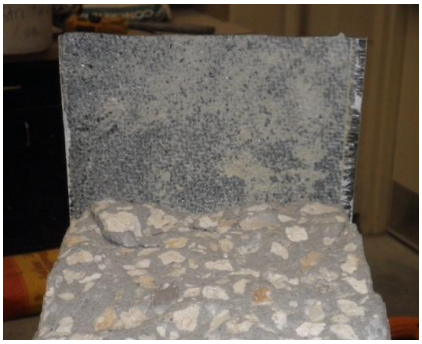

(c) Debonded Laminate

Figure 186. Beam AMB-30-1

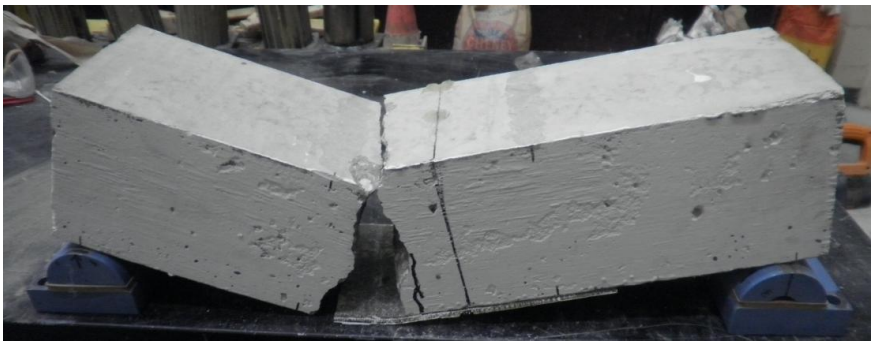

(a) Specimen at Failure

(b) Concrete Substrate

(c) Debonded Laminate

Figure 187. Beam AMB-30-2

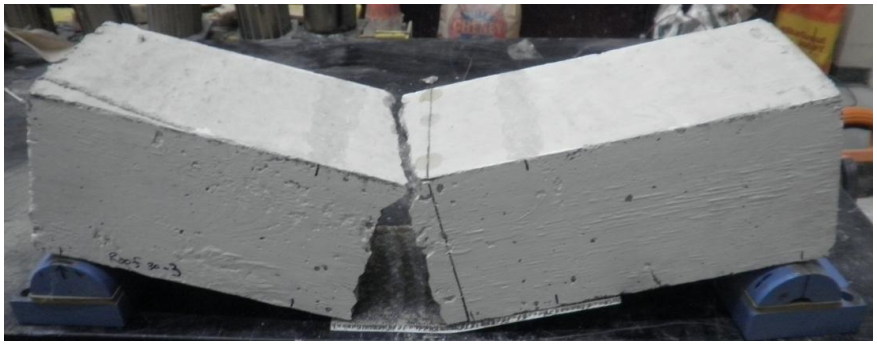

(a) Specimen at Failure

(b) Concrete Substrate

(c) Debonded Laminate

Figure 188. Beam AMB-30-3

Table 39. AMB-60 Beam Test Results Summary

ID	Cracking Load (kip)	Pre-crack Stiffness (kip/in)	Post-crack Load (kip)	Post-crack Deflection (in)	Post-crack Stiffness (kip/in)	Max Strain
AMB-60-1	8.48	346	9.11	0.070	128	4166
AMB-60-2	7.59	281	N/A	N/A	N/A	152
AMB-60-3	7.82	350	N/A	N/A	N/A	1790
Average	7.96	326	9.11	0.07	128	2036
Standard Dev.	0.464	38.6	N/A	N/A	N/A	2018
C.O.V.	0.0582	0.1184	N/A	N/A	N/A	0.9912

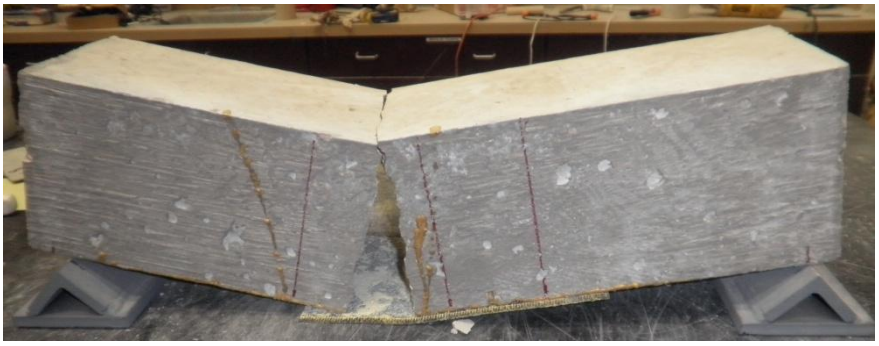

(a) Specimen at Failure

(b) Concrete Substrate

(c) Debonded Laminate

Figure 189. Beam AMB-60-1

(a) Specimen at Failure

(b) Concrete Substrate

(c) Debonded Laminate

Figure 190. Beam AMB-60-2

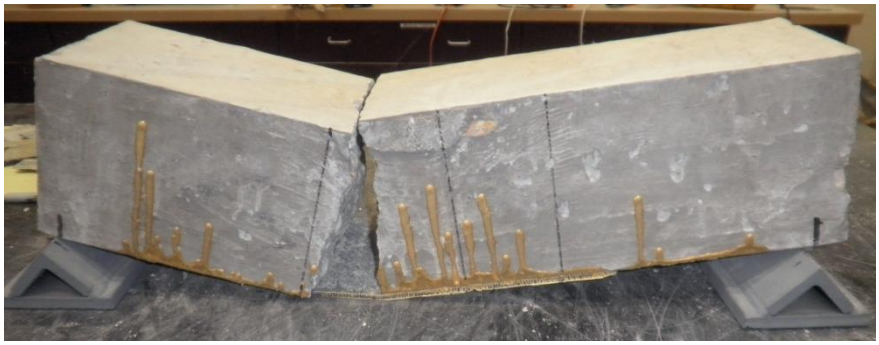

(a) Specimen at Failure

(b) Concrete Substrate

(c) Debonded Laminate

Figure 191. Beam AMB-60-3

REFERENCES

Abanilla, M. A., Li, Y., & Karbhari, V. M. (2006). Durability characterization of wet layup graphite/epoxy composites used in external strengthening. *Journal of Composites: Part B , 37,* 200-212.

Aidoo, J., Harries, K. A., & Petrou, M. F. (2004). Fatigue Behavior of Carbon Fiber Reinforced Polymer-Strengthened Reinforced Concrete Bridge Girders. *Journal of Composites for Construction , 8* (6), 501-509.

Andreopoulos, A. G., Konstantinidou, A. V., & Petsalas, H. J. (1989). Elastomeric Polyurethanes Reinforced with Aramid Fibers. *Journal of Applied Polymer Science , 38,* 2073-2978.

Apicella, A., Migliaresi, C., Nicolais, L., & Roccotelli, S. (1983). The water aging of unsaturated polyester-based composites: Influence of resin chemical structure. *Composites , 14* (4), 387-392.

Barne, R. A., & Mays, G. C. (1999). Fatigue performance of concrete beams strengthened with CFRP plate. *Journal of Composites for Construction , 3* (2), 63-72.

Bazinet, S., Cereone, L., & Worth, F. (2003). Composite FRP moves into underwater repair applications. *SAMPE Journal , 39* (3), 8-16.

Bonacci, J. F., & Maalaj, M. (2001). Behavioraly Trends of RC Beams Strengthened with Externally Bonded FRP. *Journal of Composites for Construction , 5* (2).

Buyukozturk, O., & Yu, T. (2006). Understanding and Assessment of Debonding Failures in FRP-concrete Systems. *Seventh International Congress on Advances in Civil Engineering.* Istanbul, Turkey.

Ferrier, E., Bigaud, D., Hamelin, P., Bizindavyi, L., & W., N. K. (2005). Fatigue of CFRP externally bonded to concrete. *Journal of Materials and Structures , 38*, 39-46.

Gamage, J., Al-Mahaidi, R., & Wong, M. B. (2006). Bond Characteristics of CFRP Plated Concrete Members Under Elevated Temperatures. *Composite Structures* (75), 199-205.

Gheorghiu, C., Labossiere, P., & and Proulx, J. (2006). Fatigue and monotonic strength of RC beams strengthened with CFRP's. *Journal of Composites: Part A , 37*, 1111-1118.

Grace, N. F., & Singh, S. B. (2005). Durability evaluation of carbon fiber-reinforced polymer strengthened concrete beams: Experimental study and design. *ACI Structural Journal , 102* (1), 40-53.

Karbhari, V. M., & Engineer, M. (1996). Effect of environmental exposure on the external strengthening of concrete with composites – Short term bond durability. *Journal of Reinforced Plastics and Composites , 15*, 1194-1216.

Karbhari, V. M., Chin, J. W., Hunston, D., Benmokrane, B., Juska, T., Morgon, R., et al. (2003). Durability gap analysis for fiber-reinforced polymer composite in civil infrastructure. *Journal of Composites for Construction , 7* (3), 238-247.

Kutty, S. K., & Nando, G. B. (1991). Short Kevlar Fiber-Reinforced Thermoplastic Polyurethane Composite. *Journal of Applied Polymer Science , 43,* 1913-1923.

Kutty, S. K., & Nando, G. B. (1991). Stress Relaxation Behavior of Short Kevlar Fiber-Reinforced Thermoplastic Polyurethane. *Journal of Applied Polymer Science , 42,* 1835-1844.

Mallick, P. K. (2008). *Fiber-Reinforced Composites.* Boca Raton: CRC Press.

Marom, G., & Broutman, L. J. (1981). Moisture penetration into composites under external stress. *Polymer Composites , 2* (3), 132-136.

Meier, U., Deuring, M., Meier, H., & Schwegler, G. (1992). Strengthening of structures with CFRP laminates: Research and applications in Switzerland. *Reprinted from Advanced Composite Materials in Bridges and Structures* .

Ritchie, P. A., Thomas, D. A., Lu, L. W., & Connelly, G. M. (1991). External Reinforcement of Concrete Beams using Fiber Reinforced Plastics. *ACI Structural Journal , 88* (4), 490-500.

Schutte, C. L. (1994). Environmental durability of glass-fiber composites. *Material Science Eng., R. , 13* (7), 265-322.

Setiadi, Y., Jar, P.-Y. B., Kuboki, T., & Cheng, J.-J. R. (2005). Comparison of Damage Developmentin Random Fiber-reinforced Polymers (FRPs) under Cyclic Loading. *Journal of Composite Materials , 40* (1), 71-91.

Soudki, K., El-Salakawy, E., & Craig, B. (2007). Behavior of CFRP strengthened reinforced concrete beams in corrosive environment. *Journal of Composites for Construction , 11* (3).

Szycher, M. (1999). *Szycher's Handbook of Polyurethanes.* Boca Raton: CRC Press.

Tavakkolizadeh, M., & Saadatmanesh, H. (2001). Galvanic Corrosion of Carbon and Steel in Aggressive Environments. *Conposites for Construction , 5* (3), 200-210.

Toutanji, H., Zhao, L., Deng, Y., Zhang, Y., & and Balaguru, P. (2006). Cyclic behavior of RC beams strengthened with carbon fiber sheets bonded by inorganic Matrix. *Journal of Materials in Civil Engineering , 18* (1), 28-35.

Zheng, Q., & Morgan, R. J. (1993). Synergistic thermal moisture damage mechanisms of epoxies and there carbon fiber composites. *Journal of Composite Materials , 27* (15), 1465-1478.